The Dissertation Committee for Robert Chase Cornelison Certifies that this is the approved version of the following dissertation:

AN INJECTABLE ACELLULAR NERVE GRAFT AS A PLATFORM FOR TREATING SPINAL CORD INJURY

Committee:

Lydia M. Contreras, Supervisor

Christine E. Schmidt, Co-Supervisor

Hal S. Alper

Jennifer A. Maynard

Laura J. Suggs

AN INJECTABLE ACELLULAR NERVE GRAFT AS A PLATFORM FOR TREATING SPINAL CORD INJURY

By

Robert Chase Cornelison, B.S.

Dissertation

Presented to the Faculty of the Graduate School of

The University of Texas at Austin

in Partial Fulfillment

of the Requirements

for the Degree of

Doctor of Philosophy

The University of Texas at Austin

August 2015

AN INJECTABLE ACELLULAR NERVE GRAFT AS A PLATFORM FOR TREATING SPINAL CORD INJURY

Robert Chase Cornelison, Ph.D.

The University of Texas at Austin, 2015

Supervisors: Lydia M. Contreras, Christine E. Schmidt

Spinal cord injury (SCI) affects a quarter million people in the US, and there is currently no clinical treatment option. Approximately 60% of clinical SCI results from spinal cord contusion, which causes formation of a growth-inhibitory cavity. Research with experimental SCI models has shown spinal axons can regenerate despite this cavity if supplied with appropriate conditions. Two strategies have proven particularly successful: grafting segments of peripheral nervous tissue and transplanting pro-regenerative cells such as peripheral nerve Schwann cells. While implanting fresh nerve tissue risks immune rejection, this challenge can be overcome by removing immunogenic tissue components through decellularization. Unfortunately, decellularization also eliminates the benefits of resident nerve Schwann cells, and transplanting purified Schwann cells after SCI requires the addition of a scaffold for effective cell survival. Tumor-derived Matrigel is often used experimentally to support Schwann cell therapy. For successful translation into humans, however, more clinically-relevant alternatives are needed. Acellular nerve grafts are currently available clinically for peripheral nerve repair and therefore have potential to be such an alternative, although they require some modification to be compatible with contusion injury.

Contusion cavities necessitate scaffolds be applied using minimally-invasive techniques such as injection. Additionally, injectable scaffold are easier to incorporate with other therapeutics such as cells. The goal of this dissertation was to develop and evaluate an injectable acellular nerve graft as a potential intervention for treating contusion SCI. This thermally-gelling nerve scaffold was shown to approximate the chemical composition of native nerve tissue and was optimized to match the mechanical properties of rat neural tissue. Injectable nerve scaffolds were biocompatible with Schwann cells *in vitro* and promoted a regenerative immune response *in vivo* in a rat model of cervical contusion SCI. Delivery of injectable nerve alone supported axon growth into and beyond the SCI lesion after 8 weeks. In collaboration with Dr. Mary Bunge at the Miami Institute to Cure Paralysis, transplanting Schwann cells in injectable nerve promoted equivalent yet faster recovery compared to using Matrigel. This injectable acellular nerve graft is therefore a clinically-relevant alternative to Matrigel for enhancing Schwann cell therapy and promoting recovery following traumatic SCI.

Table of Contents

List of Tables

List of Figures

Chapter 1: Introduction

A quarter million individuals in the United States currently suffer from sensory and motor damage as a result of spinal cord injury (SCI). Deficits can include limb paralysis, respiratory distress, bladder and sexual dysfunction, among others, and there are currently no clinical treatment options to help restore lost function. This paralysis persists because several factors can limit the potential of the spinal cord to regenerate after injury. First, a glial scar forms between the healthy and injured tissue that is inhibitory to axon regrowth and prevents functional recovery. Second, the injury site develops into an inflammatory, fluid-filled cavity, which also limits the potential for regeneration.

A variety of experimental strategies have shown promise to alter this environment and support tissue recovery. Grafting segments of peripheral nervous tissue into the spinal cord can enable regeneration by providing both trophic factors from Schwann cells and a growth-supportive extracellular matrix (ECM) scaffold. Although this strategy shows promise, it requires incision of the spinal cord for graft application, risking further tissue damage. Transplantation of Schwann cells into the injury site without the supportive matrix results in extremely low survival and local maintenance, yet results suggest surviving cells can promote axon regeneration and remyelination. Commercially-available Matrigel is commonly used to enhance Schwann cell survival in experimental models and affords numerous benefits to neural regeneration owing to its high laminin content. Unfortunately, the origin of Matrigel as a tumor ECM extract limits its chances of clinical approval by the FDA. Therefore, a more clinically-viable alternative is needed to achieve the full potential of Schwann cell therapy for treating SCI and improving patient quality of life.

The ECM of nerve tissue is created in part by resident Schwann cells and therefore may be optimally suited to promote survival of Schwann cells after transplantation. This ECM can be obtained through decellularization of peripheral nerve tissue. Over a decade ago, research in Dr. Christine Schmidt's laboratory yielded an optimized decellularization protocol for nerve tissue that is now used clinically with success. Hence, acellular nerve tissue may be a clinically-relevant material from which to develop a Schwann cell-supportive matrix. Reformulating acellular nerve as an injectable material would further enhance this clinical potential by facilitating cell incorporation and minimally-invasive graft application into the contused spinal cord.

The objective of this dissertation was to create and evaluate an injectable nerve scaffold as a material platform for repairing the injured spinal cord. A reproducible method was developed to reformulate acellular nerve tissue into an injectable solution that achieves thermal gelation under physiological conditions. The composition of injectable nerve was determined to be similar to the native tissue grafts known to promote spinal axon regeneration. Furthermore, the mechanical properties of injectable nerve were tuned to realize properties in range of neural tissue and optimal for neurite growth. Finally, injectable nerve scaffolds were evaluated as a stand-alone therapy to treat SCI and in combination with Schwann cell transplantation. Results indicate that injectable nerve promotes 1) immune cell bias toward regenerative phenotypes after one week *in vivo* and 2) supports Schwann cell survival, remyelination, and hindlimb functional recovery comparable to, yet faster than, clinically-irrelevant Matrigel. We conclude that injectable acellular nerve scaffolds may offer a clinically-viable and versatile platform for promoting recovery after SCI, particularly in combination with Schwann cell therapy.

Chapter 2: Background

2.1. The Spinal Cord and Impacts of Traumatic Injury

Often thought of as the "information highway" connecting the brain to the peripheral organs, the spinal cord is critical to normal neural function and can in fact mediate responses independent of the brain (Gomez-Pinilla *et al.* 2007). Unfortunately, over 12,000 people sustain a spinal cord injury (SCI) annually in the U.S., with approximately 275,000 Americans currently suffering from SCI-related deficits (NSCISC 2014). SCI results in permanent, partial or complete paralysis below the injury level, and currently there are no clinical treatment options. Since nearly 60% of injuries occur at the cervical level, many patients experience loss of sensory and motor function over a large portion of their bodies. Furthermore, the average SCI patient is 42 years old at the time of injury and therefore will live with these deficits for decades to come. The cost of managing SCI symptoms is prohibitively high at nearly three million dollars over a patient's lifetime (NSCISC 2014). There is therefore a significant need for clinically-translatable therapies to treat SCI.

2.1.1. Anatomy of the Intact Spinal Cord

The spinal cord comprises grey matter, where neuronal cell bodies reside, and white matter, where ascending and descending myelinated axons are found. The meninges (dura mater, subarachnoid mater, and pia mater) line the outside of the spinal cord and enable paraspinal flow of cerebrospinal fluid. There are four main regions of the spinal cord: cervical, thoracic, lumbar, and sacral. The cervical spinal cord contains neural pathways that innervate the upper extremities as well as the diaphragm, the major muscle of

respiration. The thoracic region is responsible for innervating the upper internal organs and abdominal muscles, and the lumbar and sacral regions innervate the lower extremities and organs, such as the bladder. Damage to the spinal cord, at any level, disturbs the harmonious orchestration between the cells and can generate a range of functional deficits.

The spinal cord is composed of four main cell types, each with distinct and important roles: (1) Neurons and their axonal projections transfer information between neural and non-neural cells via electrical impulses. Depending on the type and location, neurons either integrate sensory information about the surrounding environment or elicit muscle responses to achieve locomotion, respiration, and digestion, etc. (2) Astrocytes support healthy neuronal function by producing appropriate cytokines and managing transport of molecules from the blood via the blood brain barrier. (3) Oligodendrocytes are the myelin-producing glial cells of the central nervous system (CNS) that ensheath axons with an insulative, fatty membrane deposit that increases the speed of electrical conduction. Myelin also contains proteins that stabilize the axon and prevent aberrant sprouting. (4) Microglia are the resident immune cells of the CNS, actively monitoring the environment for abnormalities similar to resident tissue macrophages and assisting in pathogen or debris clearance following infection, injury, or disease.

2.1.2. Spinal Cord Injury: Pathophysiology and Functional Sequelae

An injury to the spinal cord severs local axons and results in death of neurons and the supporting cells near the primary insult. Damage to the blood brain barrier enables influx of circulating immune cells and other peripheral cell types, generating an inflammatory environment. The increased prevalence of excitotoxic and inflammatory

compounds then causes a secondary wave of cell death at the lesion periphery, exacerbating tissue damage. In response, astrocytes become activated or hypertrophic, actively proliferating and generating a "glial scar" to confine the injured tissue. This glial scar acts to mitigate immune cell infiltration and subsequent spread of the lesion into the remaining healthy tissue. Over time, the spinal cord lesion develops into a fluid-filled cavity that is inhibitory to tissue regeneration for a multitude of reasons.

The glial scar is primarily composed of chondroitin sulfate proteoglycans (CSPGs), molecules typical found in perineuronal nets that stabilize synapses and prevent aberrant connections. Their role is mediated through binding of NogoR or PTPσ receptors on growing axons, which induces axon retraction and growth inhibition (Cao *et al.* 2008; Lang *et al.* 2015). Although the glial scar may be acutely beneficial in minimizing spread of the injury, it acts as a physical and chemical barrier to axon regeneration at more chronic time points. Additionally, myelin contains proteins that prevent axon sprouting known as myelin associated inhibitors. These inhibitors are released into the extracellular space following injury, also contributing to regenerative failure (Fitch and Silver 2008; Cafferty *et al.* 2010). Invading immune cells are another barrier to regeneration as macrophages activated by CNS injury often induce axon retraction (Busch *et al.* 2011; Horn *et al.* 2008).

The immune response following SCI is quite unique. Typically after peripheral tissue damage, macrophages initially exhibit a pro-inflammatory (M1) phenotype to assist in disinfecting the area and clearing tissue debris for regeneration to occur (Novak and Koh 2013). The prevalent phenotype then switches toward a pro-regenerative/anti-inflammatory (M2) activation state in which the cells promote tissue repair. In contrast, SCI induces a burst response of M2 macrophages that is quickly dominated by M1

macrophages, which persist chronically (Kigerl *et al.* 2009). These M1 macrophages are most likely responsible for the immune-mediated axon retraction mentioned above. Conversely, M2 macrophages promote neural regeneration as well as neural progenitor cell differentiation of oligodendrocyte precursors (Kigerl *et al.* 2009; Miron *et al.* 2013), and transplantation of appropriately activated macrophages can enhance functional outcomes in paraplegic rats (Rapalino *et al.* 1998). Therefore, beyond glial scarring and growth inhibition, evaluating the immune response may be a critical consideration when developing new interventions for SCI.

The combination of all factors associated with traumatic neural injury (e.g., axon retraction, primary and secondary cell death, inflammation, and glial scarring) induce significant functional deficits in both humans and animal models. In broad terms, these deficits encompass loss of sensory and motor function below the level of injury. Since the majority of clinical injuries occur at the cervical level (~60%; NSCISC 2014), many SCI patients are at high risk for losing function in the upper and lower extremities, abdominal muscles including those involved in respiration (the diaphragm and intercostal muscles), as well as bladder and sexual dysfunction. Recovery of locomotion has been the focus of most research efforts to date. Injury models in rats and mice can be useful for evaluating locomotor improvement because the injury environment and observed deficits correlate well with clinical injuries (Metz *et al.* 2000; Norenberg *et al.* 2004). There is one caveat to this approach: Rodents exhibit increased neural plasticity, meaning they can recover near-normal use of their hindlimbs after incomplete cervical injury. Nonetheless, this phenomenon is a logistical advantage since caring for quadriplegic animals would require significantly more intense care procedures. Another advantage is that assessing locomotor

recovery in rodents after incomplete cervical injury only involves measures of forelimb function as the hindlimbs are unaffected.

Despite the experimental focus on locomotor recovery, respiratory complications are the number one cause of morbidity and mortality in SCI patients (NSCISC 2014). Damage to cervical, thoracic, and even lumbar spinal cord regions can result in respiratory deficit resulting from denervation of various muscle groups (Inskip *et al.* 2009). The largest motor neuron pool known as the phrenic nucleus is in the cervical region (C3-C5/6 in rats and C3-C5 in humans) and controls the diaphragm via the phrenic nerve (Zimmer *et al.* 2007). Injuries at or above this region can significantly impair voluntarily breathing. In fact, approximately one third of cervical SCI patients require mechanical ventilation (NSCISC 2014). Therefore, a definite need exists to develop therapies that not only improve locomotor function but also respiratory function after SCI.

2.2. Experimental Methods to Study Spinal Cord Repair

2.2.1. Choice of Injury Model

The choice of SCI animal model can dictate which parameters and conclusions of the investigation are relevant to human injuries. Until recently, most studies employed injuries in the thoracic region because the thoracic spinal cord is more accessible than the cervical cord (i.e., the thoracic cord is more superficial and associated with less overlaying musculature). These injuries largely cause hindlimb and bladder dysfunction, and the animals are typically still ambulatory even after extensive, bilateral injury (which affects both limbs). This characteristic is the primary advantage over cervical models since bilateral cervical injury may severely limit mobility and decrease the animal's ability to

access food and water. This limitation can be overcome using a unilateral injury (affecting only one side). As mentioned above, cervical injury is most common in humans, so cervical injury models are gaining interest given the obvious clinical relevance. In rodents, these injuries primarily affect locomotion through forelimb function. Unilateral cervical injuries largely create deficits in only one limb, thereby affecting mobility as little as possible. The next consideration is the method of conducting the injury. Three main injury types are most common: resection, clip compression, and contusion, with variations possible for each.

Resection Models Transections or hemisections involve incising the dura mater and physically removing a complete segment or a partial segment of the spinal cord. Complete transection models are most common as thoracic injuries because fully severing the spinal cord in cervical regions could result in death. This model is particularly useful for evaluating the effects of an intervention on axon regeneration (Cheriyan *et al.* 2014). Transection injuries spare no axons in the lesion, eliminating the possibility for lateral sprouting. Furthermore, there is no route around the injury, and all observable axon growth and corresponding functional recovery is therefore attributable to genuine regeneration into the lesion. Hemisection models are used to selectively study injury in one region of the spinal cord (such as the dorsal or lateral funiculi) or create "complete" but unilateral injuries (Cheriyan *et al.* 2014). This model entails potential for compensation by the uninjured side, but all ipsilateral pathways are severed such that most axon growth and functional recovery results from regeneration. Given the invasiveness of these models, however, resection models are not particularly representative of clinical injuries.

Compression Models Clip-compression improves upon transection models in terms of clinical relevance. This model involves clamping the spinal cord using modified

aneurysm clips (Poon *et al.* 2007). The severity of injury can be varied by altering the duration of clamping and the force rating of the applied clip. Clip-compression generates an incomplete injury given that some axons may be spared in the lesion, but these are primarily bilateral injuries. As such, clip-compression has mostly been applied for thoracic injury. A cervical clip-compression injury model was recently described (Forgione *et al.* 2014), demonstrating additional applicability of this model given the injury is applied in the low cervical region (at C6). Although more clinically-relevant than transection models, it is debated whether endured forces accurately mimic clinical injuries which most commonly result from rapid impacts as in sports injuries and vehicle crashes.

Contusion Models Contusion injuries are most representative of the pathophysiology observed in clinical injuries. Several models of contusion injury have been described to create mild, moderate, and severe injuries. The first device described for creating a contusion injury was the NYU (now MASCIS) weight-drop model (Basso *et al.* 1996). The injury severity in this model is governed by the mass of the weight and the height from which it is dropped. This model can provide fairly reproducible and graded injuries, yet the duration of impact is not controllable and two impacts were often observed from bouncing of the weight. A second device was then developed and used exclusively at Ohio State University based on electromechanical propulsion opposed to using gravity (Somerson and Stokes 1987). Since this device was controlled by an external computer that controlled the approach and retraction, weight bounce is eliminated. The level of expertise required to construct the unique pattern generator restricted the commercial availability of this device.

Infinite Horizons (IH) (Precision Systems and Instrumentation, LLC) eventually commercialized a device that similarly automates the approach and retraction of the

impactor. Additionally, an onboard sensor reports the biomechanical properties of the impact such as displacement and force of impact, increasing reproducibility of the injury. For these reasons, the IH device is the most common device for generating controlled contusion injuries. The injury severity is controlled both by the force on impact as well as the size of the impactor used. Mild injuries in rats can be applied using a 1.3 mm tip and more severe injuries a 2.5 mm tip, approximately half the diameter of a rat spinal cord. Similarly, lower forces around 100-150 kDynes are considered more mild whereas forces ≥200 kDynes can create more moderate to severe injuries.

Modeling Respiratory Deficits Given the prevalence of respiratory deficits and complications associated with clinical SCI, several injury models have been used to assess recovery of respiratory function after injury. In spinal injured rats, total breathing (tidal volume x frequency) can be indistinguishable from uninjured controls 2 weeks after injury (Fuller *et al.* 2006). Therefore, generating measurable respiratory deficits requires moderate to severe injuries that ensure ablation of neurons that innervate the ipsilateral (injured) hemi-diaphragm. It can be particularly important that the chosen injury model is severe enough to abolish lateral white matter, including descending bulbospinal respiratory fibers (Darlot *et al.* 2012), and ventral grey matter containing phrenic motor neuron cell bodies. Cervical hemisection models are most commonly used since they provide the most reliable removal of respiratory pathways. Achieving this extent of destruction using a contusion injury often requires considerable impact forces between 200-400 kDynes, depending on the impactor diameter (Nicaise *et al.* 2012; Lane *et al.* 2012). Despite extensive research into different methods of injury generation, no current injury model

mimics ventilator-dependent patients given the level of care and specialized equipment this would require.

2.2.2. Assessing Functional Recovery in Animal Models

The choice of animal model will dictate which established behavior tests will be useful for elucidating functional benefits of a therapy. This dependence is primarily based on the level of injury, although injury type and severity can influence the sensitivity required to detect differences. Behavioral assessments have been developed to examine recovery of several different parameters, with some tests correlating between cervical and thoracic injury models.

Motor Recovery Open-field tests such as that described by Basso, Bresnahan, and Beattie (BBB) evaluate limb function during general, unconstrained locomotion (Basso *et al.* 1995). The BBB test, as well as the forelimb equivalent Forelimb Locomotor Scale (FLS) (Cao *et al.* 2008), scores independent joint movement, weight support, paw position, and toe clearance, among others. As such, this type of test examines the broadest spectrum of movements affecting locomotion and is the most common behavioral test reported. Additional tests have been created to assess recovery of more fine motor control, such as the pasta eating test, the Irvine-Beatties-Bresnahan Forelimb recovery scale, and the Whishaw reaching task to assess digit control, object manipulation, and fine reaching/grasping movements, respectively (Allred *et al.* 2008; Irvine *et al.* 2014; Whishaw *et al.* 1993). Furthermore, electrophysiological recordings of muscle action potential can provide a more quantitative measure of functional muscle recovery. This technique is discussed in detail below.

Sensorimotor Recovery Tests to evaluate recovery of sensorimotor function involve applying a sensory stimulus to elicit a quantifiable motor response. Several sensory inputs have been studied, including visual presentation and stimulation of the skin and whiskers (or vibrissae). The cylinder paw preference test is commonly used to evaluate weight support and shifting through paw preference during vertical exploration (Khaing *et al.* 2012). After unilateral injury, animals will exclusively use their uninjured paw, gradually recovering use of the affected limb over time; hence, this test is useful for distinguishing differences in sidedness after neural injury. Vibrissae-elicited paw placing can be used to score forelimb movement following whisker-stimulation (Khaing *et al.* 2012; Schallert *et al.* 2000). The degree of forelimb movement assesses recovery of motor function as well as sensation in the ipsilateral barrel or whisker field. With thoracic injuries, the grid walk test is commonly used to evaluate sensorimotor coordination of hindlimb and forelimb movement as the animal traverses randomly spaced metal bars (Metz *et al.* 2000). Finally, the sticker test can be used to measure the animal's ability to sense and remove an adhesive sticker from the surface of the paw. This test is most common in stroke research, although it has been used with SCI, as well. (Schallert *et al.* 2000; Webb and Muir 2005).

Recovery of Sensation Sensory fibers often regenerate more readily than motor fibers, making SCI patients susceptible to increased pain sensation (A. Brown and Weaver 2012). Allodynia describes increased sensitivity to a stimulus that normally would not elicit pain, while hyperalgesia is enhanced pain sensation to a stimulus that normally would be painful. Hyperalgesia can be difficult to study in animals since the subject cannot self-report on the level of pain, but allodynia can be gauged using both mechanical and thermal stimuli. Von Frey filaments have been developed to precisely evaluate mechanical allodynia (Chaplan

et al. 1994; Fruhstorfer *et al.* 2001). These fibers bend at defined forces and therefore can be used to converge on the minimum force required to elicit a motor response. This test is most useful for thoracic injuries because, while stationary animals use their forelimbs for grooming, exploration, and eating, the hindlimbs are in constant contact with the cage bottom, providing more opportunity to probe the plantar surface of the paw. An infrared heat source is often employed to examine thermal allodynia (Kanno *et al.* 2014; Hargreaves *et al.* 1988), although this test is less common than mechanical methods given the potential to burn the footpads of the paralyzed animal.

Physiological Recovery Electrophysiology enables recording of electrical signals generated by or propagated through tissues such as muscle or nerve, thereby correlating with the degree of innervation or the functional activity of terminating axons. In thoracic injury models, bladder function can be measured by recording activity of the detrusor muscles and external urinary sphincter (Y. S. Lee *et al.* 2013). Similarly, respiratory function after cervical injury can be measured by electromyography recordings of the diaphragm (Alilain *et al.* 2011). To more precisely measure the central neural drive of respiration, recordings can alternatively be taken directly from the phrenic nerve. This preparation enables characterization of neural respiratory output under normal oxygen conditions as well as respiratory challenges such as hypoxia (low oxygen) or hypercapnia (elevated CO_2). These challenges may be experienced at higher altitudes or during hypoventilation resulting from respiratory disease; therefore recording neural activity under these parameters can provide useful information about the effects of treatment on a patient's ability to cope with challenging environmental conditions.

Understanding the advantages and disadvantages of different animal models and behavioral tests is crucial to appropriately evaluating a new therapeutic strategy. Transection and hemisection models are best for examining recovery from complete neural disconnection, while contusion models are more representative of the clinical setting. Moreover, SCI therapies can differentially affect sensory, sensorimotor, and motor recovery (both locomotor and otherwise), and multiple functional measures should therefore be used to better characterize the effects of an intervention.

2.3. Current Strategies to Promote Spinal Cord Regeneration

A spinal cord lesion does not contain a substrate for regeneration and in fact is inhibitory to recovery. Methods to overcome this barrier typically fall into two broad categories: 1) Strategies to make the lesion environment more hospitable to tissue regrowth, either using transplanted cells, biomaterials, or molecular therapy, and 2) Strategies to bypass the lesion entirely using peripheral nerve grafts. The current status of each is briefly reviewed, focusing on relevant cell- and biomaterial-based approaches as well as their combination.

2.3.1. Cell-Based Strategies and the Need for a Supporting Substrate

Stimulated Macrophages Phagocytic cells such as macrophages help to clear myelin debris after peripheral nerve and CNS injuries, thereby preparing the area for axon ingrowth. Classically-activated or M1 macrophages can be detrimental to repair after spinal cord injury, but exposure of macrophages to a peripheral nerve injury prior to application in the spinal cord would stimulate the cells toward alternative (M2) activation (Ydens *et al.* 2012). As in other injury environments, these stimulated macrophages promote repair

of the injured spinal cord and also improve hindlimb function following thoracic transection (Rapalino *et al.* 1998). In human patients, transplantation of stimulated macrophages failed to demonstrate benefits (Lammertse *et al.* 2012), and now most research focuses on methods to bias the phenotype of resident/invading macrophages.

Mesenchymal Stem/Stromal Cells Mesenchymal stem/stromal cells (MSCs) derived from bone marrow or placenta have potential to differentiate into several mesodermal cell lineages, including neuron-like and oligodendrocyte-like cells (Portmann-Lanz *et al.* 2010; H. Xu *et al.* 2010). Therefore, there is significant interest in using these cells to promote recovery after SCI. MSCs can home to SCI lesions following a simple intravenous injection (Parr *et al.* 2007), which enhances the clinical utility of this cell source. The current understanding is that MSCs primarily influence the immune response to injury via paracrine signaling, and infusion of MSC-conditioned media alone can promote locomotor recovery (Cantinieaux *et al.* 2013). Neuron-like MSCs, however, may be incapable of generating action potentials (Hofstetter *et al.* 2002), limiting the potential of MSCs to functionally replace damaged neurons.

Neural Stem/Progenitor Cells The allure and promise of stem cells for regenerative medicine entered the neural realm in 1992 when neural stem/progenitor cells (NPCs) were first identified and isolated from the adult rat subventricular zone (Reynolds and Weiss 1992). Since this discovery, several approaches have been used to transplant and attempt differentiation of NPCs from both adult and embryonic tissues after SCI. Although these cells offer potential to replace multiple neural cells types including neurons, NPCs typically differentiate exclusively into glial cell types upon transplantation, if differentiating at all (Mothe and Tator 2013; Karimi-Abdolrezaee *et al.* 2006). Similar to MSCs, NPCs have

been shown to mediate positive immune responses that can benefit recovery after SCI (Giusto *et al.* 2014; Ottoboni *et al.* 2015). Unfortunately, maintenance and survival of these cells in the lesion is often particularly low, and the injury milieu effectively hinders cell differentiation. Recent evidence suggests that degradation of the chondroitin sulfate component of the glial scar significantly enhances NPC migration and differentiation toward a desirable oligodendrocytic lineage (Karimi-Abdolrezaee *et al.* 2010). Nonetheless, undesirable heterogeneity in differentiation is currently unavoidable, and many researchers are now investigating methods to better direct differentiation *in vitro* or *in vivo* using growth factors and/or engineered materials.

Olfactory Ensheathing Cells A subpopulation of glial cells in the olfactory epithelium and nerve known as olfactory ensheathing cells (OECs) can phagocytose debris (Wewetzer *et al.* 2005) and promote axon regeneration when transplanted into the injury site after SCI (Keyvan-Fouladi *et al.* 2003; Y. Li *et al.* 2003; Ramon-Cueto *et al.* 2000). OECs have been shown to ensheath axons similar to their role in the olfactory nerve, although there is controversy over whether these cells promote remyelination and functional recovery (Imaizumi *et al.* 2000; Pearse *et al.* 2007; Rao *et al.* 2014; Takami *et al.* 2002). Differences in culture method may be the cause of these contradictory results (Novikova *et al.* 2011).

Schwann Cells Following peripheral nerve injury, Schwann cells, the resident myelinating cell type, dedifferentiate into a migratory phenotype, proliferate, and guide axon regeneration via cytokine production and formation of channel structures known as bands of Büngner (Fex Svennigsen and Dahlin 2013). These cells perform similar functions when transplanted after SCI, remyelinating regenerating axons and promoting recovery of hindlimb function (Oudega and Xu 2006; Pearse *et al.* 2004; Pearse *et al.* 2007; Takami *et*

al. 2002; X. M. Xu *et al.* 1999). Combining Schwann cell transplantation with other cell types or growth factor therapy can enhance these effects. In particular, transducing Schwann cells to express the bifunctional neurotrophin D15A, having activity similar to both brain-derived neurotrophic factor (BDNF) and neurotrophin-3 (NT3), has been shown to increase cell survival, axon regeneration length, and axon remyelination by five-fold (Golden *et al.* 2007). Being native to the peripheral nervous system, Schwann cells produce peripheral myelin which is morphologically-distinct from CNS myelin, but this fact has not been shown to be detrimental to recovery.

While several cellular interventions are currently or have previously been evaluated in clinical trials, the overarching conclusion from the preclinical research is that transplantation of cells in media results in low cell survival and maintenance in the lesion area. This outcome limits the efficacy of any transplantation strategy, regardless of cell type used or the delivery location. It is known that transplanting donor cells with a supportive scaffold can significantly improve cell survival and therapeutic impact (Patel *et al.* 2010; Christman *et al.* 2004). One explanation is that removing cells from a substrate downregulates expression of cell surface adhesion molecules, and this effect is prevented by restoring the extracellular ligands (He *et al.* 2015). Therefore, creation of clinically-translatable scaffolds to support cell transplantation into the spinal cord has significant potential to improve anatomical and functional benefits conferred through cellular therapy.

2.3.2. Biomaterial-Based Strategies

An SCI lesion provides ample space to implant polymeric scaffolds that promote spinal cord regeneration, either as an empty scaffold or in combination with cell

transplantation. A large variety of biomaterials have been developed for this purpose, both preformed scaffolds and those that form *in situ*. The mechanism of material polymerization or formation will dictate what animal model can be used in evaluation as well as the ease of incorporating additional factor. Most early biomaterials for SCI were preformed, molded and polymerized outside of the body and then implanted *en bloc* following resection of the spinal cord. Given that surgical incision into delicate neural tissue risks causing unnecessary damage, injectable biomaterials are gaining significant interest since they are less invasive to apply and more compatible with clinically-relevant contusion models. The advantages and disadvantages to both strategies are discussed below.

Preformed Scaffolds Many polymeric materials require polymerization under conditions that can damage cells and tissues, either through radiation exposure or use of harsh chemicals. Modifying polymers such as hyaluronic acid, a natural glycan residue of the extracellular matrix, with methacrylate side groups renders the polymer chains photocrosslinkable. This method is widely studied in tissue engineering as a means to easily tune scaffold mechanical properties by controlling exposure to ultraviolet (UV) light (Seidlits *et al.* 2010; Suri and Schmidt 2010; Shin *et al.* 2012). Applying this concept toward spinal cord repair, Khaing et al. found that UV-crosslinking of hyaluronic acid enabled retention of the polymer in a dorsal hemisection lesion and reduced immune cell infiltration and astrocyte activation (Khaing *et al.* 2011). Instead of UV, some scaffolds require fabrication using organic solvents such as methylene chloride or chloroform. These materials can nonetheless be useful in tissue engineering following ample washing, as is the case for biodegradable poly-lactic-co-glycolic acid (PLGA). Seeding of neural stem cells onto a composite material of PLGA and a block co-polymer of PLGA-poly-L-lysine

can be accomplished after material fabrication, and this cell-scaffold combination diminished glial scarring and significantly improved hindlimb function in a thoracic lateral hemisection model of SCI (Teng *et al.* 2002).

The bulk of research into preformed neural scaffolds has been devoted to creating structures inside scaffolds for subsequent implantation. The presence of aligned topographical cues or channels significantly increases the length of resulting neurites (Chua *et al.* 2014; Kim *et al.* 2008). Though recent advances in self-assembling peptide materials are moving the field closer (Y. Liu *et al.* 2013; Tysseling *et al.* 2010), *in situ* alignment of structures spanning the length of a lesion is currently not feasible. Several methods have been described to create nano- and microscale topographical cues *in vitro*. Electrospinning and cell-mediated tension are used to create materials with aligned fibers, and freeze drying or fabrication around sacrificial templates can create larger-scale channels.

Electrospinning can create fibers that mimic the topography of the native extracellular matrix on the nanometer and micrometer scales. Rotating the collection surface enables alignment of the electrospun fibers, and this alignment promotes neural differentiation of embryonic stem cells and also increases axon length after spinal cord transection over unaligned fibers and non-fibrous films (Xie *et al.* 2009; Hurtado *et al.* 2011). These materials can be modified with growth factors and scar-degrading enzymes to further enhance the therapeutic efficacy (Liu *et al.* 2012). Alignment of native collagen fibers during fibrillogenesis can be achieved by seeding Schwann cells into the pre-gel solution (Georgiou *et al.* 2013; Georgiou *et al.* 2015). As the collagen fibers form, with a rise in temperature, the cells exert tensile forces on the fibers through cell-matrix interactions that cause fiber alignment. These aligned mats, rolled to form tubes, enhance

the length of axon growth after peripheral nerve injury. These materials have not yet been applied toward spinal cord repair.

Other methods to create intra-scaffold architecture generate structures much larger than nanometer-sized fibers. The easiest to implement requires only a freeze dryer or lyophilizer. A solution of the base polymer, typically naturally-derived collagen or the polysaccharide agarose, is placed in a sterile mold and then subjected to freeze drying. This process creates uniaxial channels hundreds of microns in diameter (Stokols *et al.* 2006; Fuhrmann *et al.* 2010). Channels of this size enable axonal growth as large fascicles in which each individual axon contacts and supports neighboring axons, increasing the total length of axon growth over smaller channels (Fuhrmann *et al.* 2010).

Forming materials around crystal lattice templates can also achieve complex networks of interconnected pores (Hardy *et al.* 2015). Essentially, solutions of hydrogels or organic polymers can be saturated with various salt molecules, and crystal lattice formation can be induced by seeding a single crystal, creating a nucleation point. By constraining the geometry of the solution in a linear and tubular mold, long-range crystal aggregates are formed. Polymerizing the material around these structures and washing away the sacrificial crystalline molecules creates interconnected pores inside the material. The geometry and tortuosity of the remaining channels is dictated by the choice of crystalline molecule, although this can be difficult to predict *a priori*. Urea was found to create the best aligned channels resembling the peripheral nerve basal lamina.

The above methods for channel generation typically offer limited control over channel diameter. Stokols et al. overcome this limitation by forming an agarose scaffold around a template of aligned polystyrene cylinders (Stokols and Tuszynski 2006). The

cylinders are then dissolved with tetrahydrofuran, creating channels approximately 200 microns in diameter. These scaffolds supported robust axon regeneration, but the effects on functional recovery was not assessed.

Creating structural cues to guide axons across an SCI lesion certainly has potential to facilitate regeneration; however, preformed scaffolds are inherently distinct from the native tissue, often forming defined graft-spinal cord boundaries. Incorporation of the host tissue with the engineered scaffold restores the integrity and continuity of the spinal cord. Conversely, a lack of integration can result in cavity expansion and separation of the rostral stump from the scaffold, eliminating the possibility for repair (Nomura *et al.* 2006). More effective methods need to be developed that enable selective removal of only scarred tissue without damaging healthy tissue as well as molding of scaffolds to the exact lesion volume before preformed scaffolds can achieve their full clinical potential for treating SCI.

Injectable Scaffolds In contrast to preformed scaffolds, injectable or *in situ* forming materials can be implanted as a liquid precursor. Upon injection, these materials create viscoelastic networks through either physical interactions such as hydrogen bonding and entanglement or chemical crosslinking via bio-orthogonal chemistries that do not interfere with cellular processes. These fabrication schemes negate the need to resect part of the tissue and enable the material to mold to and integrate with the lesion. Furthermore, evenly incorporating additional factors such as cells, drug-eluting microparticles, or small molecules is significantly easier in liquids compared to preformed materials in which diffusion may limit uniform incorporation. The most common type of injectable material applied toward SCI are thermally gelling or form with increases in temperature. These

materials will be primarily discussed, although other formation schemes are also briefly mentioned below.

Collagen I is the most common structural component of the extracellular matrix (ECM) and is commercially available as an extract from rat tails. Solutions of collagen I undergo fibril formation as the temperature is raised from 0°C to 37°C, producing a hydrated, fibrous structure at physiological conditions. Since collagen is a native to tissue, collagen-based scaffolds benefit from its biodegradability and natural role in cell adhesion and migration. Unfortunately, collagen I in excess is also associated with fibrotic scarring and may be turned over more rapidly in the injury environment than regeneration can occur; therefore collagen alone is not always an appropriate regenerative scaffold. Marchand et al. investigated adding various crosslinking agents to stabilize collagen implants after SCI (Marchand and Woerly 1990; Marchand *et al.* 1993). These crosslinkers were able to improve scaffold retention and axon ingrowth at 6 months, with chondroitin-6-sulfate crosslinking best resisting conversion to scar. Recently, tissue engineering has shifted away from using collagen I alone in favor of more complex collagen-based materials that integrate multiple signaling and cell adhesive moieties.

Matrigel is a gelatinous mixture of proteins comprising mostly collagen IV and laminin derived from the ECM of cultured mouse sarcoma cells. Matrigel's high laminin content ensures it will have many benefits for neural engineering through enhanced cell attachment, cell survival, and neurite growth. It also contains heparin sulfate proteoglycans and large quantities of growth factors that most likely improve these outcomes, as well. As such, Matrigel is very commonly used as a positive control for *in vitro* assays, and it is used *in vivo* to improve cell transplantation strategies for SCI repair. Compared to other

ECM-based injectable materials, Matrigel achieved the most significant enhancement to Schwann cell therapy based on cell survival and proliferation criteria (Patel *et al.* 2010). Nonetheless, the FDA is unlikely to grant Matrigel clinical approval based on its tumor origins, and more clinically-relevant scaffolds that perform comparable to or better than Matrigel are greatly needed to advance therapeutic development for SCI repair.

The central nervous system has high hyaluronic acid content (Zimmermann and Dours-Zimmermann 2008), motivating its use as a scaffold for neural engineering. On its own, hyaluronic acid does not form physical crosslinks. The long polymer chain can become physically entangled, creating a highly viscous solution, but these interactions are easily disturbed in aqueous solution. These entanglements do, however, afford hyaluronic acid with shear-thinning properties as the polymer chains will align with the shear forces, temporarily decreasing solution viscosity (Gupta *et al.* 2006). Hyaluronic acid can therefore be combined with physically gelling materials such as methyl cellulose to create a composite that forms *in situ* but can also be injected following gelation. Additionally, functional groups on the disaccharide backbone can be modified for bio-orthogonal crosslinking chemistries.

Composite materials of hyaluronic acid-methyl cellulose (HA-MC) have been used to deliver multiple factors around the SCI lesion (Austin *et al.* 2012; Baumann *et al.* 2010; Gupta *et al.* 2006; Kang *et al.* 2008). Delivery of neuroprotective erythropoietin in HAMC into the intrathecal space (between the spinal cord and dura mater) resulted in decreased lesion volume and increased neuronal sparring versus the free-drug control (Kang *et al.* 2008). Moreover, sustained release of platelet-derived growth factor-A from HA-MC increased oligodendrocytic differentiation of co-transplanted neural stem cells and

decreased the number of grid walk errors observed after thoracic SCI (Mothe *et al.* 2013). More recently, the Shoichet group developed a hyaluronic acid material that crosslinks using click chemistry (Fuhrmann *et al.* 2015). This click-crosslinkable hyaluronic acid exhibited sustained drug release *in vitro*, but the effects of this delivery strategy on recovery after SCI are yet to be determined.

Aside from hyaluronic acid, other polysaccharides have been implemented to repair the injured spinal cord (Ansorena *et al.* 2013; Jain *et al.* 2006). For example, agarose is a polysaccharide derived from seaweed which, in contrast to other thermally gelling materials, requires cooling for gelation. This unique characteristic complicates the application of agarose for cell culture or tissue engineering since the high initial temperature may be damaging to cells. To overcome this limitation, Jain et al. (2006) developed a system to rapidly cool the agarose after application into the hemisected spinal cord using chilled nitrogen gas. They then used this system to deliver BDNF which encouraged neurite growth and reduced the glial scar response. The intricacies involved with this method nonetheless limit use of injectable agarose after SCI.

Using a more molecular engineering approach, peptide amphiphiles can be created that self-assemble into β-sheet rich nanofibers *in vivo*. Without incorporating cell adhesion ligands, one type of peptide amphiphile mediated recovery of hindlimb function after clip compression SCI by reducing glial scarring and minimizing the inflammatory response (Y. Liu *et al.* 2013). Modifying the peptide to contain IKVAV, an adhesive ligand found in laminin, promoted axon elongation into the scaffolds as well as plasticity of serotonergic fibers (Tysseling *et al.* 2010; Tysseling-Mattiace *et al.* 2008). By further tuning the peptide composition and therefore assembly geometry, these materials may have the potential to

achieve long-range fiber orientation *in situ*. Such a material could provide an aligned topography for increased directional growth of axons while still embodying the benefits of injectable materials for clinical translation.

The field of injectable scaffolds for SCI repair is largely dominated by natural polymers owing to their inherent biocompatibility, biodegradability, and high water content mimicking native tissue. A small selection of injectable synthetic matrices have also been developed to treat SCI (Conova, L et al., J Neurosurgery Spine 2011; Elias, P.Z. et al, J Control Release 2015; Kang Y, Hwang D, Kim B. Macromolecular Res, 2010) but are much less common. Although biomaterial strategies can effectively support axon regeneration, it is now understood that a combinatorial approach (combining matrices with cells and/or growth factors) will be necessary to achieve meaningful recovery after SCI.

2.3.3. Peripheral Nerve Grafts in the CNS: Successes and Limitations

Over the years, extensive research has focused on determining why the peripheral and central nervous systems have such dissimilar responses to injury. The resident cell types certainly play a major role. In the peripheral nervous system, Schwann cells are activated following nerve injury, actively proliferating and guiding axon regeneration (Fex Svennigsen and Dahlin 2013). Oligodendrocytes, the corresponding CNS myelinating cells, conversely do not show evidence of activation after SCI. Spinal astrocytes become activated following injury, yet these cells act to barricade the injury environment and effectively inhibit axon regeneration in the process. Furthermore, it has been proposed that the composition of the CNS ECM is a key determinant in the injury response. Peripheral ECM promotes regeneration through laminin-containing basal lamina tubes while the CNS

ECM contains factors that are inhibitory to axon regeneration (Fitch and Silver 2008). Grafting peripheral nerve tissue into the CNS can therefore provide spinal axons with a growth-supportive environment while bypassing the local inhibitory environment (David and Aguayo 1981; Levi *et al.* 2002; Tom *et al.* 2009; Alilain *et al.* 2011). Additionally, immune cells display differential effects in response to peripheral versus central tissue (Zeev-Brann *et al.* 1998). Following exposure to sciatic nerve tissue, macrophages had increased phagocytic activity and nitric oxide expression, while the opposite effects were observed following exposure to optic nerve (CNS) tissue. These results suggest peripheral nerve grafts may further promote regeneration through immune modulation.

Peripheral nerve grafts effectively combine cell and biomaterial-based therapies as they contain native Schwann cells that secrete trophic factors and guide axons as well as ECM molecules that physically support axon growth. In the CNS, this strategy is most commonly combined with enzymatic removal of chondroitin sulfate proteoglycans using chondroitinase ABC that break down the glial scar and enable axons to enter the nerve grafts. Using this approach, Tom et al. demonstrated that chronically injured axons could be coaxed to regrow into the lesion as well as several millimeters into the distal portion of the cord (Tom *et al.* 2009). Alilain et al. also used a similar peripheral nerve bridge to promote reinnervation of the respiratory motor neuron pool and achieved functional recovery of breathing after high cervical SCI (Alilain *et al.* 2011). Despite these significant findings, both of the above studies used invasive methods to apply the nerve grafts. The former study examined a clinically relevant contusion injury but aspirated the damaged tissue prior to graft implantation, risking tearing of spared axons in the lesion or damaging adjacent uninjured tissue. The latter study employed a cervical hemisection that, while an

effective model to study axon regeneration, involved laceration of functional tissue to implant the therapy. Obviously neither strategy is ideal, and an injectable alternative could alleviate the risks inherent to such invasive methods.

Furthermore, additional factors may limit the regenerative potential of nerve grafts, including that most strategies involve implantation of fresh nerve tissue. While using fresh tissue preserves beneficial Schwann cells, it also necessitates enduring immuno-suppression, not ideal for SCI patients who are already susceptible to infections and certain types of cancer (McKinley *et al.* 1999; Stonehill *et al.* 1996; Cardenas and Hooton 1995; Blam *et al.* 2003). Methods to remove immunogenic cellular components from nerve tissue for peripheral nerve repair have aided in overcoming issues associated with immunosuppression. These acellular nerve grafts retain the growth-supportive extracellular matrix but do not elicit deleterious immune responses. Our lab previously developed one such decellularization method that is now FDA approved for peripheral nerve repair and licensed by AxoGen Inc. (Hudson *et al.* 2004; Nagao *et al.* 2011). Implementing these optimized acellular nerve grafts in the CNS may provide a clinically-translatable option for regrowing spinal axons without the need to compromise the patients' immune systems.

It was shown that treatment of acellular nerve grafts with chondroitinase ABC (ChABC) to remove chondroitin sulfate proteoglycans enhances peripheral axon elongation into the grafts (Neubauer *et al.* 2007). Applying this to the CNS, unpublished research in our lab indicates that ChABC-treated acellular nerve grafts promote equivalent forelimb recovery to fresh nerve grafts as well as pre-degenerated grafts (previously subjected to clamp injury to activate the Schwann cells). These data suggest the nerve

ECM, opposed to the Schwann cells, may be the most influential component of these grafts for promoting CNS repair. Therefore, it is possible that an injectable formulation of acellular nerve ECM may provide the growth supportive benefits of fresh peripheral nerve grafts without immune complications and invasive methods of application. The remaining portion of this chapter will focus on the regenerative potential of the ECM in nerve and several organ systems and recent advances in making injectable hydrogels derived from acellular tissue. Considerations for characterizing and optimizing these materials to promote effective tissue regeneration are also discussed.

2.4. The Regenerative Potential of Acellular Tissue

The extracellular matrix or ECM is a fibrous, mesh-like network that surrounds and provides support to all cells in the body. It is a dynamic structure that is constantly being remodeled, and influences a wide array of cellular processes including cell differentiation (Z. L. Chen and Strickland 2003; Duan *et al.* 2011; Reilly and Engler 2010), cell migration (Chernousov *et al.* 2001; Agrawal *et al.* 2011; Petersen *et al.* 1992), and inflammation (Sorokin 2010; B. N. Brown *et al.* 2009), among others. As such, mimicking the ECM through engineered materials is of great interest in the fields of tissue engineering and regenerative medicine. The advent of decellularization methods to remove immunogenic cellular components from tissue and isolate beneficial ECM molecules has revolutionized these fields, providing a means to instill a level of complexity in materials otherwise unattainable. The complete regenerative potential of the ECM is only beginning to be characterized, but one concept is clear: harnessing the potential of the ECM may be the key to effectively directing tissue regeneration, including following SCI.

2.4.1. Properties and Impacts of the ECM

The ECM comprises structural proteins such as collagens and elastin, adhesion proteins like fibronectin and laminin, and glycosaminoglycans (GAGs) such as hyaluronic acid and chondroitin sulfate. Cells interact with these molecules via interactions between cell membrane receptors and extracellular ligands. The generated signals can then either directly modulate the cell cytoskeleton or can be transduced to the nucleus to influence gene expression (Stachowiak *et al.* 2014; Dupont *et al.* 2011). ECM factors that directly influence cells include ligand type and density (Frith *et al.* 2012; J. Lee *et al.* 2013), matrix mechanical properties (Flanagan *et al.* 2002; Gu *et al.* 2012; Engler *et al.* 2006), and surface topography (Fozdar *et al.* 2011; Fuhrmann *et al.* 2010). Recreating these parameters to mimic a target tissue may be important in developing new tissue engineering strategies.

Ligand Type and Density Tissue composition can also play an active role in directing cellular responses. For example, expression of fibronectin after peripheral nerve injury is associated with regeneration while expression of vitronectin results in non-regenerative outcomes (Previtali, S C.et al., Neurology 2008). It is unsurprising, then, that adhesive ligands such as those in nerve tissue (laminin, collagen) can bias MSC differentiation toward neurogenic outcomes, whereas adipogenic outcomes were observed in response to less adhesive molecules (J. Lee *et al.* 2013). Cell adhesion moieties are not necessarily required to mediate effects, however, since the presence of hyaluronic acid can enhance neurite growth in 3D collagen/laminin hydrogels (Deister et al., 2007) despite that neurons rarely express hyaluronic acid receptors beyond early developmental stages (Liu, Y. Dev Bio 2004). It is possible that an even more complex model system could reveal additional insight into these processes or further enhance outcomes.

Matrix Mechanical Properties The adult rat brain has a shear modulus near 200 Pa (Levental *et al.* 2007). Additionally, the compressive moduli for fetal and adult rat brain are approximately 2.5 and 5.5 kPa, respectively (Seidlits *et al.* 2010). In contrast, primate kidney has a compressive modulus of 150 kPa (Nakayama *et al.* 2010) while human spongy bone exhibits a compressive modulus of 88 MPa (Xiong *et al.* 2002). Modulating mechanical properties can affect cell behavior, including differentiation, migration, and morphology. Therefore, softer mechanics are expected to be more appropriate for neural applications. The optimal range of mechanical properties is often described experimentally to be near properties of the brain (Seidlits *et al.* 2010; Leipzig and Shoichet 2009; Man *et al.* 2011). Matching embryonic tissue may enable maximal neuronal differentiation, although Leipzig and Shoichet reported that matching adult brain is sufficient. Beyond properties of the adult brain, Leipzig and Shoichet also found neuronal differentiation decreased with increasing stiffness while oligodendrogenesis increased up to 10 kPa.

Mechanical properties can influence processes in adult neural cells, as well. Increasing substrate stiffness was shown to decrease Schwann cell survival, adhesion, proliferation, and migration (Gu *et al.* 2012). Furthermore, materials more closely mimicking the adult brain induce greater neurite growth compared to stiffer substrates (Leach *et al.* 2007; Man *et al.* 2011), and stiffer materials promote hypertrophy of astrocytes similar to the morphological changes that result after CNS injury (Moshayedi *et al.* 2010). These data collectively indicate not only that using soft materials is optimal, but the need to match specific developmental periods depends on the specific desired outcome.

2.4.2. The ECM in Neural Injury

The composition of the ECM is vastly different for peripheral nerve and spinal cord tissue, and this fact plays a major role in the tissue response to pathological states. In peripheral nerve, the main structural component is collagen I which surrounds linearly aligned channels of laminin and collagen IV. The composition of these channels promotes neurite growth and myelination (Deister *et al.* 2007; Podratz *et al.* 2001). Conversely, the ECM in the CNS is unique in that it is largely composed of proteoglycan and GAGs, particularly in regions around synapses known as perineuronal nets (Lau *et al.* 2013). In the mature CNS, these perineuronal nets are intended to prevent undesirable neurite sprouting and synaptic plasticity that could lead to inappropriate neural connections. The CNS also contains very little laminin restricted to the basement membrane of blood vessels (Risling *et al.* 1993). Myelin-derived inhibitors are another major ECM component. The peripheral nervous system contains one inhibitor, myelin associated glycoprotein (MAG), while the central nervous system contains three: MAG, oligodendrocyte myelin glycoprotein (OMGP) and neurite outgrowth inhibitor (Nogo) (Fitch and Silver 2008).

Consider the response following damage to the ECM when these myelin-derived inhibitors are dispersed throughout the neural injury site. In peripheral nerve, surviving laminin channels can guide regenerating axons back to their distal targets. Schwann cells become activated, migrate to span the lesion as part of a fibrin cable "bridge", and begin rebuilding the lost laminin structures (Fex Svennigsen and Dahlin 2013). These activated Schwann cells, as well as infiltrating macrophages/monocytes, also rapidly phagocytose and clear myelin inhibitor debris (Fex Svennigsen and Dahlin 2013). In contrast, damage to the CNS ECM results in spread of chondroitin sulfate proteoglycans and the three myelin

inhibitors throughout the injury site (Cafferty *et al.* 2010; Fitch and Silver 2008). Invading phagocytic cells unfortunately are unable to remove the multitude of extracellular inhibitors, which may actually downregulate phagocytosis by macrophages (Zeev-Brann *et al.* 1998). Although activated astrocytes upregulate laminin expression, they also markedly upregulate expression of inhibitory chondroitin sulfate proteoglycans that effectively dominate the cellular response (Liesi and Kauppila 2002).

Modifying the CNS ECM after injury is a promising approach to overcome matrix-mediated inhibition. The most widespread approach is using the bacterial enzyme chondroitinase ABC to digest local CSPG molecules. This enzyme can be introduced using either direct injection (Bradbury *et al.* 2002; Karimi-Abdolrezaee *et al.* 2010), transgenic cells (Kanno *et al.* 2014), or viral transduction of the host (Bartus *et al.* 2014). While this method increases the regenerative potential of injured axons, it can also increase aberrant sprouting of uninjured axons with potential off-target effects (Barritt *et al.* 2006). An alternative method is to block receptors for CSPG or myelin inhibitors on the cell surface of regenerating axons. Inhibitors to both NogoR and PTPσ receptors have been developed and confer significant benefits to regeneration (Cao *et al.* 2008; Lang *et al.* 2015). Achieving the full potential of receptor inhibition will require developing new paradigms for delivery that overcome the limitations of sustained intrathecal injection (risk of inflammation, infection, etc.).

Even with modification of the local milieu, the SCI lesion remains devoid of its own ECM to support effective regeneration. While synthetic materials can provide excellent control over physical and chemical properties, materials composed of native ECM better mimic the pre-injury tissue environment and provide endogenous cells with a

multitude of cues that are otherwise difficult to recreate. Decellularized tissue scaffolds therefore hold significant promise for repair after SCI. In this vain, it will be important to consider the differential effects of ECM from different tissue sources on regeneration, especially peripheral versus central nervous ECM.

2.4.3. Methods and Considerations for Tissue Decellularization

Several protocols have been developed to remove cells from tissue and preserve the ECM. Each method of decellularization is characterized by positive and negative attributes; hence, the optimal method often depends on the tissue type as well as the application. Decellularization methods must strike a balance between cellular removal and ECM preservation since these parameters are inversely related. Although the FDA does not currently list criteria for limiting remaining DNA content in acellular tissue, investigators typically focus on achieving high levels of DNA removal (>95%), therefore regretfully ignoring the importance of ECM preservation.

The animal source and decellularization method are important considerations in developing an acellular scaffold for tissue engineering. Ensuring compete removal of immunogenic material is crucial to avoid detrimental immune responses (B. N. Brown *et al.* 2009), particularly for xenotransplantation models (cross-species transplantation). For example, some species, such as porcine, carry α-galactose epitopes that must be removed for human transplantation or can result in eventual graft rejection (Gilbert 2012). Regardless of animal source, the effectiveness of decellularization as well as the effects on the structure and composition of the resulting acellular scaffold are major considerations for implementing acellular tissue grafts.

The majority of decellularization protocols start by lysing the cells, typically with a hypotonic solution such as water, to release intracellular proteins. Following cell lysis, these proteins can be removed from the tissue using a variety of methods, including alternating freeze/thaw cycles, detergents, acids and bases, hypertonic and hypotonic solutions, enzymatic digestion, or a combination of these. Gilbert et al present a more complete review of possible methods (Gilbert et al., Biomaterials 2006). Detergents are most commonly used to solubilize and facilitate removal of cellular proteins and nucleic acids. The electrostatic charge of a detergent molecule influences its ability to remove proteins, lipids, and nucleic acids, although this can differ based on the charge or hydrophobicity of the target molecule(s).

Non-ionic detergents disrupt lipid-lipid and protein-lipid interactions without disrupting protein-protein interactions. Therefore, non-ionic detergents are least likely to denature the extracellular matrix proteins. Using non-ionic detergents alone are often ineffective at removing cellular components in tissues, however (Faulk *et al.* 2014). Ionic detergents are effective at solubilizing both cellular proteins and nucleic acids but entail a higher risk for protein denaturation. Since many proteins carry an overall negative charge, anionic detergents are commonly used. In general, strongly anionic detergents such as sodium dodecyl sulfate (SDS) best remove cellular protein as well as DNA; however, they are similarly efficient at removing extracellular matrix proteins as well as denaturing the remaining matrix (Faulk *et al.* 2014). Zwitterionic detergents conduct functions similar to both non-ionic and ionic detergents given the presence of charged and uncharged domains. If chosen correctly, a zwitterionic detergent can serve to solubilize cellular proteins with minimal effects on protein denaturation.

Protocols employing anionic SDS account for a large percentage of current decellularization research. Similar methods have been used to prepare acellular heart (Ott *et al.* 2008), liver (Uygun *et al.* 2010; Shupe *et al.* 2010), lung (Ott *et al.* 2010; Nagao *et al.* 2013), brain and spinal cord (Guo *et al.* 2010; Medberry *et al.* 2013), as well as other tissue types. Many of these acellular constructs effectively support recellularization or improve regenerative outcomes in vivo. Unfortunately, the tissue structure was commonly disrupted according to histological analysis, and the composition of the ECM may also have been equally damaged (Faulk *et al.* 2014). This does not discount the potential for effective regeneration, but does limit it. The anionic detergent Triton X-200 is gentler on the ECM while still achieving effective cell removal. In combination with zwitterionic detergents sulfobetaine-10 and sulfobetaine-16, Triton X-200 was used to optimize decellularization of peripheral nerve tissue (Hudson *et al.* 2004). This method best preserved the microstructure of the basal lamina channels important for nerve regeneration versus other detergents, eliminated immunogenicity, and resulted in grafts that promoted significant functional recovery following nerve injury (Nagao *et al.* 2011). Given these results, this optimized method likely also achieves better preservation of the ECM composition.

Ultimately, the optimal method of decellularization will vary based on animal source and the type of tissue being used. Some tissues require very little processing while others necessitate much longer protocols. New information is constantly being garnered about the effects of different decellularization methods on tissues as well as this significance to cellular response. Currently, a large body of evidence demonstrates that acellular scaffolds have great potential to direct tissue repair, including in the CNS.

2.4.4. Acellular Tissue for CNS Repair

Acellular tissue has been used extensively to direct repair of peripheral organs, yet only recently has it been applied to treat CNS trauma. Several types of decellularized tissue scaffolds have been created for neural engineering, mostly focused on *in vitro* cell culture (DeQuach *et al.* 2011; Medberry *et al.* 2013; De Waele *et al.* 2015; Zhu *et al.* 2015). To date, three such scaffolds have been implemented *in vivo* based on decellularized spinal cord (J. Chen *et al.* 2014; J. Liu *et al.* 2013), peripheral nerve (C. Li *et al.* 2012), and skeletal muscle (J. Chen *et al.* 2014; Zhang *et al.* 2012). In the former study, decellularized spinal cord was first seeded with mesenchymal stem cells derived from umbilical cord blood and then implanted into a unilateral transection model of thoracic spinal cord injury. The authors found the acellular spinal cord fused with the host tissue, and oligodendrocytes were the primary cell type present after 8 weeks. The presence of oligodendrocytes may explain the observation of myelinated axons in these grafts. Furthermore, the authors found acellular spinal cord alone promoted recovery of hindlimb function, and adding mesenchymal stem cells further improved functional scores obtained via BBB testing.

Similar to studies using fresh peripheral nerve grafts, decellularized peripheral nerve has been evaluated to treat SCI (C. Li *et al.* 2012). In this study, acellular nerves were lyophilized to enable incorporation of BDNF into the scaffolds via rehydration. Growth-factor laden nerves were then implanted into a thoracic model of complete transection SCI. The nerve scaffold increased the number of neurons present in the lesion as well as decreased the latency and increased the amplitude of sensory evoked potentials in the hindlimb sensory cortices. Nonetheless, no hindlimb locomotor recovery was observed. These results are in contrast to an unpublished study conducted in our laboratory

in which using the acellular nerve graft as a "bridge" across the lesion demonstrated recovery of forelimb function. There are several potential sources for this discrepancy. 1) Our decellularization method may better preserve the nerve basal lamina channels such that the tissue provides enhanced guidance cues to regenerating axons. 2) The study above lyophilized the acellular nerve scaffold, potentially further damaging the channel architecture. 3) Using the nerve graft as a bridge across the lesion instead of implanting into the lesion can avoid detrimental effects from axon interactions with the glial scar, myelin-derived inhibitors, and inflammatory immune cells.

The final study employed a unique approach examining acellular skeletal muscle tissue to treat thoracic spinal cord hemisection injury (Zhang *et al.* 2012; J. Chen *et al.* 2014). The linear organization of the muscle fiber matrix guided axons into the lesion with increased axonal sprouting over the untreated control. The first study was terminated after 4 weeks without behavioral analysis, but the authors conducted a follow up study. The acellular skeletal muscle was evaluated as a blank scaffold as well as seeded with amniotic epithelial cells. This cell type has stem cell properties and potential to differentiate into neural cells (Miki *et al.* 2005). Both the blank and cell-seeded muscle scaffolds were shown to significantly improve hindlimb motor funtion after thoracic hemisection, with the cell-seeded scaffold achieving the best results.

Thinking outside of *en bloc* decellularized scaffolds, unique and innovative hybrid materials are also being developed based on acellular CNS tissue. For example, two studies have examined incorporation of powdered brain or cauda equina ECM into electrospun fibers (Baiguera *et al.* 2014; Wen *et al.* 2015). This technique combines the benefits of natural ECM with controllable fiber production and enables generation of aligned

composite fibers to direct and enhance neurite growth *in vitro* (Wen *et al*. 2015). Future studies will demonstrate if this method is effective at promoting neural recovery *in vivo*.

The above acellular tissue strategies focus on preformed scaffolds, which again require less clinically-relevant transection or hemisection models of SCI. Recently, it has been recognized that not all injury paradigms are compatible with preformed materials. This realization motivated the study towards methods to create injectable acellular tissue scaffolds. Derived using the same decellularization processes, these injectable tissue scaffolds enable tissue engineers to harness the regenerative potential of the ECM for both injury models requiring less invasive methods of scaffold implantation as well as new and innovative cell culture systems.

2.5. INJECTABLE ACELLULAR TISSUE: TRENDS IN REGENERATIVE MEDICINE

Freytes et al. were the first to describe a method to create injectable scaffolds derived from decellularized urinary bladder tissue (Freytes DO et al., Biomaterials 2008). Since this report, injectable ECM materials have been described for a vast and continually expanding array of tissues, including but not limited to heart, skeletal muscle, cartilage, kidney, brain, spinal cord, and bone (Duan *et al.* 2011; Kwon *et al.* 2013; Medberry *et al.* 2013; O'Neill *et al.* 2013; Sawkins *et al.* 2013; Seif-Naraghi *et al.* 2012; DeQuach *et al.* 2012). The process to create these ECM hydrogels has remained largely the same, with only small variations. Briefly, the acellular tissue is micronized either by hand or a tissue mill and is then digested in an acidic solution of pepsin. The enzyme pepsin is natively found in the stomach where it assists in digestion of organic matter by cleaving proteins between hydrophobic and aromatic residues (Powers *et al.* 1977). This fairly non-specific

cleavage pattern enables pepsin to break down many proteins, including those in the ECM. The extent and rate of ECM digestion can be controlled through parameters such as digestion duration, concentration, temperature, and method of agitation. Optimizing these parameters allowed Freytes et al. and their predecessors to realize a solution of ECM that undergoes thermal gelation at physiological conditions, creating a tissue-based hydrogel. Moreover, neutralizing the pH of the pre-hydrogel solution inactivates the enzyme, negating the need for costly and time-consuming separation processes.

Injectable ECM has been used as a pre-gel solution as well as a hydrogel with promising results. The pre-gel solution can be added to cell culture media or used to produce coated tissue culture substrates that better match the physiological environment. Adding digested, acellular brain or spinal cord to the media over neural stem cells significantly increased neuronal differentiation over both a negative control and cells receiving non-CNS-derived ECM (Crapo et al., Tissue Eng A 2014). Furthermore, plating neurons derived from induced pluripotent cells exhibited an increased number of primary and secondary dendrites on brain ECM coated substrates versus Matrigel controls. Using hydrogels of digested ECM have demonstrated similarly positive effects. For example, hybrid gels of collagen I and cardiac ECM were used to culture human embryonic stem cells in 3D with and without a defined growth factor regimen (Duan *et al.* 2011). The gels effectively directed the stem cells toward a cardiac lineage, with substrates containing 75% ECM (the highest tested) achieving the most cardiomyocytes, without the need for growth factor treatment. Clearly, physiologically-relevant ECM matrices improve upon previous *in vitro* cell culture methods, and similar benefits have been demonstrated *in vivo*.

It has been discovered that pepsin digestion of the ECM exposes a cryptic peptide in collagen III that promotes recruitment of several cell types *in vitro*, including progenitor cells and immune cells. These results also have been confirmed in animal models. Catheter delivery of a cardiac ECM hydrogel promoted cellular recruitment in small and large animal models of myocardial infarction, increasing cardiac muscle and improving left ventricular function (Singelyn JM et al., J Am Coll Cardiol. 2012 or 2013; Seif-Naraghi SB et al., Sci Transl 2014; Wang RM & Christman KL, Advanced Drug Delivery Reviews 2015). Furthermore, injectable skeletal muscle increased infiltration of muscle progenitors and proliferating muscle cells in a rat model of hindlimb ischemia (DeQuach JA et al., Eur Cell Mater 2012 or 2013). These recruited cells aided in restoring muscle mass and promoting neovascularization. Recruitment of progenitor cells is not the explanation for these benefits, however.

Macrophage phenotype can predict whether a biological scaffold will promote regeneration or result in chronic inflammation (Badylak *et al.* 2008; B. N. Brown *et al.* 2012). It has been shown that digested ECM effectively directs macrophages away from pro-inflammatory, M1 phenotypes and toward pro-regeneration, M2 phenotypes *in vitro* (Sicari *et al.* 2014). This biasing affect was also demonstrated *in vivo* by comparing uncoated and ECM-coated polypropylene meshes. The ECM coating significantly increased the M2 to M1 ratio over the uncoated controls and minimized the foreign body response typical of this material (Wolf MT et al., Biomaterials 2014). Currently, no study has examined the effects of ECM hydrogel injection into the spinal cord on immune cell phenotype after injury.

As with structured acellular scaffolds, implementation of ECM hydrogels to treat CNS trauma has been explored less than in other tissues. One such material has been evaluated *in vivo* thus far: A solubilized, injectable version of acellular urinary bladder matrix was assessed in combination with neural progenitor cells to limit neurological deficits following traumatic brain injury and stroke (Wang *et al.* 2013; Bible *et al.* 2012). Both studies demonstrated that this injectable scaffolds based on bladder ECM can improve neurological and functional outcomes. Nonetheless, this urinary bladder matrix was previously found to underperform CNS-derived ECM in promoting neurite growth and neuronal differentiation of stem cells (Crapo *et al.* 2014). Using injectable ECM derived from neural tissue may, therefore, provide additional or enhanced neurological benefits.

In looking to develop a new intervention for clinical translation, the most efficient pathway is to build off of an existing market product. Based on a technology developed in our laboratory, acellular human nerves have been used in many patients to enhance peripheral nerve regeneration. Recent experiments also from our laboratory show that acellular nerve grafts promote functional recovery after SCI equivalent to fresh nerve grafts and therefore may provide a clinical option for SCI patients. An "off the shelf" product would negate the need for a second surgery normally used to obtain a nerve biopsy. Additionally, since structured nerve grafts require tissue resection for implantation, an injectable form of acellular nerve would further reduce the invasiveness of the surgical procedure. The objectives of this dissertation are to 1) develop and characterize an injectable, thermally gelling nerve scaffold, 2) determine the therapeutic baseline of injectable nerve application after SCI, and 3) evaluate the injectable nerve scaffold to support Schwann cell transplantation and promote recovery following SCI.

2.6. SPECIFIC AIMS

2.6.1. Specific Aim 1: Develop and Characterize an Injectable Acellular Nerve Graft

- Optimize a process to achieve injectable, thermally gelling acellular nerve
- Determine the scaffold composition and compare to native nerve tissue
- Characterize the mechanical properties of injectable nerve hydrogels
- Assess biocompatibility of injectable nerve with Schwann cells in vitro
- Examine material effects on macrophage polarization acutely after application

Rationale: Fresh and acellular nerve grafts have shown great potential to promote spinal axon regeneration and functional recovery after SCI, in part because of the growth-supportive ECM. Since these structured nerve grafts require invasive application methods, an injectable scaffold based on nerve ECM would provide a more clinically-relevant therapeutic option. This scaffold should have mechanical properties in range of neural tissue to achieve its maximum potential. Biomaterials need to be compatible with cells and tissues to provide a therapeutic benefit. Therefore, the biocompatibility of injectable nerve will be evaluated *in vitro* using Schwann cell culture and *in vivo* acutely after application to the injured spinal cord based on immune cell infiltration and polarization.

2.6.2. Specific Aim 2: Determine the Therapeutic Baseline of Injectable Nerve in a Rat Model of Cervical Contusion SCI

- Assess histological outcomes 8 weeks after application of injectable nerve
- Evaluate the effects of injectable nerve application on forelimb recovery following cervical spinal cord injury

- In collaboration with Dr. David Fuller, also examine the effects of injectable nerve application on respiratory recovery using phrenic nerve recordings

Rationale: In developing a material platform for combination SCI therapies, it is important to determine the influence of the material alone on functional and histological recovery. This analysis defines the therapeutic baseline and potential for supplementation by other therapeutics. Limb paralysis is the most evident deficit following SCI, although respiratory complications are the leading cause of death for SCI patients. Functional outcome measures for both forelimb and respiratory recovery will be used to evaluate the therapeutic baseline of injectable nerve, as well as various histological measures.

2.6.3. Specific Aim 3: Assess Injectable Nerve as a Clinically-Viable Alternative to Matrigel for Schwann Cell Therapy in a Rat Model of Thoracic Contusion SCI

- In collaboration with Dr. Mary Bunge, examine injectable nerve for supporting Schwann cell transplantation and promoting recovery following SCI
- Compare functional and histological results of Schwann cell therapy using injectable nerve versus Matrigel matrices

Rationale: Schwann cell therapy holds significant promise to treat SCI, yet effective cell survival requires supplementation with a supportive matrix. Commercial Matrigel is currently the best option for enhancing cell survival and transplantation efficacy; however, Matrigel will likely not be translated to the clinic because of its origins as a tumor cell matrix. Since acellular nerve grafts are currently used clinically, this injectable acellular nerve graft will be examined as a clinically-viable alternative to Matrigel for enhancing Schwann cell transplantation after thoracic contusion SCI.

Chapter 3: Injectable Extracellular Matrix Hydrogels of Optimized Acellular Nerve for Treating Spinal Cord Injury

3.1. INTRODUCTION

Following contusion SCI, an inflammatory cavity develops that inhibits tissue repair and functional recovery. Peripheral nerve grafts, both fresh and acellular, have shown particular promise to bridge this cavity and provide a substrate for spinal axon regeneration; yet, they also require resection of the spinal cord, potentially inducing additional tissue damage. This chapter details development and characterization of a novel injectable scaffold derived from acellular nerve suited for minimally-invasive application following contusion SCI. This material was examined for the ability to 1) mimic the composition of native nerve extracellular matrix (ECM), 2) achieve mechanical properties of rat neural tissue, 3) support cell attachment and survival *in vitro*, and 4) influence the immune response acutely after *in vivo* application. Collectively, these analyses reveal implications of the material's therapeutic potential to promote tissue repair and functional recovery following debilitating neural injury.

3.2. MATERIALS AND METHODS

3.2.1. Tissue Harvest and Decellularization

Sciatic nerves were aseptically harvested from adult Sprague Dawley rats, separated from the epineurium, and decellularized according to the optimized acellular method previously developed in the Schmidt lab (Hudson *et al.* 2004). The procedure is outlined in **Table 3.1**. Briefly, sciatic nerves were individually transferred to 15 mL

Table 3.1: Overview of nerve decellularization process prior to lyophilization.

	Solution composition	Duration	Purpose
1.	Sterile water	7 hours	Lyse cells
2.	125 mM sulfobetaine 10	18 hours	Wash out cell debris
3.	100 mM Na / 50 mM PO_4	1 x 15 minutes	Remove detergents
4.	0.14% Triton X-200 and 0.6 mM sulfobetaine 16	24 hours	Wash out cell debris
5.	100 mM Na / 50 mM PO_4	3 x 15 minutes	Remove detergents
6.	125 mM sulfobetaine 10	7 hours	Wash out cell debris
7.	100 mM Na / 50 mM PO_4	1 x 15 minutes	Remove detergents
8.	0.14% Triton X-200 and 0.6 mM sulfobetaine 16	18 hours	Wash out cell debris
9.	50 mM Na / 10 mM PO_4	3 x 15 minutes	Remove detergents
10.	0.02 U/mL chondroitinase ABC	16 hours	Cleave inhibitory CSPG
11.	10 mM phosphate buffer	3 x 3 hours	Wash out CSPG fragments
12.	Sterile water	3 x 15 minutes	Remove salts before drying

conical tubes filled with sterile ddH_2O to lyse the cells. After 7 hours, the water was aspirated and replaced with a detergent solution of 125 mM sulfobetaine-10 (SB-10) in phosphate-buffered 50 mM saline for 18 hours. The tissue was then transferred to a buffered solution of 0.6 mM sulfobetaine-16 (SB-16) and 0.14% Triton X-200 for 24 hours. Following rinsing in 100 mM sodium/50 mM phosphate buffer 3x15 minutes, the detergent cycle was repeated with shorter durations (7 and 18 hours for SB-10 and SB-16/Triton, respectively). The tissue was then rinsed in a 50 mM sodium/10 mM phosphate buffered solution 3x15 minutes to remove residual detergents. All processing was performed under sterile conditions at room temperature on a vertical agitator set to 14 rpm.

Peripheral nerve tissue contains chondroitin sulfate proteoglycans (CSPGs) that inhibit axonal extension (Neubauer *et al.* 2007). Therefore, acellular nerves were treated with 200 μL of 0.02 U/mL chondroitinase ABC (Sigma) for 16 hours at 37°C to remove inhibitory CSPGs. The tissue was then washed thrice in sterile 1X phosphate buffered saline (PBS) for 3x3 hours, thrice in sterile ddH_2O for 3x15 minutes, flash frozen, and lyophilized prior to storage at -20°C.

3.2.2. Developing a Protocol for Injectable, Thermally Gelling Acellular Nerve

Several methods to solubilize nerve tissue were explored, including using a tissue grinder, using a probe sonicator, grinding with a mortar and pestle, and finally manually dicing the tissue followed by digestion in pepsin. Only pepsin digestion was able to solubilize the tissue, so digestion parameters were optimized to produce a homogeneous solution that thermally gelled at 37°C. Based on previously published protocols (Medberry *et al.* 2013; DeQuach *et al.* 2012; DeQuach *et al.* 2011; Seif-Naraghi *et al.* 2010; Freytes

et al. 2008), the following parameters were examined to achieve a homogeneous solution and subsequent hydrogel formation at 37°C: tissue and enzyme concentration, reaction duration and temperature, and method of agitation. At the end of the digestion, the enzyme was inactivated by neutralizing the pH to 7.4 using 1 M NaOH and 10X PBS. To test gel formation, 30 uL of each solution was incubated in a humidified incubator at 37°C for 30-45 minutes. Saline solution was then added to examine the ability of the final product to hold its shape. A schematic representation is shown in **Figure 3.1**.

3.2.3. Protein Identification

The effect of decellularization on nerve tissue protein content was examined using tandem high performance liquid chromatography-mass spectrometry (LC-MS/MS). Samples of fresh and acellular nerve were digested at 10 mg ECM/mL in 0.25% trypsin-ethylene diaminetetraacetic acid (EDTA) for 24 hours at 37°C. Because trypsin is known to specifically cleave proteins on the C-terminal side of arginine and lysine residues, the protein content can be determined by comparing molecular weights of the resulting protein fragments to an existing fragment library. Following digestion, protein concentrations were estimated based on absorbance at 280 nm, and 20 μL of sample at 1 μg protein/μL was submitted to the Proteomics Facility at the University of Florida's Interdisciplinary Center for Biotechnology Research for LC-MS/MS. Results were reported in units of spectral abundance, with proteins in highest abundance being identified first. This reporting method enables intra-sample comparisons to determine relative protein abundance in individual samples but is incompatible with performing inter-sample comparisons.

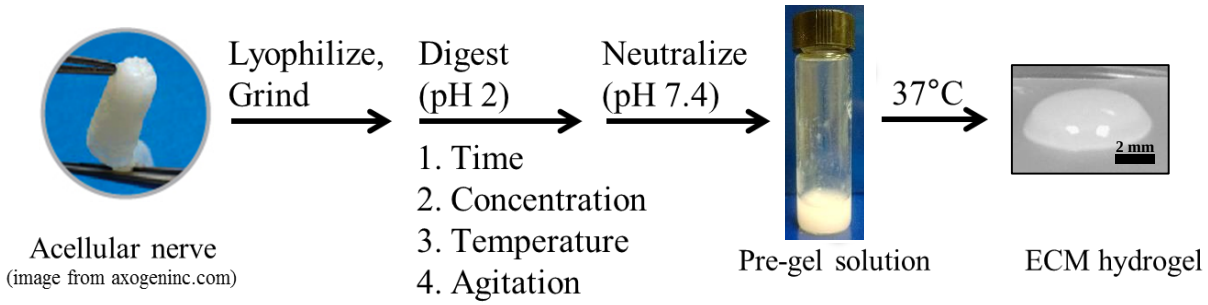

Figure 3.1: Schematic of proposed method to achieve an injectable, thermally gelling nerve hydrogel using pepsin digestion. The variables used to optimize the digestion are listed below the arrow.

3.2.4. Collagen and Glycosaminoglycan Quantification

The collagen and sulfated glycosaminoglycan (sGAG) content of acellular nerve were determined using Sircol and Blyscan assay kits, respectively, (Biocolor Ltd, UK) performed according to manufacturer's instructions. For the collagen assay, nerve tissue was digested at 20 mg/mL in 1 mg/mL pepsin for 64 hours at room temperature, and for the sGAG assay, tissue was digested at 20 mg/mL in a solution of 0.1 mg/mL papain (Sigma) (containing 0.2 M monobasic sodium phosphate, 0.1 M sodium acetate, 5 μM EDTA, and 5 μM cysteine) for 18 hours at 65°C. sGAG content was measured both before and after chondrointinase ABC treatment to determine the effects of enzyme treatment. All data were normalized to the initial dry weight of the tissue and are represented in units of mg/mg (n = 11 in duplicate for collagen content, and n=5 in duplicate for sGAG content). Additionally, since peripheral nerve tissue is linear, tissues from age- and sex-matched animals were also normalized to tissue length to account for mass changes during decellularization that may skew the results. These data are represented in units of μg/mm (n = 5 in duplicate or triplicate for both assays).

3.2.5. Turbidity Gelation Kinetics

The gelation kinetics of injectable nerve solution was assessed by incubating 100 μL of cold nerve solution to the well of an ice-cold 96-well plate. The plate was immediately transferred from ice to a Biotek Synergy HT spectrophotometer preheated to 37°C. Absorbance at 405 nm was measured every 2 minutes for 30 minutes to detect protein aggregation or crosslinking. Normalized absorbance was calculated according to Equation 1 (Medberry *et al.* 2013) and used to determine the lag time of gelation, t_{lag}; the

slope of gelation, s; and the time to achieve 50% and 95% maximum absorbance, $t_{1/2}$ and t_{95}, respectively. The analysis was repeated three times in duplicate.

$$\text{Normalized Absorbance} = \frac{A - A_0}{A_{max} - A_0} \quad (1)$$

3.2.6. Scanning Electron Microscopy

Scanning election microscopy was used to examine the surface topography of nerve hydrogels. Injectable nerve solution was incubated at 37°C for 15 minutes for thermal gelation. Hydrogels were fixed in 4% paraformaldehyde (PFA) for 10 minutes, washed briefly in ddH_2O to eliminate salts, and dehydrated onto glass slides using the following graded solutions: 15 minutes each in 30, 50, 70, 85, 90, 95, and 100% ethanol and 30 minutes each in 25, 50, 75, 100% hexamethyldisilazane (Sigma). After dehydration, a second volume of 100% HMDS was added, and the samples were left to dry overnight in a fume hood. For comparison, 10 μm thick longitudinal cryosections of fresh nerve were fixed in 4% paraformaldehyde for 10 minutes and similarly dehydrated. Conductive tape (Electron Microscopy Sciences) was applied to establish an electrical connection between the metal chuck and the dehydrated hydrogel sample. Mounted samples were then sputter coated with 10 nm of Au/Pd and imaged on a field emission gun scanning electron microscope (FEI).

3.2.7. Mechanical Characterization

Compressive and shear testing were performed to examine the mechanical properties of nerve hydrogels for comparison to native rat neural tissue. Nerve hydrogels at 16.5, 13, and 9.5 mg/mL were molded to a defined geometry using 8 mm cylindrical

silicon molds (Grace Biolabs) by incubation at 37°C for 15 minutes. The compressive modulus of the hydrogels at each concentration was measured using an Instron 5542 (Instron Corp). Samples were compressed at a rate of 0.1 mm*sec^{-1} until 60% extension (Seidlits *et al.* 2010). The slope of the linear region (within the first 20% of strain) for the resulting stress-stain curve was calculated and represents the compressive modulus. Additionally, the material's viscoelastic properties were examined using an Anton Paar MCR 302 rheometer with parallel plate geometry according to established methods (Johnson *et al.* 2011; Zuidema *et al.* 2014). A sandblasted, 8 mm top load cell was used to decrease slipping during testing. To mimic physiological conditions, the Peltier plate was pre-heated to 37°C and the samples were enclosed by a humidity chamber. Amplitude sweeps from 0.01% to 100% were first conducted at 6 rad/s to determine the linear viscoelastic (LVE) range. The storage (G') and loss (G") moduli were then determined using frequency sweeps from 0.1 Hz to 100 Hz at a strain value in the middle of the LVE, chosen as 0.5% for all concentrations.

3.2.8. In Vitro Schwann cell Culture and Live/Dead Assessment

Schwann cells were cultured on substrates coated with injectable nerve solution to ensure no cytotoxic degradation products were generated during pepsin digestion and that the presence of denatured pepsin did not affect cell attachment or survival. The surface of glass coverslips was etched in nitric acid for 3 days to increase surface area for protein adsorption, washed in ddH_2O 3x2 hours, and autoclaved. Etched coverslips were coated with a 20 µg/mL solution of poly-D-lysine (PDL; Fisher ICN15017510) overnight at room temperature, washed with ddH_2O, and allowed to dry in

the sterile hood. A solution of 1 mg/mL injectable nerve solution was then used to coat the coverslips for 1 hour at 37°C. The final coated coverslips were again washed in ddH_2O and allowed to dry. Neonatal rat Schwann cells (passage number 2; Sciencell, Carlsbad, CA) were plated onto glass PDL or PDL-injectable nerve coated coverslips in 70 µL at 30,000 cells per coverslip (approximately 27,000 cells/cm^2). The cells were allowed to adhere for 20 minutes at 37°C, and then the wells were flushed with 430 µL of 3:1 DMEM:F12 medium (both from Invitrogen) containing 1% penicillin-streptomycin, 2% N2 neural supplement (Invitrogen), 5 µM forskolin (Sigma), and 50 ng/mL neuregulin (R&D Systems).

A live/dead assay was performed after 3 days in culture by incubating the cells in media containing 2 µM calcein AM and 4 µM ethidium homodimer for 30 mins at 37°C to label all cells and dead cells, respectively. The media was subsequently replaced with fresh media, and fluorescent images were obtained at 10X magnification using an Olympus IX70 with DP80 dual color digital camera and CellSens software. The number of total cells and dead cells was counted using the "Analyze Particles" function in ImageJ (NIH). For live cell images, individual cells were discriminated using the standard Watershed function in binary mode prior to analysis. Cell numbers were averaged for three frames in each sample (n=5 samples for each group, and the experiment was repeated three times).

3.2.9. Initial in vivo Assessment – Cervical Contusion Spinal Cord Injury

The initial immune response to nerve hydrogel implantation was assessed using a clinically-relevant model of unilateral, cervical contusion spinal cord injury in adult rats. All procedures involving animals were approved by the Institutional Animal Care and

Use Committee (IACUC) at the University of Florida. Briefly, Sprague Dawley rats (Charles River) weighing 250-300 g were anesthetized using isoflurane (3% to induce, 2% to maintain). Following incision into the skin and muscle layers, the spinal cord was exposed by performing a laminectomy at the third and fourth cervical vertebrae (C3/4). A unilateral contusion between C3 and C4 was applied using an Infinite Horizon impactor equipped with a 2.5 mm impactor tip at a set force of 200 kDynes. Only animals receiving impacts within 10% of the desired force were included in the study. A small piece of adipose tissue was placed over the spinal cord to prevent unwanted adhesions. The muscle layers and skin were then closed using resorbable 5-0 Vicryl suture and monofilament 5-0 nylon sutures, respectively, and buprenorphine (0.03 mg/kg; Patterson Veterinary) was given subcutaneously for three days for pain management. This injury affects a single forelimb and therefore should not significantly hamper the animals' ability to ambulate. Nonetheless, animals were monitored for excessive deficits (bilateral opposed to unilateral injury) as well as the ability to access food and water three times a day for the first three days after surgery, then twice a day until material injection, after which postoperative care procedures were repeated.

3.2.10. Lesion Volume Determination

The lesion volume specific to this particular injury model was first determined to approximate the volume of material/solution required for injection. Similarly, lesion volume was calculated one week following material injection to assess the acute effects of material injection. For the initial assessment, a spinal cord injury was induced at C3/4 as described above (n = 5). The animals were transcardially perfused one

week later with 200 mL of 1X PBS followed by 200 mL of 4% PFA. The spinal columns were harvested and post-fixed overnight in 4% PFA before being transferred to 30% sucrose for cryopreservation. Cryopreserved spinal cords were equilibrated in Optimal Cutting Temperature (OCT; Tissue Tek) medium overnight and frozen in blocks on dry ice. Spinal cord cross-sections were obtained at 12 μm using a Leica CM1950 cryostat and adhered to gelatin coated slides on a slide warmer at 45°C.

The Cavalieri method for quantifying biological volumes was then used to approximate the lesion volume (West 2012). This method uses a sampling of tissue sections with known and equidistant spacing to estimate the total volume. Briefly, every tenth slide containing six sections at 120 μm apart was stained with Harris hematoxylin & eosin (H&E) or Luxol Fast Blue to discriminate healthy and injured tissue. A grid of equally spaced points with known dimensions (based on image magnification) was randomly overlaid onto stained images. The third and sixth section of every tenth slide was used to obtain 20 data points for each tissue. As few as 10-12 sections are required to accurately approximate biological volumes using this method (Jakeman 2012). The number of points occurring in injured tissue for each section was used to calculate the total lesion volume based on $V = T * \frac{a}{p} * \sum P$, where **T** is the section thickness, **a** is the area of the overlaid grid based on the image scale, **p** is the number of points in the grid, and $\sum \boldsymbol{P}$ is the total number of points counted in the lesion. Refer to **Figure 3.9** for a graphical depiction.

3.2.11. Material Injection following SCI

One week after injury, the spinal cord was re-exposed and 6 μL of either 1X PBS or injectable nerve solution was injected into the lesion over 6 minutes using a 34

gauge needle on a Nanofil syringe mounted to an UltraMicroPump3 microinjection system (World Precision Instruments). Following injection, the needle was left in place for 2 minutes then slowly retracted to prevent overflow from the lesion. Six animals were included in each injection group. Administration of buprenorphine was repeated and supplemented with three days of meloxicam (1 mg/kg; Norbrook). Gentamicin (4 mg/kg; Patterson Veterinary) was also given subcutaneously for five days starting the day prior to the injection surgery to minimize the risk of infection. One week after injection (two weeks post-injury), animals were transcardially perfused with 1X PBS and 4% paraformaldehyde. Spinal columns were isolated and post-fixed in paraformaldehyde overnight before being transferred to 30% sucrose for cryopreservation.

3.2.12. Immunohistochemistry and Digital Image Analysis

Cryopreserved spinal cords were prepared for cryosectioning as stated above. The tissue was assessed for total macrophage infiltration and macrophage polarization toward either an M1, pro-inflammatory phenotype or an M2, pro-regenerative phenotype using antibodies against ED1 (Abd Serotec MCA341R, 1:200), CCR7 (Abd Serotec, 1:200), and CD206 (Abcam ab64693, 1:200), respectively. Tissue sections were incubated with blocking buffer containing 3% goat serum and 0.3% Triton X100 for 1 hour at room temperature. Following blocking, primary antibody solutions in blocking buffer were added and incubated overnight at 4°C. Samples were then washed 3x10 minutes with 1X PBS, and secondary antibodies in blocking buffer were added for 1 hour in the dark at room temperature. The PBS washes with were repeated, and DAPI was added (1:1000 in water) for 5 minutes in the dark to label cell nuclei. Stained samples were then mounted

with Fluoromount-G (SouthernBiotech) and coverslipped for imaging. Images were obtained using a Zeiss Axio Imager.Z2 and Zen software. Immune cell number was quantified using Zen image analysis software (Zeiss). Image threshold criteria can be found in the appendix. Each antibody was assessed on twelve sections, six distal and six proximal positions, approximately 120 μm apart.

3.2.13. Statistics

One-way analysis of variance (ANOVA) on GraphPad Prism software was used to identify statistical differences within multiple groups for collagen and glycosaminoglycan analysis, rheological measurements, compressive testing, and biocompatibility studies. A student's t-test was then used to determine significance between the individual groups.

3.3. RESULTS

3.3.1. Optimized ECM Hydrogel Preparation

Achieving a homogenous solution of acellular nerve capable of thermal gelation under physiological conditions required enzymatic digestion with pepsin. A matrix study to optimize this procedure revealed that constant agitation and room temperature conditions during gelation were required to achieve gelation. Results for the digestion concentration and duration analyses are summarized in

Table 3.2 below. The following process achieves maximum homogeneity and thermal gelation: Dried acellular nerve was weighed and then comminuted into 1-2 mm segments using microscissors. The tissue pieces were digested at room temperature with constant stirring and a concentration of 20 mg ECM/mL in a solution of 1 mg/mL porcine pepsin (Sigma) and 0.01 M HCl.

Table 3.2: Determining optimal parameters for pepsin digestion. Small check marks indicate solutions that achieved gelation, but the resulting gels dissociated with gentle agitation in medium. Digestion for 64 hours produced the most robust, easy to handle gels and therefore this reaction duration was used for all future material preparation.

Digestion duration →	**30 hr**		**36 hr**		**48 hr**		**64 hr**	
Tissue concentration ↓	*Stays in solution*	*Gels*	*Stays in solution*	*Gels*	*Stays in solution*	*Gels*	*Stays in solution*	*Gels*
10 mg/mL	✘	✘	✓	✘	✓	✓	✓	✓
20 mg/mL	-	-	-	-	✓	✓	✓	✓

After 62-64 hours, the enzyme was deactivated by raising the pH to 7.4 using sterile 1 M NaOH ($1/100^{th}$ original volume) and sterile 10X PBS (to 1X final dilution). Nerve solution was diluted to the desired concentration using 1X PBS for *in vitro* material characterization or *in vivo* implantation, as described below.

3.3.2. Compositional Characterization

Using high performance liquid chromatography in tandem with mass spectrometry, multiple ECM proteins were identified in both fresh and acellular nerve samples. The results are summarized in **Table 3.3**. The α1 and α2 subunits of collagen type I were the most abundant ECM proteins in both tissues, comprising 30.8% each of fresh nerve and 27.5% and 20.2% of acellular nerve, respectively. Collagen I is primarily a structural protein with cell adhesive properties and should provide molecular structure to an injectable nerve scaffold. It is unclear if having differential percentages of α1 and α2 will affect this property. Laminin was the next most abundant protein, with the α2 subunit making up 23.1% and 9.2% of fresh and acellular tissues. Laminin also contains cell adhesive peptides and is known to promote and enhance neurite growth (Deister *et al.* 2007). Furthermore, the γ1 subunit of laminin is critical for induction of Schwann cell myelination (Z. L. Chen and Strickland 2003). The remaining ECM spectra was attributed to fibrillin-1, which provides elasticity to connective tissue. Fresh and acellular nerve samples surely contain additional proteins, however the proteins are identified based on abundance in the sample, so the presence of innate or residual cellular proteins may overshadow less abundant ECM proteins.

For a more quantitative assessment, we also examined the total collagen and glycosaminoglycan content of fresh and acellular nerve tissue using Sircol and Blyscan assays (Biocolor Ltd, UK), respectively. Collagen content for fresh and acellular nerves is reported in **Figure 3.2** normalized to both tissue mass and length. Normalized to mass, the collagen content of fresh and acellular nerves was significantly different at 8.90% and 23.7% collagen, respectively ($n=11$, $p<0.0001$). An apparent increase in percent collagen after decellularization may be an artifact of removing cellular proteins that skew mass normalization. Since nerve tissue is linear, collagen content was also normalized to tissue length for age and sex matched animals yielding 27.2 and 15.3 μg/mm for fresh and acellular nerve ($n=5$, $p=0.07$), respectively. These data are not statistically different regardless of normalization method, indicating that decellularization does not significantly alter total nerve collagen content.

The presence of glycosaminoglycans (GAGs) can increase localization and bioavailability of growth factors upon implantation (Colin *et al.* 1999; Jiao *et al.* 2007). As shown in **Figure 3.3**, fresh and acellular nerves contain 250 and 87 ng GAG/mm, respectively, indicating a significant reduction in sulfated GAG content following decellularization ($p=0.01$). Certain GAGs such as CSPGs are proven inhibitors of neurite growth and therefore should be removed from tissue-based scaffolds to enable maximum neural regeneration. Therefore, acellular nerves are treated with the enzyme chondroitinase ABC (ChABC) prior to solubilization to remove inhibitory chondroitin sulfate proteoglycans. Following this treatment, nerve tissue retained 40 ng GAG/mm, which is also significantly different from fresh nerves as well as untreated acellular nerves ($p=0.01$).

Table 3.3: Extracellular matrix proteins and their spectral abundance in nerve tissue as determined using tandem chromatography-mass spectrometry.

Protein	Spectrum Counts (% of ECM)	
	Fresh	*Acellular*
Collagen type I (α 1)	30.8	27.5
Collagen type I (α 2)	30.8	20.2
Collagen type VI (α 3)		5.5
Collagen type IV (α 2)		5.5
Total collagen	***61.6***	***58.7***
Laminin subunit (α 2)	23.1	9.2
Laminin subunit (β 2)	7.7	8.3
Laminin subunit (γ 1)	7.7	8.3
Total laminin	***38.5***	***25.7***
Fibrillin-1		15.6

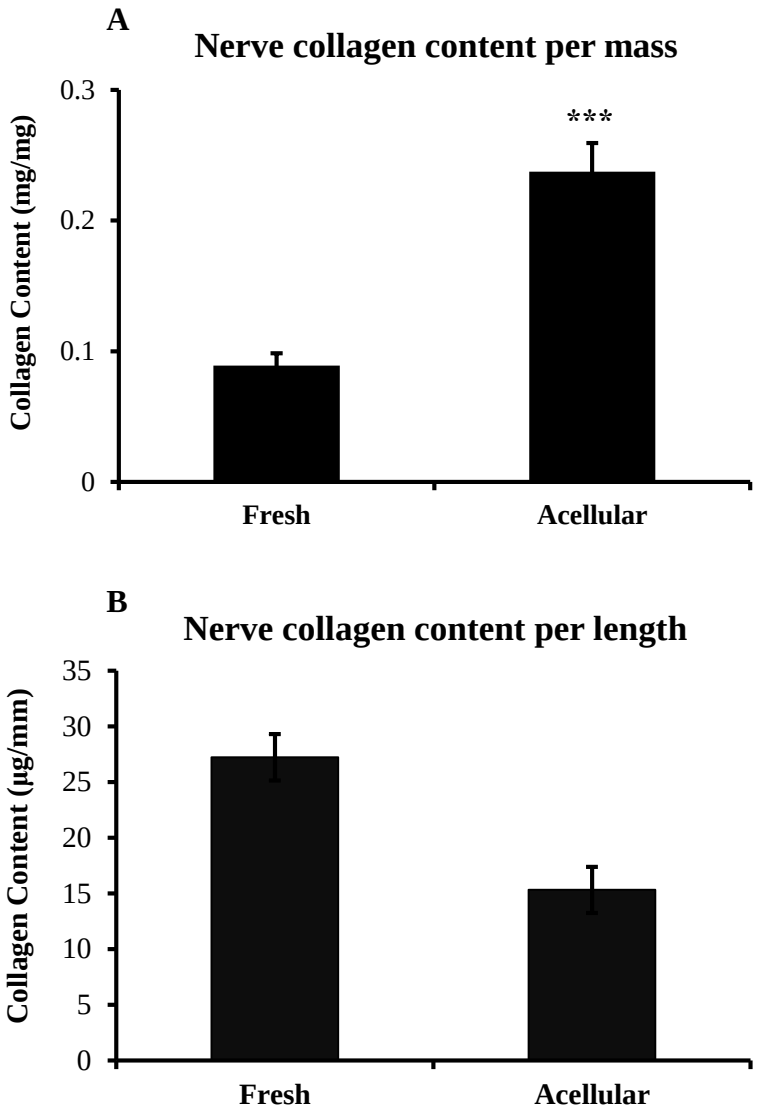

Figure 3.2: Optimized decellularization of peripheral nerve does not significantly alter total collagen content. Collagen content was determined using a Sircol assay and normalized to tissue mass (n=11) and length (n=5). Normalizing to mass shows a statistically significant increase in collagen content after decellularization ($p<0.0001$), potentially as a result of cell protein loss. Normalizing to mass reveals a more intuitive trend, with decellularization preserving 56% of total collagen content. No statistically difference was found in B ($p = 0.07$).

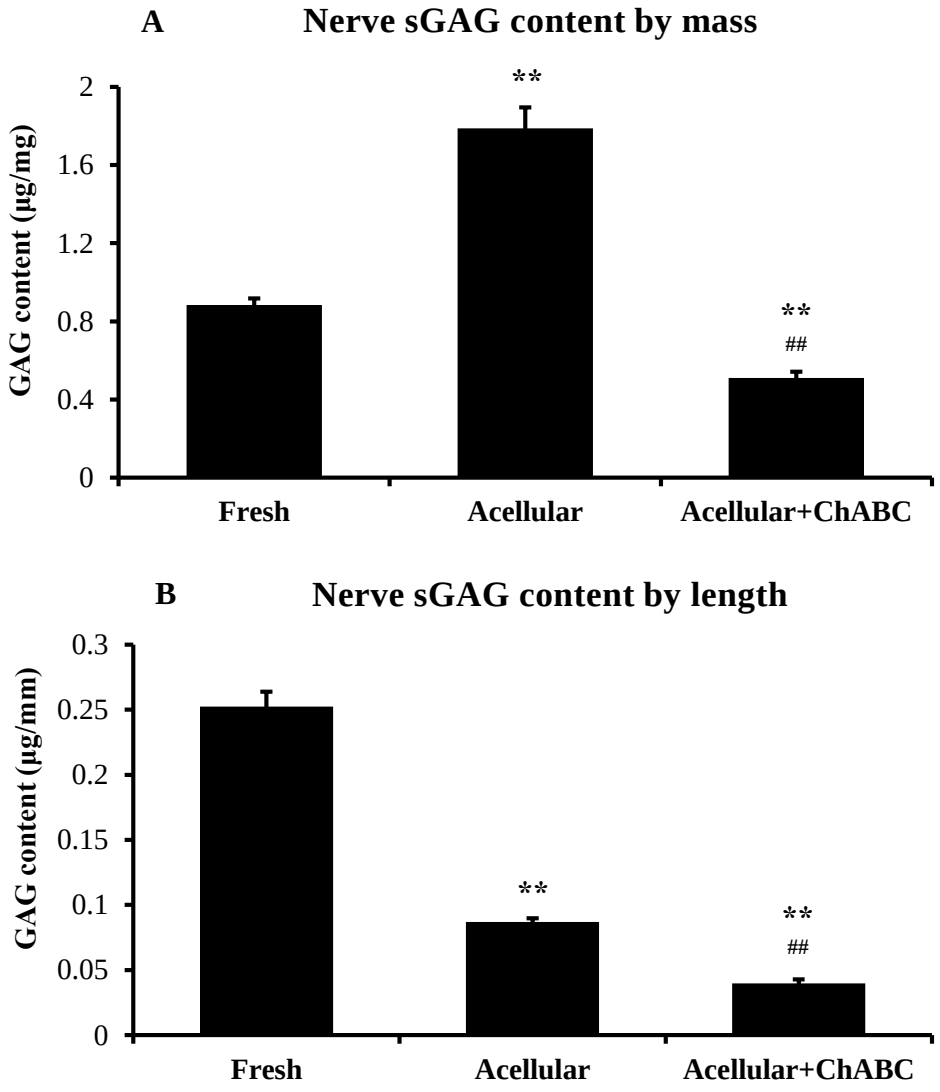

Figure 3.3: Nerve glycosaminoglycans are retained after processing but are significantly reduced following decellularization and chondroitinase ABC treatment. Sulfated glycosaminoglycan (sGAG) content was measured using Blyscan assays and normalized to tissue mass and length. As with collagen content, mass normalization ineffectively portrays the effects of decellularization. When normalized to tissue length, 34% of the sGAGs are retained following decellularization. After treating with chondroitinase ABC, an expected reduction in sGAGs is observed, with 15% and 46% retention compared to fresh and untreated, acellular nerve, respectively. These results indicate that 54% of sGAGs in acellular nerve are neurite-inhibiting chondroitin sulfate proteoglycans. Symbols ** and $^{\#\#}$ indicate significance ($p < 0.01$) compared to fresh nerve and untreated acellular nerve, respectively.

3.3.3. Assessing Hydrogel Formation

The turbidity or absorbance of nerve solutions at 16.5, 13, and 9.5 mg/mL was measured over 30 minutes at 37°C (**Figure 3.4**). Unsurprisingly, less concentrated solutions were slower to initiate gelation, with lag times of 4.9, 5.8, and 6.5 min for 16.5, 13, and 9.5 mg/mL, respectively (**Table 3.4**). All solutions achieved 95% gelation in 10-11 minutes, and the rate of gelation did not correlate with concentration. Following gelation, scanning electron microscopy revealed that the resulting hydrogels were fibrous structures with fiber diameters on the same length scale as those in native nerve tissue, approximately 100 μm. These fibers were also similar in size to those in collagen I hydrogels (**Figure 3.5**), signifying that collagen I fibrillogenesis may be the cause of thermal gelation for nerve hydrogels.

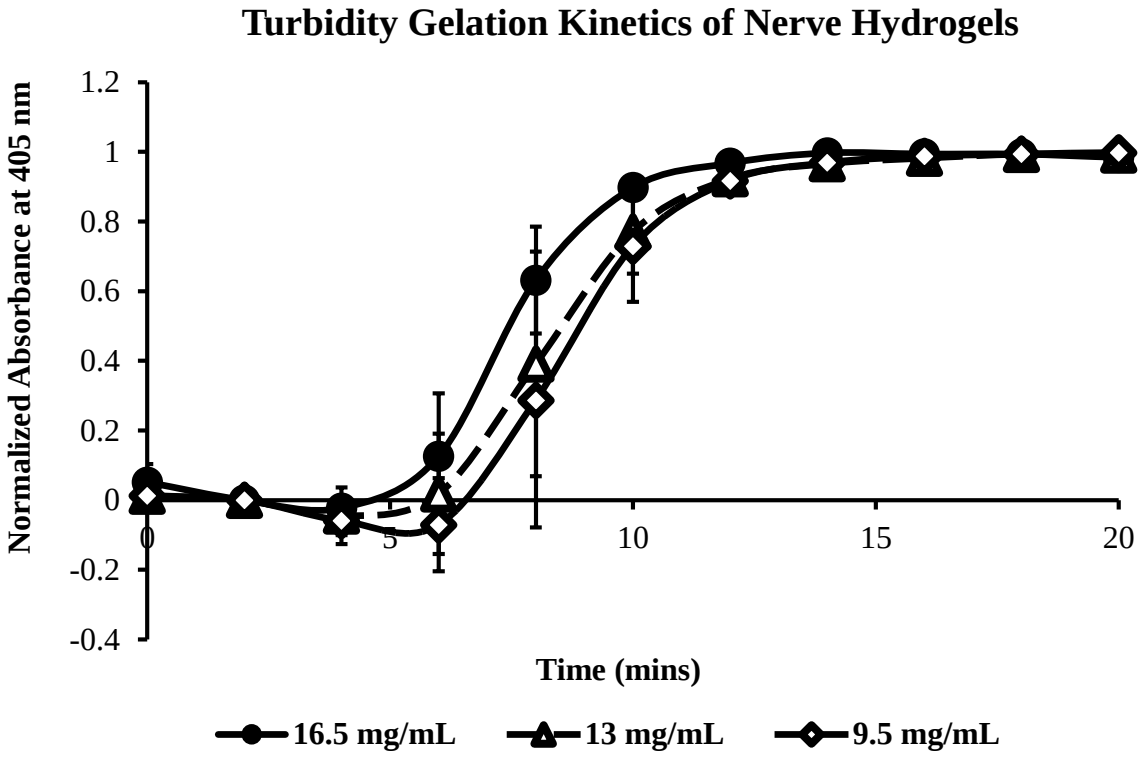

Figure 3.4: Injectable nerve rapidly gel at 37°C. Protein crosslinking was measured via absorbance at 405 nm using a spectrophotometer. Solutions at 16.5 mg/mL initiated gelation faster than lower those at lower concentrations, though all solutions achieved gelation in 10-11 minutes.

Table 3.4: Calculated parameters for gelation kinetics of injectable nerve at 37°C. 100 μL of solution was transferred from ice to a preheated spectrophotometer, and absorbance at 405 nm was measured every 2 minutes for 30 minutes. Lag time, t_{lag}, is the time from t=0 until the region of linear increase; $t_{1/2}$ and t_{95} are the times to achieve 50% and 95% gelation, respectively; s is the speed of gelation calculated as the slope of the linear region.

Parameter	**Reported Value (Mean ± SEM)**		
	16.5 mg/mL	***13 mg/mL***	***9.5 mg/mL***
t_{lag}	4.88 ± 1.25	5.82 ± 1.24	6.46 ± 1.05
$t_{1/2}$	7.50 ± 0.61	8.30 ± 0.87	8.70 ± 0.86
t_{95}	10.0 ± 0.19	10.9 ± 0.87	11.2 ± 1.18
s	0.19 ± 0.04	0.18 ± 0.01	0.20 ± 0.01

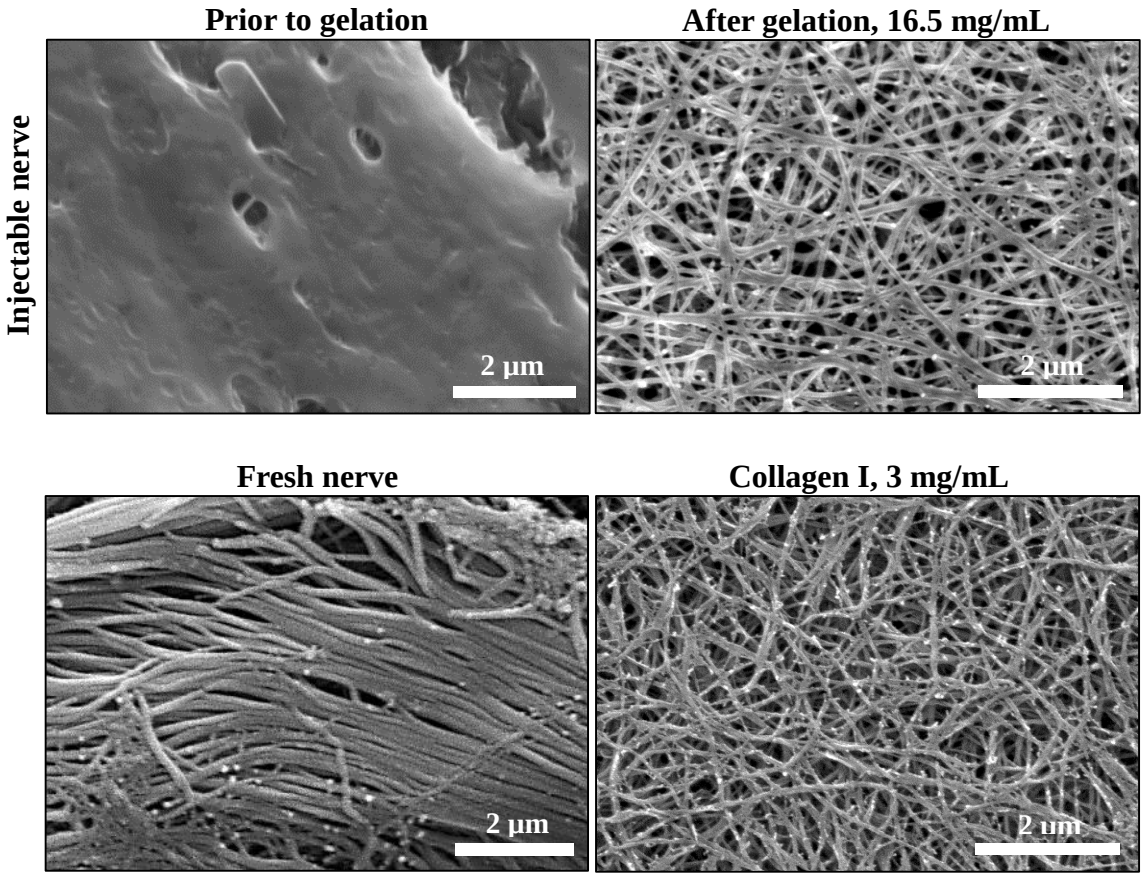

Figure 3.5: Gelation is most likely attributable to collagen fibrillogenesis. Scanning electron micrographs for injectable nerve prior to (A) and after (B) gelation, fresh nerve (C), and collagen I hydrogels (D) demonstrate that incubating nerve solution at 37°C induces fiber formation, and the resulting fibers are on a similar length scale as those found in native nerve tissue and pure solutions of collagen I.

3.3.4. Mechanical Characterization

The response of nerve hydrogels to shear was determined using rheometry for three hydrogel concentrations (16.5, 13, and 9.5 mg/mL). The storage and loss moduli for nerve hydrogels decreased approximately linearly with concentration (**Figure 3.6**). Hydrogels at 16.5 mg/mL exhibited a storage modulus of 171 ± 8.3 Pa and was most similar to rat brain and human grey matter with moduli of approximately 200 Pa (Flanagan *et al.* 2002; Ju *et al.* 2007). Since this concentration was better able to mimic neural tissue, gels at 16.5 mg/mL were also assessed for their response to compression force. Nerve hydrogels at this concentration had a compressive modulus of 4.5 ± 0.35 kPa (**Figure 3.7**). This value is between the moduli for neonatal and adult rat brain previously measured in our lab (Seidlits *et al.* 2010). Notably, compressive moduli at and below 4.5 kPa have been shown optimal for promoting 3D neurite growth i*n vitro* (Man *et al.* 2011).

3.3.5. Biocompatibility

Prior to *in vivo* application, injectable nerve solution was examined to support cell attachment and survival *in vitro*. Rat Schwann cells were plated on 2D glass coverslips coated either with PDL or PDL-injectable nerve, and cell attachment and survival was assessed after 3 days in culture. A live/dead assay revealed no significant difference in cell survival on the two substrates, with over 95% survival on both coatings (**Figure 3.8A)**. Additionally, cell attachment was approximately the same for the control and nerve substrates at 750 ± 31 and 775 ± 25 cells/frame, respectively (**Figure 3.8B)**.

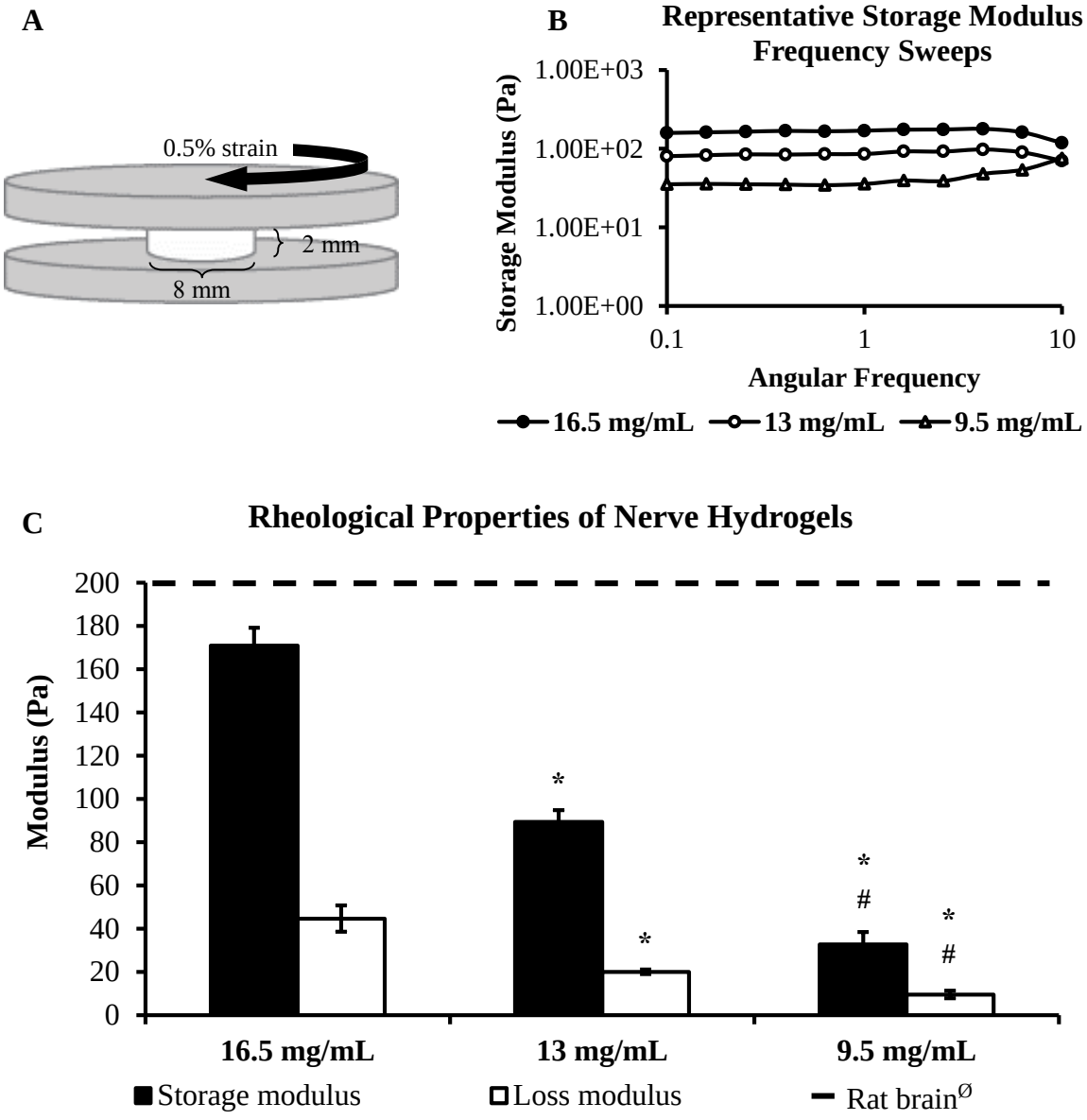

Figure 3.6: The concentration of nerve hydrogels influences mechanical properties. Storage and loss moduli were measured using an ARES rheometer at 0.5% strain and 37°C. (A) Graphical representation of the testing setup. Nerve hydrogels were subjected to shear stress at 0.5% strain. (B) Representative frequency sweeps for 16.5, 13, and 9.5 mg/mL nerve hydrogels. (C) Hydrogels at 16.5 mg/mL (n=7) exhibited a storage modulus most similar to rat spinal cord. Reference data in dashed line from ØLevantal et al., 2007. Symbols * and # indicate significant differences ($p<0.05$) compared to 16.5 mg/mL data and 13 mg/mL, respectively.

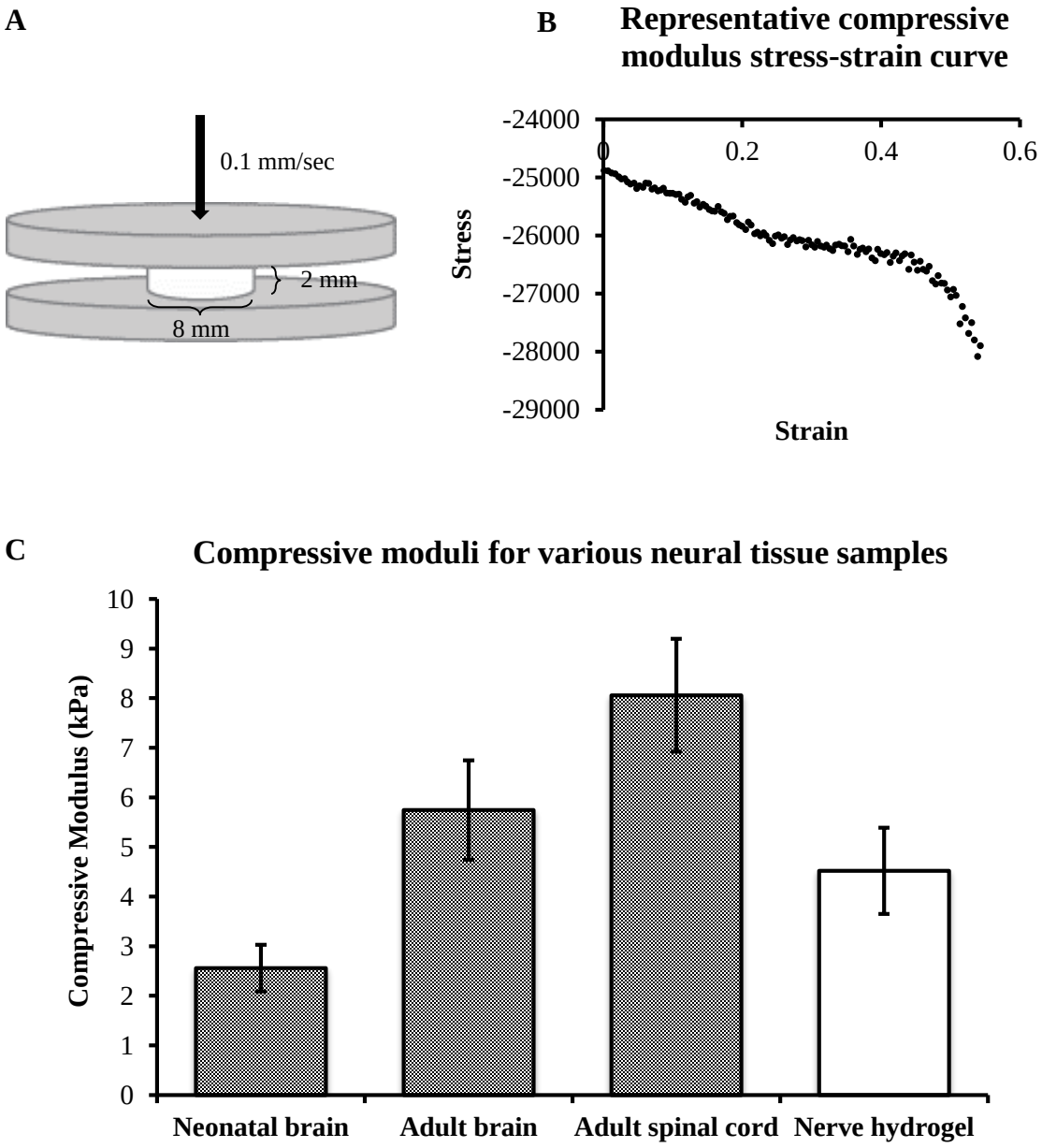

Figure 3.7: Nerve hydrogels exhibit similar a compressive modulus to rat neural tissue. (A) Graphical representation of the testing setup. Nerve hydrogels were subjected to compressive forces at 0.1 mm/sec. (B) Representative stress-strain curve. The compressive modulus was taken as the slope of the linear region, typically within the first 20% of strain. (C) Compressive moduli for various rat neural tissue (black pattern) and nerve hydrogels at 16.5 mg/mL (white). Black patterned data was reproduced from Seidlits *et al*., 2010. Error bars represent standard deviation.

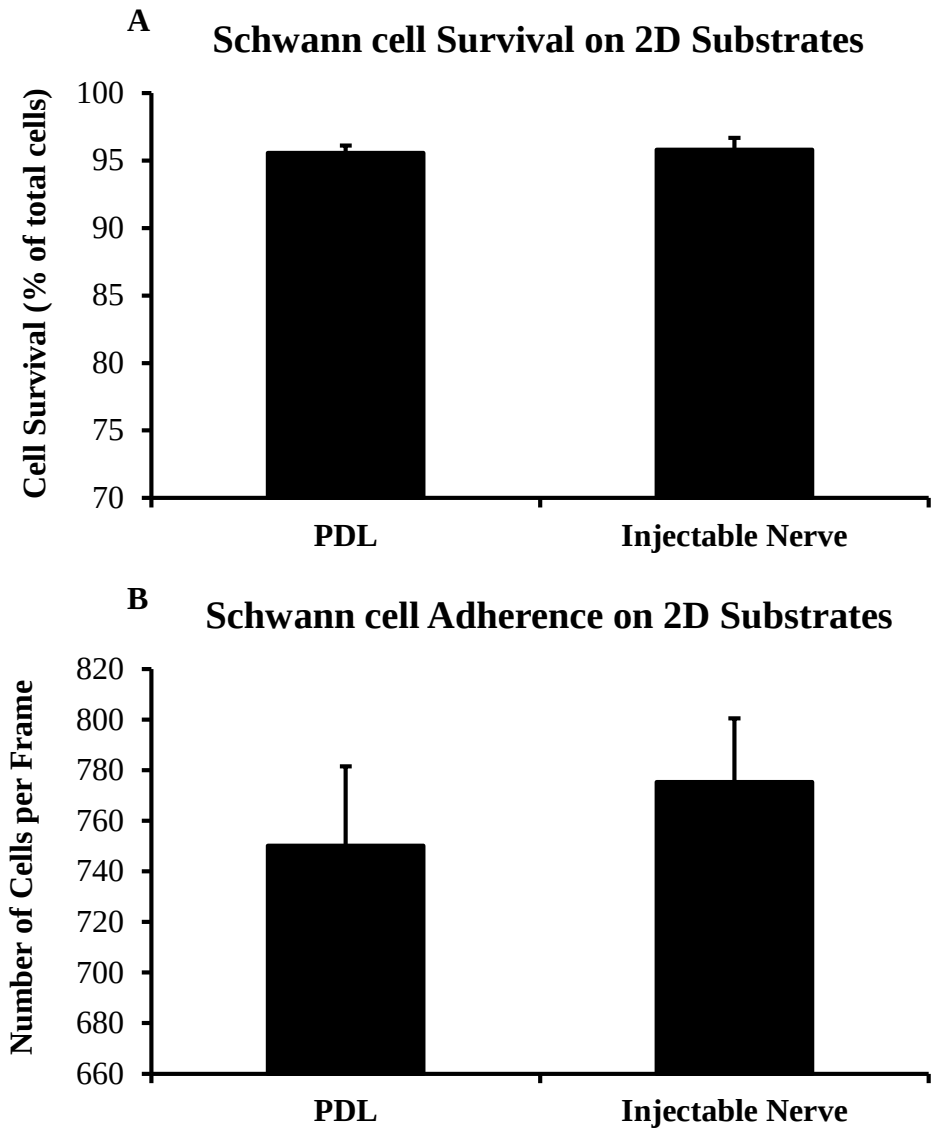

Figure 3.8: Injectable nerve solution supports cell attachment and survival comparable to controls. Adult rat Schwann cells were cultured on glass coverslips coated with either poly-D-lysine (PDL) or injectable nerve solution. Three days after plating, a live/dead assay was performed and cell number was manually counted for three frames per sample (n=6 per group). The percentage of live cells (A) and the cell density (B) reveal injectable nerve coatings supported cell survival and adherence comparable to controls ($p=0.75$ for A and $p=0.47$ for B).

3.3.6. Lesion Volume Assessment

The volume of injured spinal cord tissue was calculated for two animal cohorts to determine 1) the volume of nerve solution required to fill the cavity one week after injury and 2) the acute effect of injectable nerve on cavity volume during the first week following injection (two weeks after injury). Using the Cavalieri method on H&E stained tissue sections, the average lesion volume one week after injury was calculated to be approximately 6.16 ± 0.18 μL (average ± SEM; n=5). Representative stained tissue sections used in this analysis are shown in **Figure 3.9 A** and **B**. Since overfilling the cavity may result in unnecessary pressure and additional tissue damage, a conservative 6 μL was used for all injection surgeries. In a separate study, 6 μL of either PBS or injectable nerve solution was injected into the injured spinal cord of 12 animals, 6 per group. After one week *in vivo*, the spinal cords were harvested, and the lesion volume was again calculated. It was determined that injection of nerve solution did not negatively contribute to spread of the injury, with lesion volumes of 5.08 ± 0.56 and 5.12 ± 0.32 μL for PBS and injectable nerve, respectively (**Figure 3.9D**). These data suggest that a degree of tissue inflammation/swelling is resolved between one and two weeks post-injury for all animals, and any therapeutic effect on lesion volume would be mediated over a longer time period.

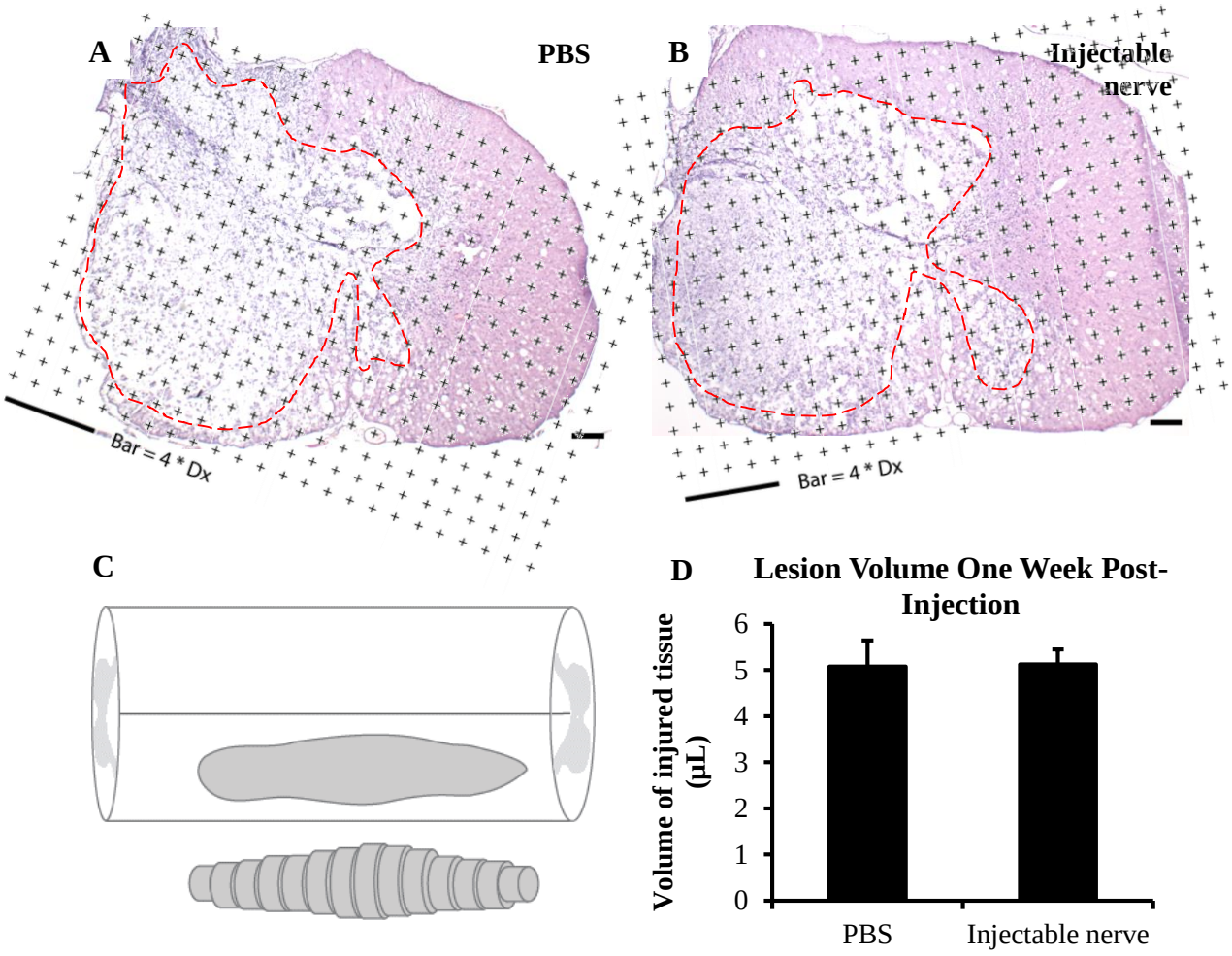

Figure 3.9: Injectable nerve does not affect SCI lesion volume after one week. Twelve micron sections, 360 µm apart, were stained using H&E. Lesion volume was calculated using the Cavalieri method. (A and B) Representative stained sections used for volume analysis. The lesion area was approximated by counting the number of points in the lesion (outlined). Scale bars are 200 µm. (C) Graphical representation of how the lesion volume was calculated based on summation of area projections. (D) Calculated lesion volumes show no detrimental effects for injectable nerve compared to PBS injection.

3.3.7. Acute Inflammatory Response following Application of Nerve Hydrogels

We investigated the ability of injectable nerve hydrogels to bias invading macrophages/monocytes toward a pro-regenerative or M2 phenotype after application in the injured spinal cord. Immunofluorescence staining for the pan-macrophage marker ED1 revealed an extensive macrophage/microglia presence inside the lesion and occasionally on the uninjured side (not shown). A portion of these cells could be identified as M1 cells by CCR7 staining while others were found to express markers of M2 cells such as CD206 (**Figure 3.10 A** and **B)**. Most notably, spinal cords receiving an injectable nerve scaffold displayed a large presence of M2 cells immediately adjacent to the injection site (**D** and **H**). The ratio of M1 to M2 (inflammatory to regenerative) macrophages has been shown to correlates with neuro-regenerative outcomes (Mokarram *et al.* 2012). Using digital image analysis, injectable nerve scaffolds were found to reduce the M1:M2 ratio two-fold compared to saline injection, demonstrating a bias away from inflammation and toward promoting regeneration. This effect may help alleviate development of chronic inflammation that is characteristic of SCI and hinders regeneration.

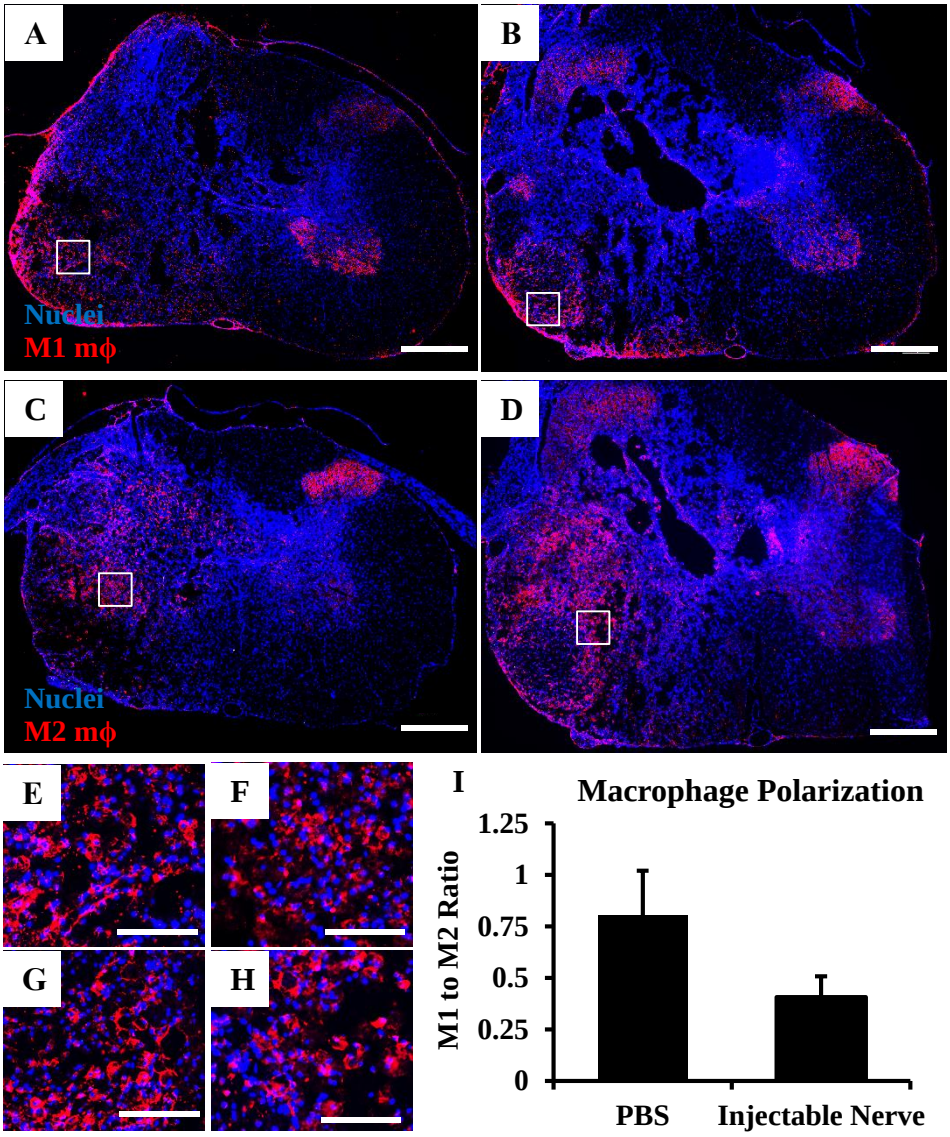

Figure 3.10: Injectable nerve hydrogels alter macrophage phenotype following injection into the injured spinal cord. Spinal cord cross-sections were stained for CCR7 (red, M1 macrophages (mϕ)) in A and B and CD206 (red, M2 mϕ) in C and D. Tissue in A and C was treated with PBS and in B and D, injectable nerve. Nuclei are counterstained with DAPI (blue). (E-H) Inset images of A-D, respectively. Scale bars are 200 μm (A-D) and 50 μm (E-H). (I) Cell number was digitally quantified for each stain at two locations in the lesion to obtain the ratio of M1 to M2 cells (n=6 per group). A two-fold reduction was observed in M1:M2 one week following injectable nerve application compared to saline control, indicating a bias toward pre-regenerative phenotypes (p=0.1).

3.4. DISCUSSION

Materials for implantation into the injured spinal cord can be rationally designed to address several hindrances to regeneration, including lack of a growth supportive substrate in the lesion cavity, inhibition of axonal growth via the glial scar and extracellular inhibitors, and persistence of chronic inflammation. Injectable scaffolds are preferred as they minimize the potential to cause additional damage during application in clinically-relevant contusion models of SCI. Furthermore, *in situ*-forming materials directly integrate with host tissue to enhance astrocyte/axon interactions as well as improve functional recovery (Williams *et al.* 2015). In developing an injectable material to treat SCI, it is important to consider that neural specific matrices (i.e., derived from neural tissue) have been shown to enhance neurite outgrowth and neural cell differentiation compared to non-neural tissue sources (Medberry *et al.* 2013; DeQuach *et al.* 2011). Decellularized brain or spinal cord may retain residual myelin-associated inhibitors; therefore, we sought a different approach by using acellular peripheral nerve as it instead contains components that promote axon regeneration such as laminin.

Using an FDA-approved decellularization process, an injectable hydrogel of peripheral nerve was realized via enzymatic digestion of acellular nerve and optimization of digestion parameters. Under optimal conditions, the resulting ECM hydrogel exhibits relatively rapid gelation (t_{95} is approximately 12 minutes), which may allow for effective cell encapsulation and transplantation without hindering delivery into the spinal cord. Additionally, injectable nerve retains chemical cues found in the naïve tissue, demonstrated by retention of 56% of the original collagen content and 34% of the original sulfated GAGs. The collagen portion of the matrix is most likely contributing to hydrogel formation, based

on comparing the surface topography of injectable nerve and collagen I hydrogels, and maintenance of certain GAGs may increase growth factor binding and bioactivity (Colin *et al.* 1999; Jiao *et al.* 2007) with potential to enhance outcomes upon re-implantation *in vivo* (Seif-Naraghi *et al.* 2012).

Conversely, GAGs of the CSPG classification, normally beneficial in stabilizing mature synapses, are upregulated after injury and serve to potently inhibit axon regrowth (Fitch and Silver 2008). Selective removal of these molecules by the bacterial enzyme Chondroitinase ABC can increase neurite growth into peripheral nerve grafts (Neubauer *et al.* 2007), and this strategy was employed here to maximize the potential for nerve hydrogels to promote neural regeneration. Since Chondroitinase ABC removes both chondroitin and dermatan sulfate, the remaining GAGs types are keratin sulfate and heparan sulfate, the latter of which is known to enhance neurite growth (J. J. Hill *et al.* 2012). Furthermore, nerve hydrogels also contain a high proportion of laminin I, another ECM molecule that promotes extensive neurite outgrowth *in vitro* and *in vivo* (Deister *et al.* 2007; Cheng *et al.* 2007). Collectively, these data suggest nerve hydrogels may enhance axon regeneration *in vivo* to improve outcomes following neural injury.

The mechanical properties of nerve hydrogels can be tuned simply by adjusting the hydrogel concentration. The compressive and storage moduli of nerve hydrogels at 16.5 mg/mL (original 20 mg/mL) were both in the range of rat neural tissues (Seidlits *et al.* 2010; Levental *et al.* 2007), and the former is in an optimal range to promote neurite growth, at least for 3D culture (Man *et al.* 2011). Notably, this is the first account of ECM hydrogels exhibiting a storage modulus similar to the target tissue. Others have reported storage moduli for similar ECM-based materials at 25 Pa or less, with intention to implant

into tissues with much higher mechanics than neural tissue (Johnson *et al.* 2011; Freytes *et al.* 2008). Given the impact of mechanical properties on a broad range of cellular processes (Man *et al.* 2011; Engler *et al.* 2006; Seidlits *et al.* 2010), the soft nature of neural tissue affords an advantage in applying ECM hydrogels for treating neural damage.

Beyond more aptly mimicking native tissue, acellular scaffolds also bias invading macrophages toward regenerative, as opposed to inflammatory, phenotypes after injury (B. N. Brown *et al.* 2009). Since pro-inflammatory macrophages persist chronically following spinal cord injury (Kigerl *et al.* 2009), capitalizing on this phenomenon may offer significant potential to promote wound resolution and enhance recovery. We demonstrated that, in fact, injectable nerve did alter the immune response to spinal cord injury. The ratio of M1 to M2 macrophages decreased one week after application, indicating a bias toward regenerative phenotypes. These data suggest that injectable nerve hydrogels may enhance recovery outcomes not only by providing a growth supportive scaffold but also by modulating the chronic inflammatory environment.

3.5. CONCLUSIONS

As technology progresses, the list of benefits for using decellularized organs in tissue engineering and regenerative medicine continues to grow. In treating contusion spinal cord injury, an injectable version of acellular tissue would enable less invasive methods of application and potentially decrease formation of a rigid glial scar by increasing host integration. Hydrogels derived from optimized acellular nerve approximately mimic the mechanical properties of host neural tissue and recreate the chemical milieu known to support axon regeneration in the PNS and CNS. Furthermore, these injectable nerve

hydrogels modulate the spinal cord injury environment by biasing immune cells toward a regenerative, anti-inflammatory phenotype. Given these results, this novel material demonstrates significant therapeutic potential for aiding regeneration following debilitating neural injury or disease.

Chapter 4: Hydrogels of Injectable Nerve Extracellular Matrix for Application after Spinal Cord Injury

4.1. Introduction

Injectable materials can be excellent mediums to deliver cells or other therapeutics to augment the repair after spinal cord injury (SCI). These matrices can serve either as blank templates that act in synergy with the added therapeutics or may mediate partial recovery on their own. It is therefore important to establish a therapeutic baseline from material implantation prior to addition of supplemental components. In this chapter, we examined a novel injectable material derived from acellular peripheral nerve with potential to act as a supportive template for cell delivery following contusion SCI in rats. A cervical contusion model was chosen to mimic the majority of clinical injuries. To analyze the effects of injectable nerve on functional recovery, forelimb function was assessed using three behavior tests over 8 weeks post-injection. Additionally, respiratory complication is the leading cause of fatality after SCI (NSCISC 2014). Therefore, respiratory function was also examined using neurophysiological recordings in collaboration with Dr. David Fuller at the University of Florida. These analyses provided a comprehensive portrayal of the material's therapeutic baseline when applied after cervical contusion SCI.

4.2. Materials and Methods

4.2.1. Nerve Decellularization and Digestion

Sciatic nerves were aseptically harvested from adult Sprague Dawley rats, separated from the epineurium, and decellularized according to the method previously

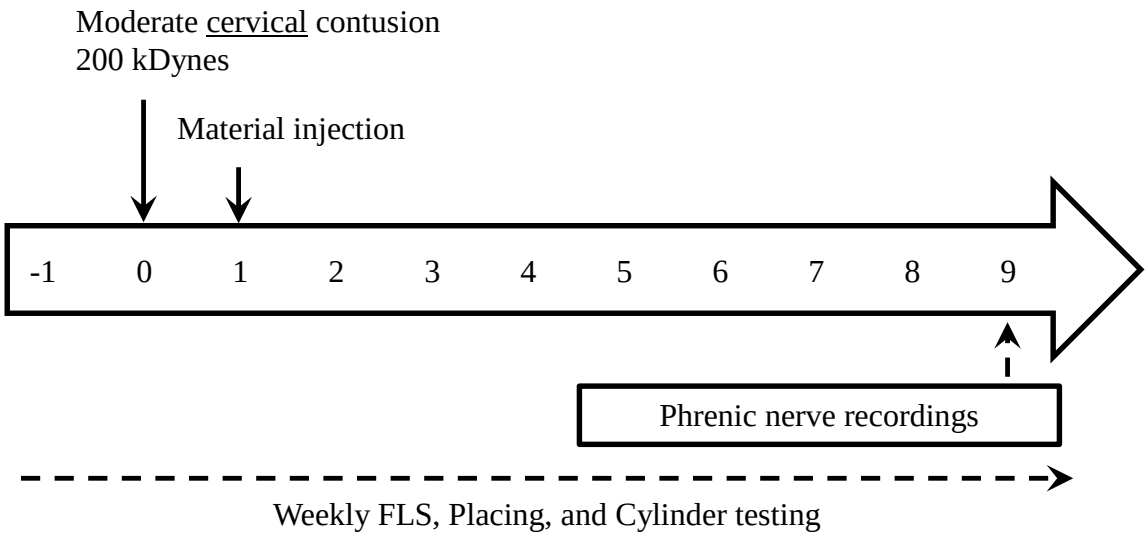

Figure 4.1: Experimental timeline for Chapter 4 animal study. A moderate cervical contusion was induced at C3/4. One week later, the injectable nerve material was injected to fill the lesion cavity. Recovery of forelimb function was monitored over the following 8 weeks using weekly FLS, placing, and cylinder behavior tests. Neurophysiological activity of both phrenic nerves was recorded just prior to termination of the experiment.

developed by Hudson et al. (Hudson *et al.* 2004). All processing was performed under sterile conditions at room temperature on a vertical agitator set to approximately 10 rpm. Following decellularization, nerve tissue was treated with 200 μL of 0.02 U/mL chondroitinase ABC (Sigma) for 16 hours at 37°C to remove inhibitory chondroitin sulfate proteoglycans (CSPGs) (Neubauer *et al.* 2007). The tissue was then washed thrice in sterile 1X PBS for 3x3 hours, thrice in sterile ddH_2O for 3x15 minutes, flash frozen, lyophilized, and stored at -20°C. For pepsin digestion, dried, acellular nerves were weighed and diced into 1-2 mm segments using microscissors. The tissue pieces were digested at room temperature under constant stirring at 20 mg ECM/mL in a solution of 1 mg/mL porcine pepsin (Sigma) and 0.01 M HCl. After 62-64 hours, the enzyme was deactivated by raising the pH to 7.4 using sterile 1 M NaOH ($1/100^{th}$ original volume) and sterile 10X PBS (to 1X final dilution). Nerve solution was diluted to 16.5 mg/mL using 1X PBS for *in vivo* application.

4.2.2. Cervical Contusion Spinal Cord Injury

All procedures involving animals were approved by the Institutional Animal Care and Use Committees (IACUC) at the University of Florida. A model of cervical contusion spinal cord injury in young adult rats was used to evaluate the capacity of iOA to limit spreading of the initial lesion and enhance recovery of locomotor and respiratory function, two deficits causing significant detriment on patient quality of life. This specific injury model was chosen to be analogous to the majority of clinical injuries (NSCISC 2014). Briefly, adult Sprague Dawley rats (250-300 g; Charles River) were anesthetized using isoflurane. Following incision into the skin and muscle layers, the spinal

cord was exposed by performing a laminectomy at the third and fourth cervical vertebrae (C3-4). Animals then sustained a bilateral contusion at C3-4 applied using an Infinite Horizon impactor, the 2.5 mm impact tip, and a force of 200 kDynes. Only animals receiving impacts within 10% of the desired force remained in the study. A section of adipose tissue was used to cover the spinal cord to prevent unwanted adhesions. The muscle layers and skin were then closed using resorbable 5-0 Vicryl suture and monofilament 5-0 nylon sutures, respectively. Buprenorphine (0.03 mg/kg; Patterson Veterinary) was given subcutaneously for three days to manage pain. Animals were monitored three times daily until the injection surgery for excessive deficits (bilateral opposed to unilateral injury) as well as the ability to access food and water.

4.2.3. Material Injection

The spinal cord was re-exposed one week after injury, and 6 μL of either injectable nerve or PBS control (n=14 per group) was injected into the lesion epicenter over 6 minutes using a micromanipulator and a microinjector (World Precision Instruments). Following injection, the needle was kept in place for 2 minutes to minimize leakage during retraction. One group of animals received a laminectomy only (n=13) and therefore served as an uninjured, surgical control. A regimen of buprenorphine was repeated for three days to help with pain management. Forelimb functional recovery was assessed for 8 weeks after material injection (9 wks post-injury) using three behavior test, as described below. Additionally, recovery of respiratory function was examined using electrophysiological recordings at 8 weeks post-injection.

4.2.4. Cylinder Paw Preference Test

Asymmetry in paw use was examined using the Cylinder Paw Preference test. Animals were placed in a Plexiglass cylinder 20 cm in diameter, and forelimb use was scored during vertical exploration. The first forelimb to contact the wall was scored as independent use of that limb, receiving either a "left" or "right" score. If the opposite limb was then placed on the wall, no score was given until the first limb was moved, requiring independent use of the second limb for support. A score of "both" was given if both forepaws contacted the wall simultaneously. Alternation in limb use to climb the wall was also scored as "both" for each set of forelimb movements. To score again, both forepaws had to be removed from the wall. Only paw placement on the way up the wall or in a lateral direction were scored for a total of 20 scores. The percent of ipsilesional paw use was calculated by adding the percentage of ipsilesional placements and half the percentage of "both" placements.

4.2.5. Forelimb Locomotor Score (FLS)

The Forelimb Locomotor Score (FLS) was used to examine voluntary forelimb recovery during open field locomotion (Cao *et al.* 2008). As detailed **Table 4.1**, in FLS is an 18-point rating system (0–17), where 0 indicates no function and 17, normal function. This test assesses forelimb use during locomotion based on joint movement, the ability to bear weight on the affected limb, and the ability to achieve to clearance during stepping. Two blinded investigators performed the test by placing individual rats or pairs of rats on a textured, round table top for four minutes each (six minutes for pairs), scoring independent use of both forelimbs. Testing was performed weekly, starting the week prior to injury as

Table 4.1: Forelimb Locomotor Scale (FLS) Scoring System.

Score	Observable behavior
0	No movements of the forelimb (shoulder, elbow or wrist joints)
1	Slight movements of one or two joints of the forelimb
2	Extensive movement of one joint and slight movement of another joint of the forelimb
3	Slight movement of all three joints of the forelimb
4	Extensive movement of one joint and slight movement of two joints of the forelimb
5	Extensive movement of two joints and slight movement of one joint of the forelimb
6	Extensive movement of all three joints of the forelimb
7	Plantar placement of the forelimb with no weight support
8	Dorsal stepping only
9	Dorsal stepping and/or occasional plantar stepping
10	Frequent plantar stepping
11	Continuous plantar stepping
12	Continuous plantar stepping with paw position rotated (either at initial contact, lift off or both)
13	Continuous plantar stepping with paw position parallel (either at initial contact, lift off or both)
14	Continuous plantar stepping with paw position rotated (either at initial contact, lift off or both) and occasional toe clearance
15	Continuous plantar stepping with paw position parallel (either at initial contact, lift off or both) and occasional toe clearance
16	Continuous plantar stepping with paw position parallel (either at initial contact, lift off or both) and frequent toe clearance
17	Continuous plantar stepping with paw position parallel (either at initial contact, lift off or both) and continuous toe clearance

a baseline for comparison. Animals were enticed to follow a pencil or piece of paper if there were hesitant to walk across the open field.

4.2.6. Vibrissae-Elicited Placing Test

Recovery of sensorimotor function was assessed based on the animals' ability to place their forelimb on a tabletop in response to whisker stimulation. The test is a 5 point scale (0-4) where 0 indicates no movement; 1, slight movement; 2, movement sufficient to touch the side of the table; 3, the ability to reach the tabletop but with atypical paw position; and 4, placing on the tabletop with normal paw position. Animals were held by their torsos with the forelimbs and tail unconstrained. While holding the animal, gentle up and down movements in space were used prior to testing to promote muscle relaxation and eliminate resistance to handling. Each forelimb was tested individually by brushing the respective whiskers on the edge of a table. Ten trails were conducted for each side for each animals, and the average placing score was then calculated for each forelimb. Uninjured animals quickly place the forelimb of both sides onto the tabletop for a score of 4. Depending on the extent of injury, animals with unilateral damage will exhibit varying degrees of deficit in placing of the injured paw while reliably placing the uninjured paw.

4.2.7. Spared Tissue Assessment

Eight weeks after injection, animals were transcardially perfused with 1X PBS and 4% paraformaldehyde. Spinal cord tissue was post-fixed in paraformaldehyde overnight, then transferred to 30% sucrose for cryopreservation. The tissue was cryosectioned at 12 microns using a Leica CM1950 cryostat and mounted onto gelatin-coated glass slides. The Cavalieri method was then used to approximate the volume of spared tissue as described

previously. This modification was implemented based on observable deterioration of the injured side, preventing accurate calculation of the lesion volume. Briefly, every tenth slide containing six sections at 120 μm apart was stained with Luxol Fast Blue and cresyl violet to distinguish healthy and injured tissue. A grid of equally spaced points with known dimensions (based on image magnification) was randomly overlaid onto images for the third and sixth section on each slide, yielding approximately 20 data points per tissue. As few as 10-12 sections are required to accurately approximate biological volumes using this method (Jakeman 2012). The number of points occurring in uninjured tissue for each section was used to calculate the total volume of spared tissue using the equation $V = T * \frac{a}{p} * \sum P$, where **T** is the section thickness, **a** is the area of the overlaid grid based on the image scale, **p** is the number of points in the grid, and $\sum \boldsymbol{P}$ is the total number of points.

4.2.8. Immunohistochemistry

Cryopreserved spinal cords were equilibrated in Optimal Cutting Temperature (OCT; Tissue Tek) medium overnight and frozen in blocks on dry ice. Longitudinal and cross-sections were obtained at 20 μm using a Leica CM1950 cryostat and adhered to gelatin coated slides. Samples were incubated in blocking buffer containing 3% goat serum and 0.3% Triton X100 for 1 hour at room temperature. Following blocking, antibody solutions in blocking buffer were added to the samples and incubated overnight at 4°C. The following primary antibodies were used for tissue analysis: mouse anti-neurofilament (RT97, Developmental Studies Hybridoma Bank) or chicken anti-neurofilament (Aves Labs) to label neurons, rabbit anti-glial fibrillary acidic protein (GFAP, Abcam) to label

astrocytes, and mouse anti-ED1 (Abd Serotec) to label macrophages/microglia. Samples were then washed 3 x 10 minutes with 1X PBS.

Secondary antibodies in blocking buffer were added for 1 hour in the dark at room temperature. Washes with PBS were repeated, and DAPI in water was added for 5 minutes in the dark. Stained samples were then mounted with Fluoromount-G (SouthernBiotech) and coverslipped for imaging. Images were acquired using a Zen Axio Imager.Z2. Each antibody was assessed at multiple locations in the injury epicenter to confirm any histological trends.

4.2.9. Phrenic Nerve Recordings

Nerve recording procedures were adapted from previous publications in the Fuller lab (Doperalski *et al.* 2008; Fuller *et al.* 2008; Fuller *et al.* 2009) and were conducted at 8 weeks post-transplantation. Isoflurane anesthesia (3-4% in O_2) was induced in a closed chamber. A catheter was inserted into the tail vein to enable intravenous (i.v.) infusion of urethane (1.6 g/kg, Sigma). The trachea was cannulated with polyethylene (PE-240) tubing, and rats were mechanically ventilated for the remainder of the experiment (FIO_2:= 0.50). The tracheal pressure was monitored with a pressure transducer (DTXPlus Pressure Transducer, Argon Critical Care Systems, Singapore; Model TA-100 strain gauge amplifier, CWE Inc.) connected to the tracheal cannula. The vagus nerves were sectioned in the mid-cervical region to prevent entrainment of phrenic motor output with the ventilator. A catheter (PE-50) was inserted into the femoral artery to measure blood pressure (DTXPlus Pressure Transducer, Argon Critical Care Systems, Singapore; Model TA-100 strain gauge amplifier, CWE Inc.) and to periodically withdraw blood samples.

Arterial PO_2 (PaO_2) and PCO_2 ($PaCO_2$) and pH were determined from ~0.2 ml arterial blood samples using an i-Stat blood gas analyzer (Heska). Rectal temperature was maintained at 37±1°C using a rectal thermistor connected to a servo-controlled heating pad (model TC-1000, CWE, Ardmore, PA, USA). The carbon dioxide partial pressure ($PETCO_2$) was measured using a rapidly responding mainstream CO_2 analyzer positioned a few centimeters from the tracheostomy tube (Capnogard, Novametrix Medical Systems). Animals received the neuromuscular paralytic pancuronium bromide (2.5 mg/kg, i.v., Hospira, Inc.) to minimize spontaneous breathing efforts. After paralysis, blood pressure and phrenic nerve responses to toe pinch were carefully monitored to ensure adequate depth of anesthesia. Urethane supplements were given as necessary. Blood pressure and fluid homeostasis were maintained by slow, i.v. infusion of a 1:3 solution of sodium bicarbonate (8.4%) and Lactated Ringers.

Bilateral phrenic nerve output was recorded using custom-made, bipolar silver wire suction electrodes filled with 0.9% saline. Compound action potentials were amplified (x10,000), band-pass filtered (3–30,000 Hz) using a differential A/C amplifier, and digitized (CED Power 1401 data acquisition interface) and integrated in real time (time constant = 20ms) using Spike2 software (Cambridge Electronic Design Limited, Cambridge, England).

The protocol for nerve recording was as follows: the ventilator rate was adjusted to maintain $PETCO_2$ between 38 and 45 mmHg throughout the surgical portion of the experiment, then the end-tidal CO_2 apneic threshold for inspiratory activity was determined by gradually decreasing the inspired CO_2 until inspiratory bursting ceased in both phrenic nerves. The ensuing apnea was maintained for 2-3 minutes, and inspired CO_2 was gradually

increased until inspiratory activity re-appeared. The $PETCO_2$ associated with the onset of inspiratory bursting was noted, and the inspired CO_2 was adjusted to maintain $PETCO_2$ ~ 2mmHg above this value throughout the remainder of the experiment. The $PETCO_2$ measurements were used as a guide to help maintain isocapnia. CO_2 levels were determined exclusively by arterial blood analyses. An arterial blood sample was drawn following a stable 10 minute baseline period (50% O_2; CO_2 as determined by apneic threshold; balance N_2). Rats were then exposed to a five minute bout of hypoxia (11% O_2; CO_2 as determined by apneic threshold; balance N_2). Following a 10 minute recovery period, rats were then exposed to a five minute bout of hypercapnia (50% O_2; 9% CO_2; balance N_2). Following another 10 minute recovery period, rats were exposed to a brief period of asphyxia to determine maximal phrenic output. At the conclusion of the experimental protocol, rats were euthanized via systemic perfusion.

4.2.10. Statistics

One-way analysis of variance (ANOVA) was performed for tissue sparing and functional data to determine if treatment resulted in a statistical difference. If so, a student's t test was used to compare individual data points to identify significant differences.

4.3. RESULTS

4.3.1. Spared Tissue Assessment

Because SCI results in deteriation of the spinal cord, the Cavalieri method was used to calculate the volume of tissue that was spared from degeneration following treatment

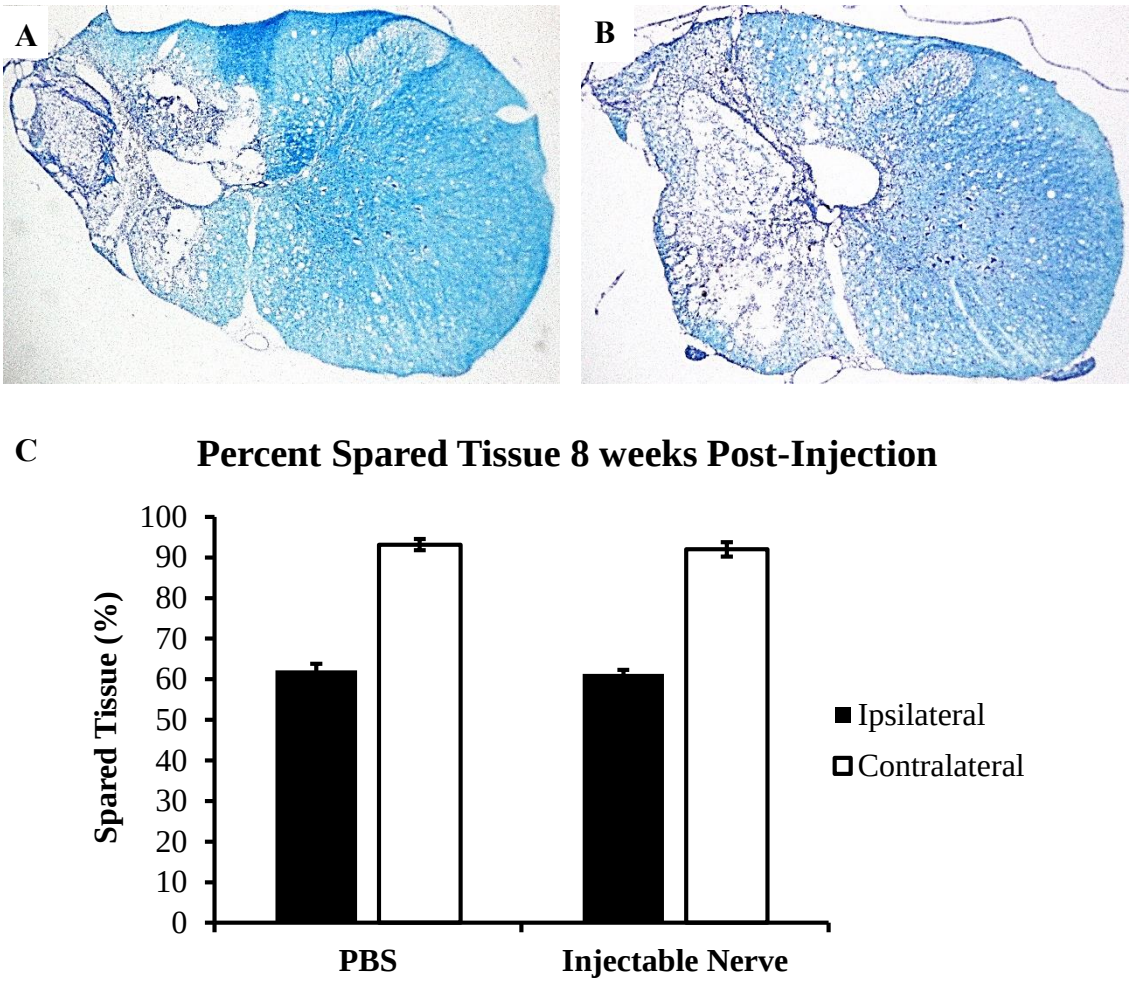

Figure 4.2: Injectable nerve supports similar tissue sparing to PBS injection. The total volume of spared tissue was estimated by applying the Cavalieri method on tissue sections stained for Luxol fast blue and cresyl violet. Representative sectioned are shown for (A) PBS and (B) Injectable nerve treated animals. Spared white matter is shown in blue and cell bodies in purple. (C) Quantifying tissue sparing revealed no difference between treatment groups (n=7). Ipsilateral and contralateral tissue volume was normalized to the volume of a similar length of intact spinal cord (based on the average area of spinal cord rostral and caudal to the injury). Error bars show standard error of the mean.

(West 2012; Jakeman 2012). Spinal cord cross-sections were stained for luxol fast blue to label spared myelin and cresyl violet to label cell nuclei (**Figure 4. A** and **B**). The volume of tissue remaining after injury was calculated and normalized to the volume of a similar length of intact spinal cord. Both experimental groups resulted in similar percentages of spared tissue at 8 weeks, with PBS and injectable nerve treatment promoted sparing of approximately 62.2±1.6% and 61.3±1.4% ipsilateral tissue and 93.1±1.0% and 92±1.8% contralateral tissue, respectively (**Figure 4.2C**). This analysis demonstrates that injectable nerve hydrogels do not adversely effect spreading of the SCI lesion.

4.3.2. Immunohistochemistry

Longitudinal tissue sections were used to evaluate the cellular level response to PBS and injectable nerve application after cervical contusion SCI. Eight weeks after injection, both groups exhibited axonal staining in the lesion epicenter. The staining was mostly punctate in animals treated with PBS (**Figure 4.3 A** and **B**), but fine fiber projections could be found in the lesion and at the distal interface between the lesion and intact tissue for animals treated with injectable nerve (**C-D**). Moreover, the punctate staining observed with PBS injection often co-localized with macrophages, suggesting the identified neurofilament proteins may actually be neuronal debris that was recently phagocytosed (**Figure 4.4 A** and **B**). Co-labeling of axons and macrophages was rare in animals treated with injectable nerve (**C-D**). These results indicate that injectable nerve grafts support axonal projection into and beyond the lesion at a time when macrophages are still clearing neuronal debris in saline treated animals.

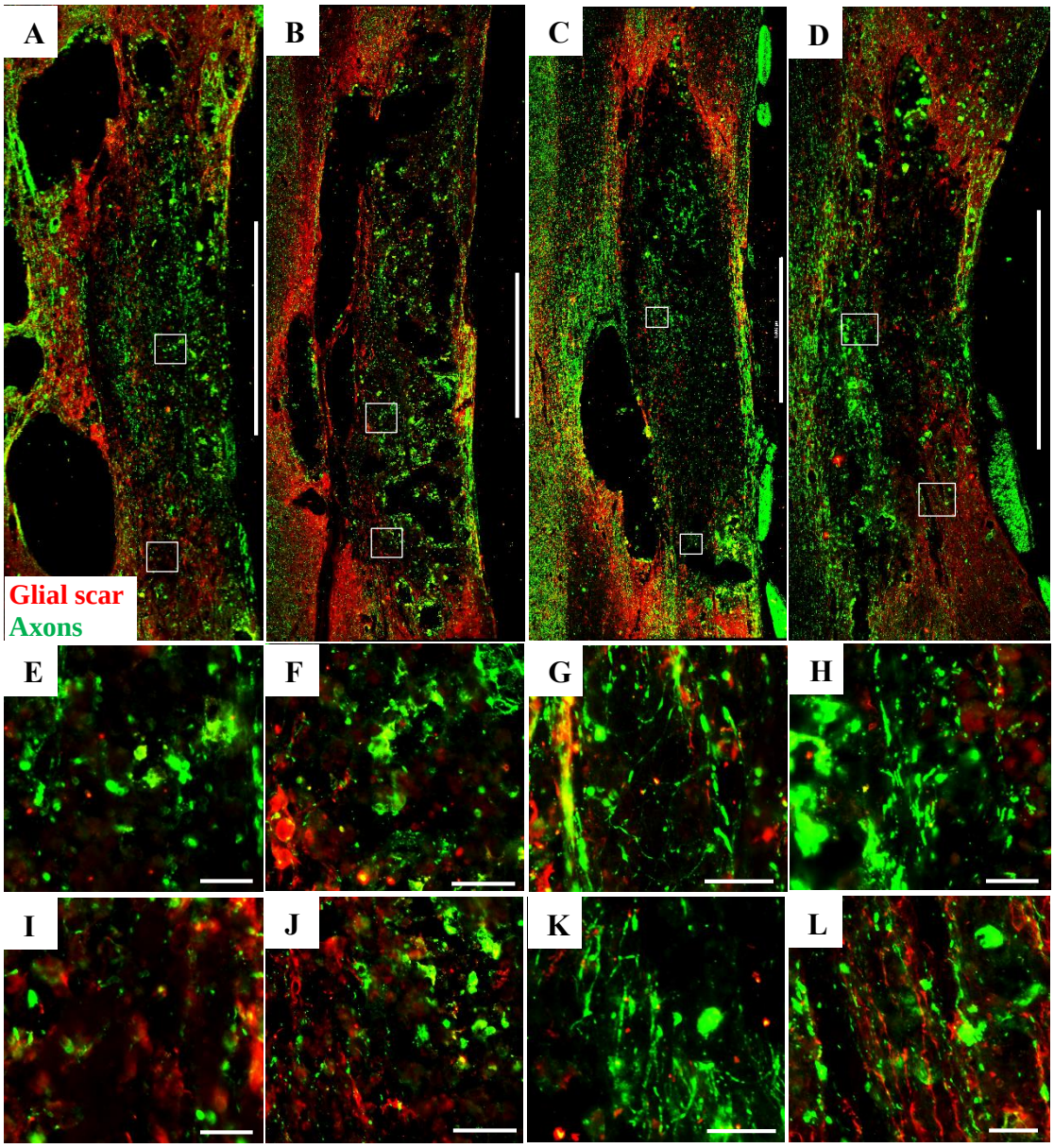

Figure 4.3: More axonal projections are found in the lesion and entering the distal interface after injectable nerve treatment. Fluorescence images of longitudinal sections stained for astrocytes (GFAP, red) and axons (neurofilament, green). Axon staining in PBS treated animals (A-B) was mostly punctate in the lesion (E-F) with sparse staining at the distal interface of healthy tissue (I-J). Conversely, treatment with injectable nerve (C-D) resulted in fine fiber projections in the lesion (G-H), and many fibers could be found reentering the intact spinal cord (K-L). Inset images in A-D are in the corresponding lesions (E-H) and at the distal interfaces (J-L). Scale bars are 1000 μm (A-D) and 50 μm (E-L).

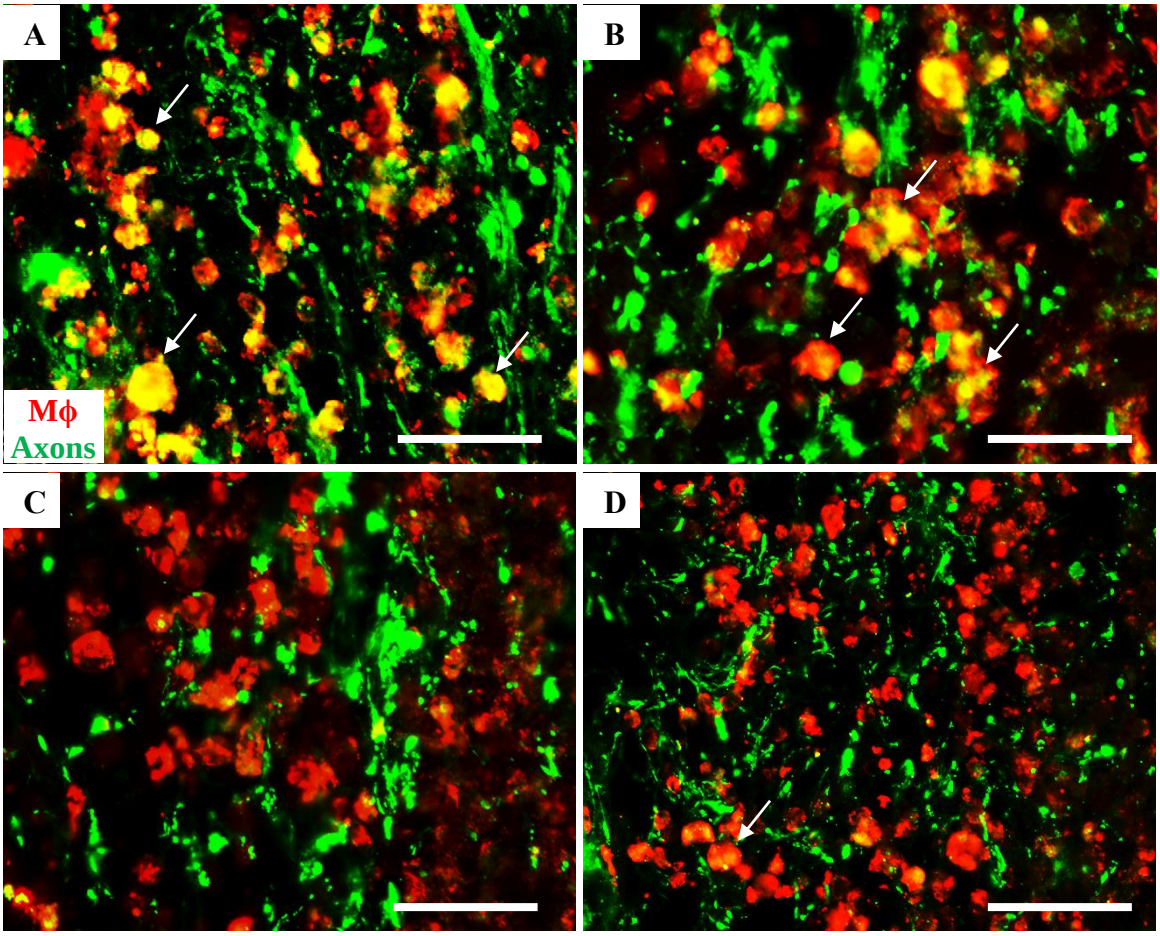

Figure 4.4: Punctate staining of axons in PBS treated animals may represent neuronal debris for clearance by phagocytes. Fluorescence images of longitudinal sections stained for macrophages (ED1, red) and axons (neurofilament, green). Co-labeling of axons with macrophages (mϕ) occurred more often after PBS injection (A-B) than application of injectable nerve (C-D), suggesting neurofilament proteins remain in the process of undergoing phagocytic clearance at 8 weeks post-injection of PBS but not injectable nerve. White arrows indicate representative axon-mϕ co-localization. Scale bars are 50 μm.

4.3.3. Assessing Recovery of Forelimb Function

Forelimb function was longitudinally assessed for 8 weeks after injection using three behavior tests: cylinder paw preference, forelimb locomotor scale, and vibrissae-elicited paw placing. Despite histological evidence, no significant differences were observed between the PBS and injectable nerve experimental groups for any test conducted. At 8 weeks post-injection (9 weeks post-injury), animals treated with injectable nerve and PBS used their injured paw for vertical exploration approximately 8.5 and 6.6%, respectively (**Figure 4.5**). Both groups received FLS scores between 12 and 13 out of 17 for the ipsilateral paw, indicating continuous plantar support of the injured paw during walking with either rotated (12) or parallel (13) paw placement on stepping (**Figure 4.5A**). The contralateral paw did not demonstrate any functional deficits and was consistently scored at 17. Using vibrissae-elicited paw placing, a slow decline in neural function was evident as animals in both groups demonstrated forelimb placement acutely after injury, but this function approached zero over time (**Figure 4.5B**). Again, the contralateral side consistently received the maximum score throughout the testing period (not shown), suggesting the injury did not significantly spread to the opposite side of the spinal cord in either treatment group. FLS and paw placing tests also did not reveal differences between the groups (**Figure 4.6**).

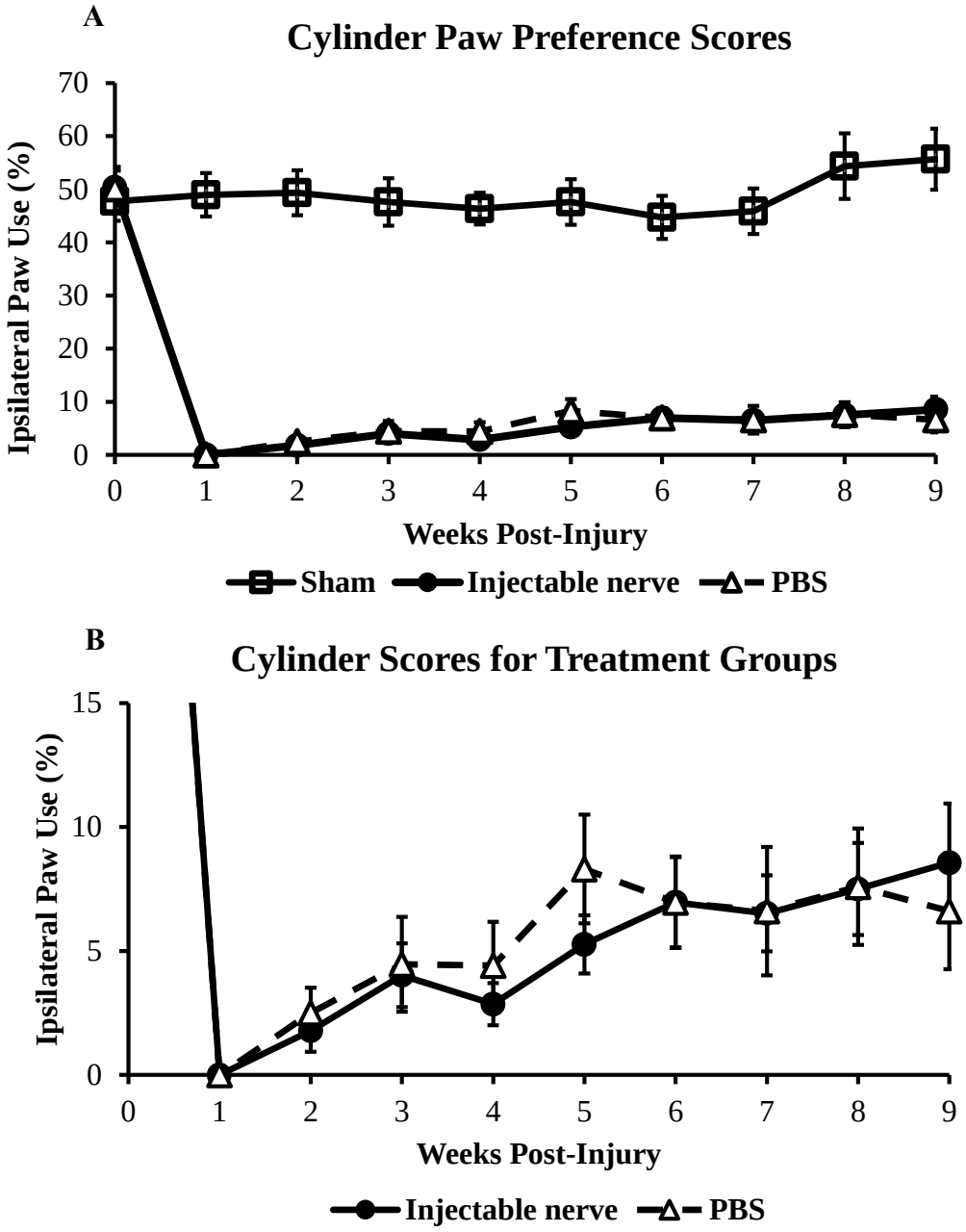

Figure 4.5: Injectable nerve was not detrimental to forelimb recovery after SCI based on Cylinder Paw Preference assessment. Rats received cervical contusion SCI and treatment with PBS or injectable nerve hydrogels one week post-injury. Forelimb functional recovery was examined for 8 weeks post-injection using Cylinder Paw Preference behavioral assessment. No difference was observed between treatment groups at approximately 8% usage compared to 50% in sham animals. B is zoomed in view of A.

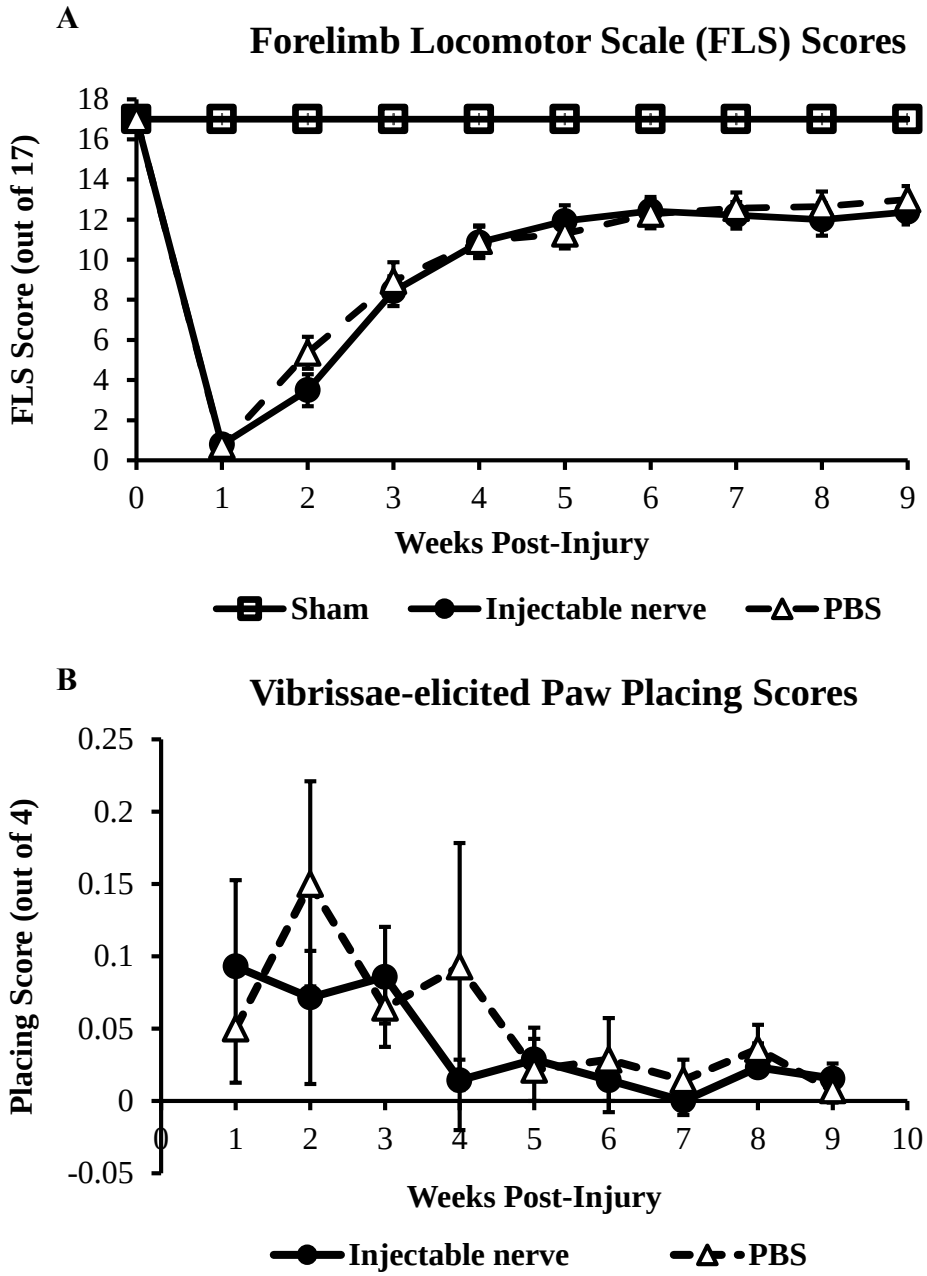

Figure 4.6: Injectable nerve was not detrimental to forelimb recovery after SCI based on FLS and Paw Placing assessment. Rats received cervical contusion SCI and treatment with PBS or injectable nerve hydrogels one week post-injury. Forelimb functional recovery was examined for 8 weeks post-injection using (A) FLS and (B) Paw Placing behavioral assessments. No significant difference was observed between groups, with animals scoring near 13 in FLS (17 for sham) and approaching 0 for placing (4 for sham, not shown).

4.3.4. Respiratory Functional Evaluation

Respiratory function was also quantified by recording activity of both phrenic nerves in mechanically ventilated, vagatomized rats. Representative tracings for one PBS-treated and one injectable nerve-treated animal are show in **Figure** . Phrenic output was recorded under baseline conditions, hypoxia, and hypercapnia. The maximum possible response was elicited by switching off the ventilator, effectively inducing asphyxia at termination of the preparation. In **Figure** , ipsilateral phrenic amplitude is presented as raw data for each animal (**A** and **B**) and normalized to contralateral activity (**C**) or baseline (**D**). A representative trace is also shown containing raw and integrated data as well arterial blood pressure. Significant variation was observed in both groups, although activity in injectable nerve-treated animals was more consistent across animals. No difference was observed between the experimental averages for any measure or normalization method. These functional assays collectively demonstrate that injectable nerve hydrogels provide a therapeutic baseline similar to PBS injection.

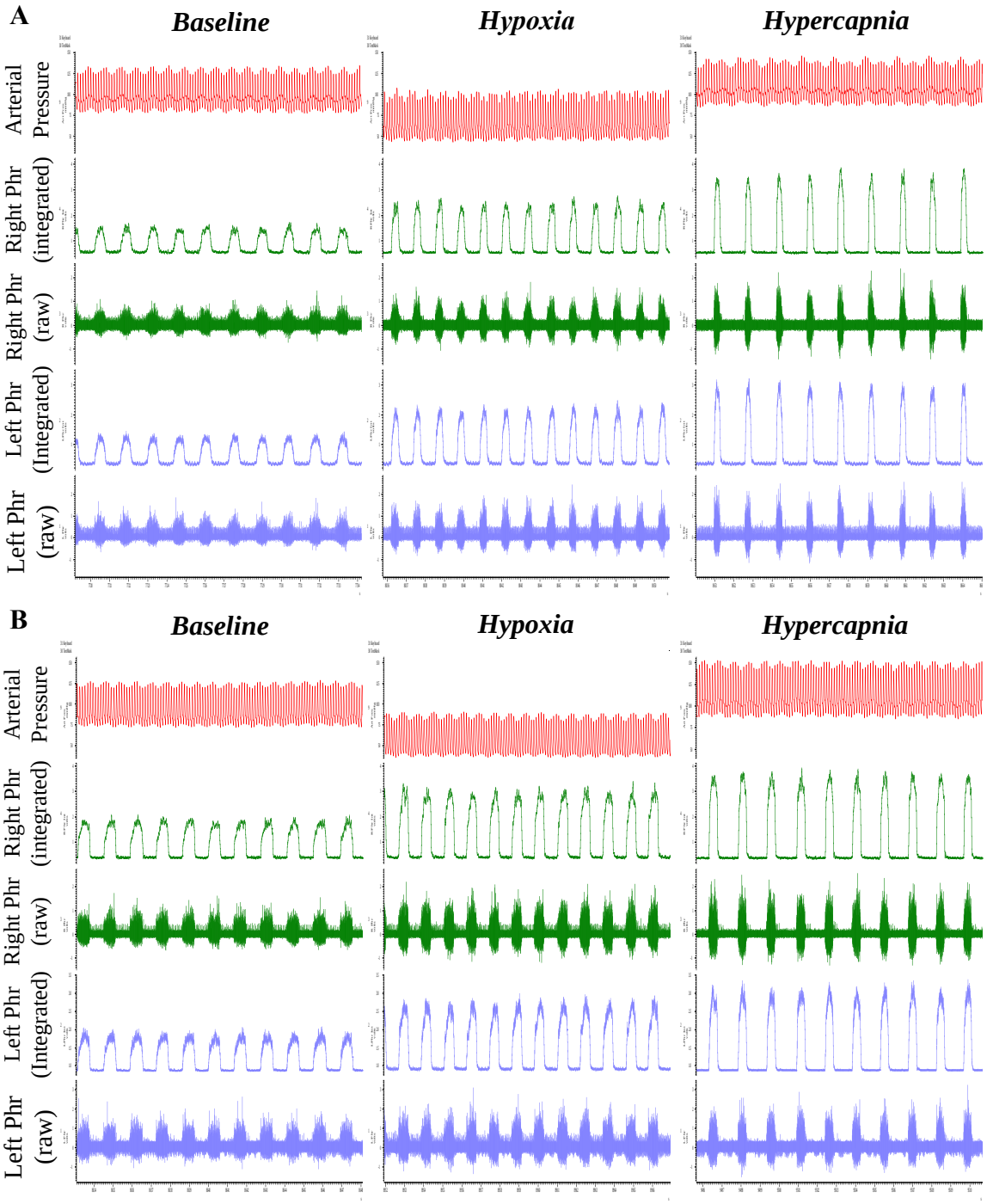

Figure 4.7: Representative phrenic nerve recordings. Treatment groups are (A) PBS and (B) injectable nerve. Each spike is one fictive breath. Baseline = 50% O_2; Hypoxia = 11% O_2; Hypercapnia = 50% O_2 7% CO_2. All gases were balanced to 100% using N_2.

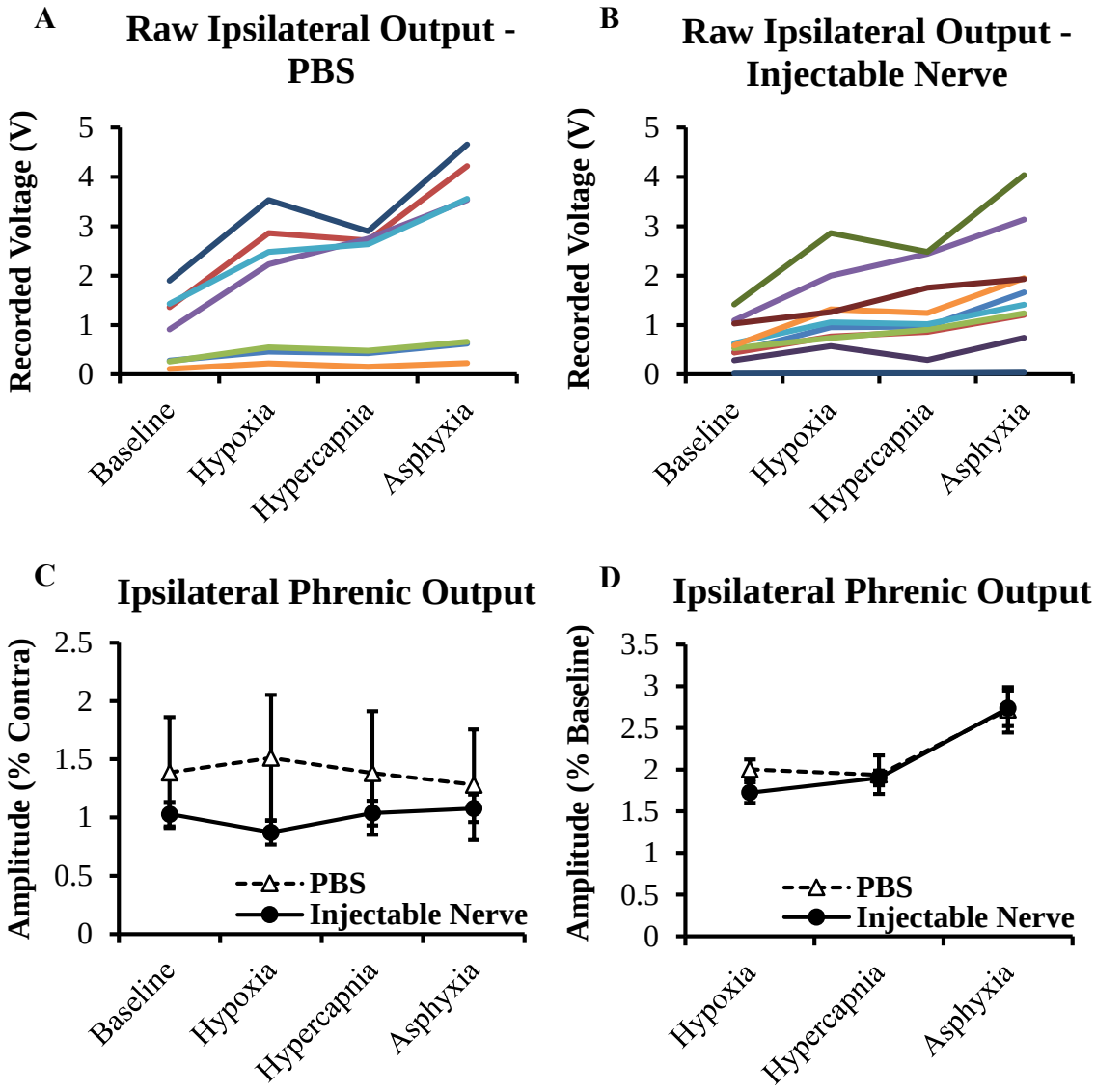

Figure 4.8: Phrenic nerve recordings reveal no difference between PBS and injectable nerve treatment. Recordings from bilateral phrenic nerves were taken 8 weeks post-injection. Neural output was recorded under baseline conditions (50% O_2), hypoxia (11% O_2), hypercapnia (50% O_2 7% CO_2), and asphyxia (ventilator disabled). Raw amplitude data for ipsilateral nerves of each animal are shown in the top panel. (A) PBS-treated animals (n=7) displayed a bimodal distribution while (B) injectable nerve-treated animals (n=8) showed a more distributed response. Ipsilateral phrenic amplitude was averaged for each treatment group and normalized to (C) contralateral output or (D) baseline response. No difference was observed between treatment groups for either normalization method.

4.4. DISCUSSION

The cavity generated after contusion SCI offers a great challenge to neural regeneration but also an opportunity to implant scaffolds that promote repair. Decellularized tissue has only recently been explored as a therapeutic scaffold to promote spinal cord regeneration, although always using preformed scaffolds that require tissue resection prior to application (Alilain *et al.* 2011; J. Chen *et al.* 2014; C. Li *et al.* 2012; Xue *et al.* 2013). Just over five years ago, it was first described how to create an injectable version of acellular urinary bladder tissue using pepsin digestion (Freytes *et al.* 2008). This method has been used to develop injectable tissue grafts from numerous source tissues for a variety of applications (Crapo *et al.* 2014; DeQuach *et al.* 2012; DeQuach *et al.* 2011; Duan *et al.* 2011; Seif-Naraghi *et al.* 2012; Singelyn *et al.* 2012). Injectable tissue has potential to provide similar mechanical support and extracellular matrix cues as the preformed scaffold but can be applied using less invasive methods. Given that SCI commonly results in cavity formation, the ability to inject a therapeutic without causing additional tissue damage may have significant implications. To date, injectable tissue grafts have yet to be reported for *in vivo* application into the spinal cord. In the present study, we chose to evaluate an injectable version of acellular peripheral nerve and its ability to be applied into a cervical contusion SCI without generating negative effects.

Eight weeks after injection, several axonal projections were found in the lesion and at the distal interface in animals treated with injectable nerve. Animals receiving saline conversely exhibited punctate axonal staining that often co-labeled with macrophages, suggesting the positive staining was residual or previously-phagocytosed neuronal debris. Nonetheless, injectable nerve was found to promote equivalent functional recovery to PBS

injection as measured using forelimb behavioral tests. Similar results were obtained via neurophysiological recording of the phrenic nerves through collaboration with Dr. David Fuller. This material is therefore a potential medium for delivery of additional therapeutics to treat SCI without the risk of unnecessary damage. Unlike saline, injectable nerve solution contains cell adhesive ligands that aid in preventing transplanted cell death due to substrate detachment, thereby enhancing the therapeutic potential of cellular therapies. Furthermore, the ability of this material to alter the inflammatory state of the lesion (reported in Chapter 3) and promote axonal re-entry into the spinal cord could provide additional benefits toward increasing therapeutic efficacy of cell transplantation.

The rate of material degradation may offer an explanation for why injectable nerve alone did not demonstrate observable functional benefits. The enzymatic pre-treatment of acellular tissue required to create an injectable tissue graft essentially pre-degrades the ECM such that the material residence time may be substantially decreased. And because the onset of axon regeneration is typically 4-6 weeks post injury, materials to promote spinal cord regeneration may require longer residence times than those found to promote functional recovery in other injury paradigms. Therefore, injectable tissue grafts for treating SCI may require the addition of exogenous cells that can produce their own extracellular matrix as the original delivery vehicle degrades. This approach would not only increase the initial survival or viability of transplanted cells but could also indirectly provide a newly deposited matrix to support axonal ingrowth and functional recovery.

4.5. CONCLUSIONS

An injectable scaffold of acellular peripheral nerve was found to support equivalent functional recovery as saline injection. This conclusion was corroborated using three separate behavior tests, including locomotor and sensorimotor tests, as well as electrophysiological recordings from the phrenic nerve. A lack of detrimental effects suggests this material may provide means to deliver additional therapeutics into the injured spinal cord without interference from the delivery vehicle. In fact, since injectable nerve solution contains adhesive ligands, it may increase cell survival cues compared to delivery in cell medium. In this manner, while this injectable nerve did not afford functional benefits on its own after SCI, it is a blank slate for delivery of other therapeutics with the capacity to enhance the efficacy of those interventions.

Chapter 5: Injectable Nerve Hydrogels as a Clinically-Relevant Alternative to Matrigel for Supporting Schwann Cell Transplantation following SCI

5.1 INTRODUCTION

Autologous Schwann cell transplantation has demonstrated significant therapeutic potential to promote functional recovery following spinal cord injury (SCI). According to the National Institute of Health, this intervention strategy is currently being investigated in separate phase I clinical trials for sub-acute and chronic SCI. These trials will test the safety of implanting cells alone, yet extensive research has demonstrated the need for supportive matrices to enhance cell survival and integration with the host (Christman *et al.* 2004; Patel *et al.* 2010). Commercially-available Matrigel is most often used for its easy accessibility and high laminin content, which enhances Schwann cell survival and axon regeneration (Patel *et al.* 2010). Given its origins as a tumor-derived substrate, however, Matrigel lacks potential for translation into a clinical setting. Schwann cells are native to peripheral nerve, and, a nerve-based scaffold may provide a more translatable option, particularly with acellular nerve grafts already on the market.

The goal of this research was to examine an injectable version of acellular peripheral nerve in comparison to Matrigel to deliver Schwann cells after SCI. Because this injectable nerve scaffold may not contain the plethora of growth factors present in Matrigel, the novel matrix was also tested in combination with growth factor therapy: One group received Schwann cells genetically modified to express the bi-functional

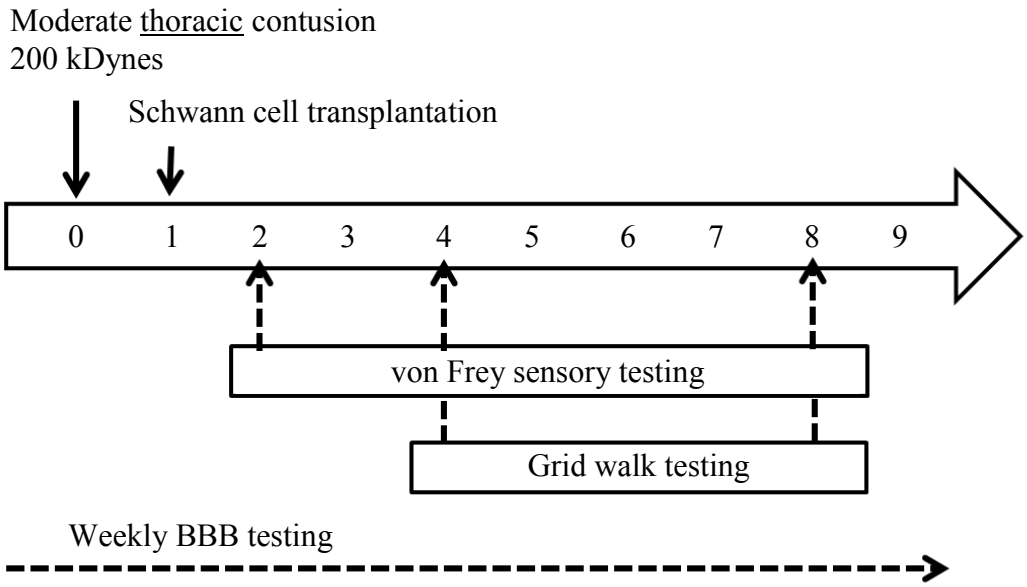

Figure 5.1: Experimental timeline for Chapter 5 animal study. All animal work was performed in Miami. A moderate thoracic contusion was performed at T7-9 using an IH impactor at 200 kDynes. One week after injury, Schwann cells in Matrigel or injectable nerve were transplanted into the lesion. Functional recovery was assessed for 9 weeks after injury using weekly BBB testing, grid walk testing at weeks 4 and 8 post-injury, and von Frey sensory testing at weeks 2, 4, and 8 post-injury. At 9 weeks after injury, spinal cord tissue was assessed using immunochemistry and transmission electron microscopy.

neurotrophin D15A, previously shown to enhance several histological and functional outcomes after SCI (Golden *et al.* 2007; Kanno *et al.* 2014). **Figure 5.** illustrates the overall experimental plan as carried out by Dr. Bunge's lab personnel at the Miami Institute to Cure Paralysis.

5.2. MATERIALS AND METHODS

5.2.1. Nerve Decellularization and Digestion

Sciatic nerves were aseptically harvested from adult Sprague Dawley rats, separated from the epineurium, and decellularized according to the method previously developed by Hudson et al. at the University of Florida (Hudson *et al.* 2004). All processing was performed under sterile conditions at room temperature on a vertical agitator set to approximately 10 rpm. Following decellularization, nerve tissue was treated with 200 µL of 0.02 U/mL chondroitinase ABC (Sigma) for 16 hours at 37°C to remove inhibitory chondroitin sulfate proteoglycans (CSPGs) (Neubauer *et al.* 2007). The tissue was then washed thrice in sterile 1X PBS for 3x3 hours, thrice in sterile ddH_2O for 3x15 minutes, flash frozen, lyophilized, and stored at -20°C. For pepsin digestion, dried, acellular nerves were weighed and diced into 1-2 mm segments using microscissors. The tissue pieces were digested at room temperature under constant stirring at 20 mg ECM/mL in a solution of 1 mg/mL porcine pepsin (Sigma) and 0.01 M HCl. After 62-64 hours, the enzyme was deactivated by raising the pH to 7.4 using sterile 1 M NaOH ($1/100^{th}$ original volume) and sterile 10X PBS (to 1X final dilution). Nerve solution was diluted to 16.5 mg/mL using 1X PBS, shipped at -20°C to our collaborators in Miami, and stored until use.

5.2.2. Thoracic Contusion Spinal Cord Injury

All procedures involving animals were approved by the Institutional Animal Care and Use Committees (IACUC) at the University of Miami. A model of thoracic contusion spinal cord injury in adult rats was used to evaluate the capacity of injectable nerve to support and enhance Schwann cell transplantation over current practices. This injury model was chosen to be analogous to the injuries of patients currently enrolled in the clinical trial for Schwann cell transplantation at the Miami Institute to Cure Paralysis. Briefly, adult Fischer rats (160-180 g; Harlan Laboratories) were anesthetized using isoflurane. Following incision into the skin and muscle layers, the spinal cord was exposed by performing a laminectomy at the seventh, eighth, and ninth thoracic vertebrae (T7-9). Animals then sustained a bilateral contusion at T7-9 applied using an Infinite Horizon impactor, the 2.5 mm impact tip, and a force of 200 kDynes. Only animals receiving impacts within 10% of the desired force were included in the study. A piece of adipose tissue was used to cover the spinal cord and prevent unwanted adhesions. The muscle layers and skin were then closed using resorbable 5-0 Vicryl suture and monofilament 5-0 nylon sutures, respectively. Buprenorphine (0.03 mg/kg; Patterson Veterinary) was given subcutaneously for three days for pain management. Animals were monitored for the ability to access food and water three times a day until the transplantation surgery one week later.

5.2.3. Schwann cell Transplantation

Adult Schwann cells were isolated from Fischer rats and virally transfected with a gene for green fluorescent protein (GFP) to facilitate post-transplantation identification.

An additional set of cells were transfected with a gene for the bi-functional neurotrophin D15A to assess the addition of growth factor therapy in our treatment strategy. Cultured transduced SCs were resuspended in one of two mediums for transplantation: Matrigel™ or injectable nerve solution. Two distinct groups received injectable nerve solution, one containing only GFP Schwann cells and one containing half GFP Schwann cells and half D15A/GFP Schwann cells. One week after injury, the spinal cord was re-exposed0, and 6 μL of $2x10^6$ cells in one of the three mediums was injected into the lesion epicenter over 3 minutes using a micromanipulator and a microinjector (World Precision Instruments). Following injection, the needle was kept in place for 3 minutes to minimize leakage during retraction. Administration of buprenorphine was repeated for three days to help with pain management. Ten animals were included in Matrigel and injectable nerve groups and eight animals in the D15A-SC+injectable nerve group. Functional recovery was assessed for 8 weeks after cell transplantation using three behavioral assessment, as described below.

5.2.4. Basso, Beattie, Bresnahan (BBB) Scoring

The Basso, Beattie, Bresnahan (BBB) score was used to examine voluntary hindlimb recovery during open field locomotion (Basso *et al.* 1995). The BBB scale is a 22-point (0–21) rating system to assess hindlimb recovery during locomotion. The scores reflect the ability to move individual joints, bear weight on the affected limbs, coordinate limb movement between forelimbs and hindlimbs, and exhibit trunk stability during walking. A score of 21 indicates unimpaired hindlimb locomotion. A subscore can be obtained from the original BBB scores to better evaluate recovery of higher motor functions such as paw position, toe clearance, trunk stability, and tail position. The BBB

subscore is a 7 point scale, with 7 representing normal function. Two blinded investigators performed the tests by placing individual rats or pairs of rats on a textured, round table top for four minutes each (six minutes for pairs). Testing was performed weekly, starting the week prior to injury as a baseline for comparison.

5.2.5. Grid Walk Analysis

Grid walk analysis was used to examine the animals' ability to accurately walk across a 1 m long wire grid using fine forelimb–hindlimb coordination, i.e. placement of the hindlimb on a bar previously occupied by the coordinating forelimb (Metz *et al.* 2000). The grid consisted of irregular gaps between round metal bars, with bar distances randomly assigned each testing session between 0.5–5 cm. Three complete trials were conducted for each animal at weeks 4 and 8 post-injury. The number of steps required to cross the grid was recorded, as was the number of footfall errors (missteps resulting in foot placement into a gap) and footslip errors (missteps resulting in foot slippage but without placement into a gap). The percent error was calculated for the number of footfalls, footslips, and total errors relative to the total number of steps.

5.2.6. von Frey Sensory Testing

Von Frey filaments that flex at defined forces were used to examine mechanical allodynia, an increased sensitivity to mechanical stimuli that would not have elicited pain prior to injury (Chaplan *et al.* 1994; Kanno *et al.* 2014). Eight graded filaments were used ranging from 0.41 to 15.1 g (force at flexion). Testing was performed once pre-injury and at 2 and 8 weeks post-transplantation. Animals were placed in a plastic cage with a wire mess bottom, enabling access to the plantar surface of the hindpaws. Behavioral

acclimation in the cage was allowed for 15 minutes prior to testing. Filaments were examined starting at the lowest flexion rating. The middle of each hindpaw footpad was perpendicularly probed until the filament was slightly bent, and pressure was maintained for 6-8 seconds. If no response was observed, the experimenter progressed to the next force rating. Foot withdrawal initiated within the 6-8 second period was noted, as was the force rating of the filament. The filaments above and below the minimum response force were tested three times at five minute intervals to ensure accuracy. Both hindpaws were tested each session with five minutes between each paw.

5.2.7. Tissue Harvest and Immunohistochemistry

Eight weeks after cell transplantation, animals were transcardially perfused with 1X PBS and 4% paraformaldehyde. The spinal cords were post-fixed in paraformaldehyde overnight before being transferred to 30% sucrose for cryopreservation. Alternatively, tissue for assessing myelination was prepared as detailed in section *5.2.8* below. Following cryopreservation, spinal cords were equilibrated in Optimal Cutting Temperature (OCT; Tissue Tek) medium overnight and frozen in blocks on dry ice. Longitudinal sections were obtained at 20 μm using a Leica CM1950 cryostat, adhered to gelatin coated slides for 2 hours, and then stored at -80°C until use. Thawed sections were incubated in blocking buffer containing 3% goat serum and 0.3% Triton X100 for 1 hour at room temperature to permeabilize the tissue and cover non-specific binding sites.

Following blocking, primary antibodies in blocking buffer were added to the samples and incubated overnight at 4°C in a humidified environment. Spinal cords were labeled using rabbit anti-glial fibrillary acid protein (GFAP, Dako) to label astrocytes and

chicken anti-green fluorescent protein (Chemicon) to label transduced Schwann cells. Samples were washed 3x10 minutes with 1X PBS, and coordinating secondary antibodies in blocking buffer were added for 1 hour in the dark at room temperature. Washes in PBS were repeated, and Hoescht was added for 5 minutes in the dark to label nuclei. Stained samples were then mounted with Fluoromount-G (Southern Biotech), coverslipped, and imaged using a confocal microscope.

5.2.8. Toluidine Blue Assessment of Myelination

Fifteen millimeter spinal cord segments around the lesion epicenter (n=5 per group) were post-fixed overnight in 2% glutaraldehyde in 0.1 M PBS and then treated with 1% osmium tetroxide in 0.1 m cacodylate buffer for 1 h. Tissues were rinsed in distilled water, dehydrated in graded ethanol and propylene oxide, and embedded in Epon/Araldite resin for sectioning (C. E. Hill *et al.* 2012). Semi-thin, plastic cross sections (1 μm) were stained with toluidine blue and photographed by light and transmission electron microscope. The g-ratio of myelinated axons was calculated by dividing the axon circumference by the myelin circumference at the widest point. A theoretically optimum g-ratio has been calculated to be 0.77 for CNS axons (Chomiak and Hu 2009).

5.2.9. Statistics

One-way analysis of variance (ANOVA) was performed for behavioral data to determine if treatment resulted in a statistical difference. If so, a student's t test was used to compare individual data points to identify significant differences.

5.3. RESULTS

5.3.1. Immunohistochemistry

Maintenance of transplanted Schwann cells was examined by labeling longitudinal sections for eGFP along with GFAP-staining to identify the astrocytic glial scar. Both injection matrices helped to maintain the cells in the lesion cavity (**Figure 5.2**). Additionally, astrocytes are occasionally observed in the Schwann cell graft, suggesting the materials promoted integration of the transplant and host spinal cord. These images will be used to assess transplanted cell survival, and additional staining will be performed to better characterize the effects on neuronal regeneration and immune cell presence.

5.2.2. Assessing Axon Myelination by Transplanted Schwann cells

Plastic sections from the epicenter of Schwann cell grafts revealed a plethora of Schwann cell-myelinated axons in both the Matrigel and injectable nerve groups (**Figure 5. A-D**). Preliminary analysis suggests there is no significant difference in the g-ratio of myelinated axons in the two matrices (**Figure 5.4E**) (n=3 images per group). Moreover, the Schwann cell implants showed no distinct borders with the host tissue, suggesting 1) both of these injectable matrices promoted effective integration with the host tissue and 2) the Schwann cells grafts did not exhibit excessively negative interactions with host astrocytes as is known to occur (Santos-Silva *et al.* 2007).

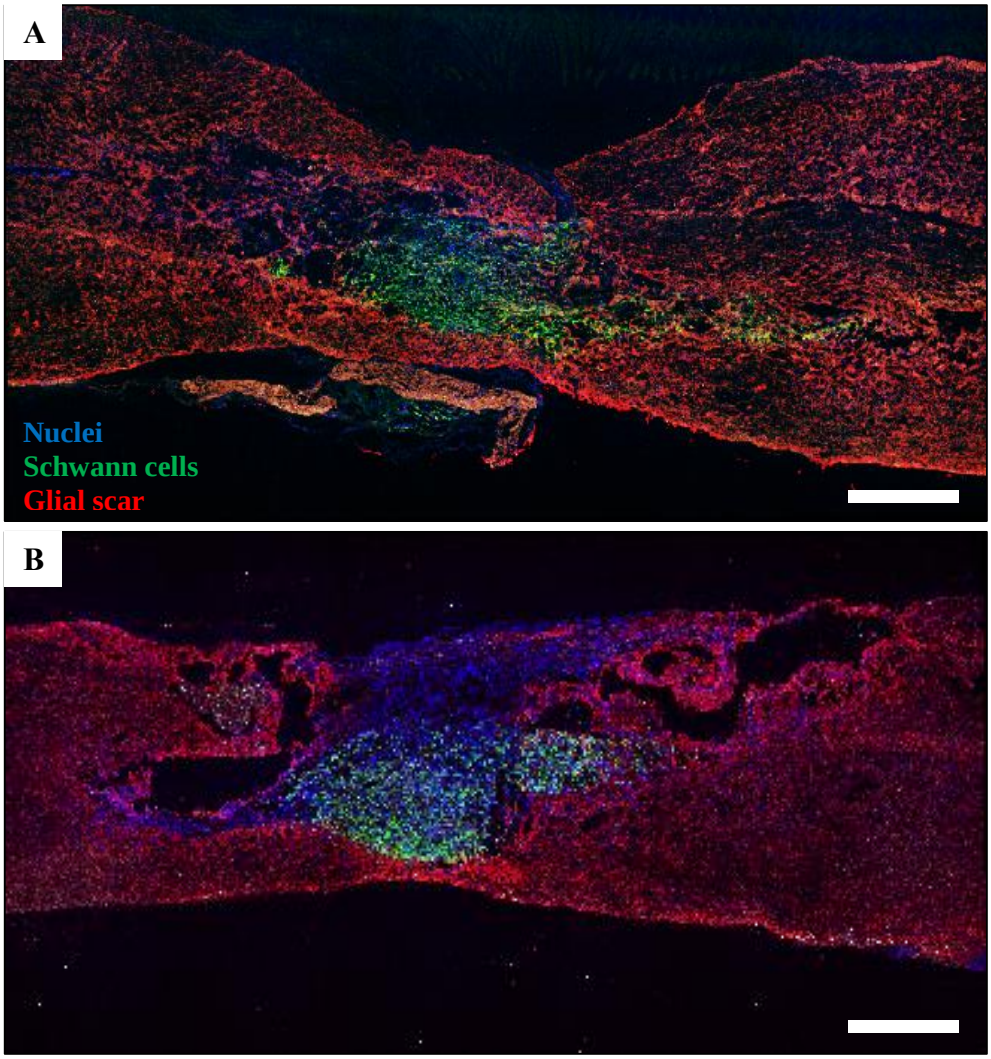

Figure 5.2: Matrigel and injectable nerve both support Schwann cell survival and maintenance in the SCI lesion. Longitudinal tissue sections were stained for GFAP (red, astrocytic glial scar) and GFP (green, Schwann cells). Nuclei are counterstained with Hoescht (blue). Representative sections are shown in A for Matrigel and B for injectable nerve. Scale bars represent 1 mm.

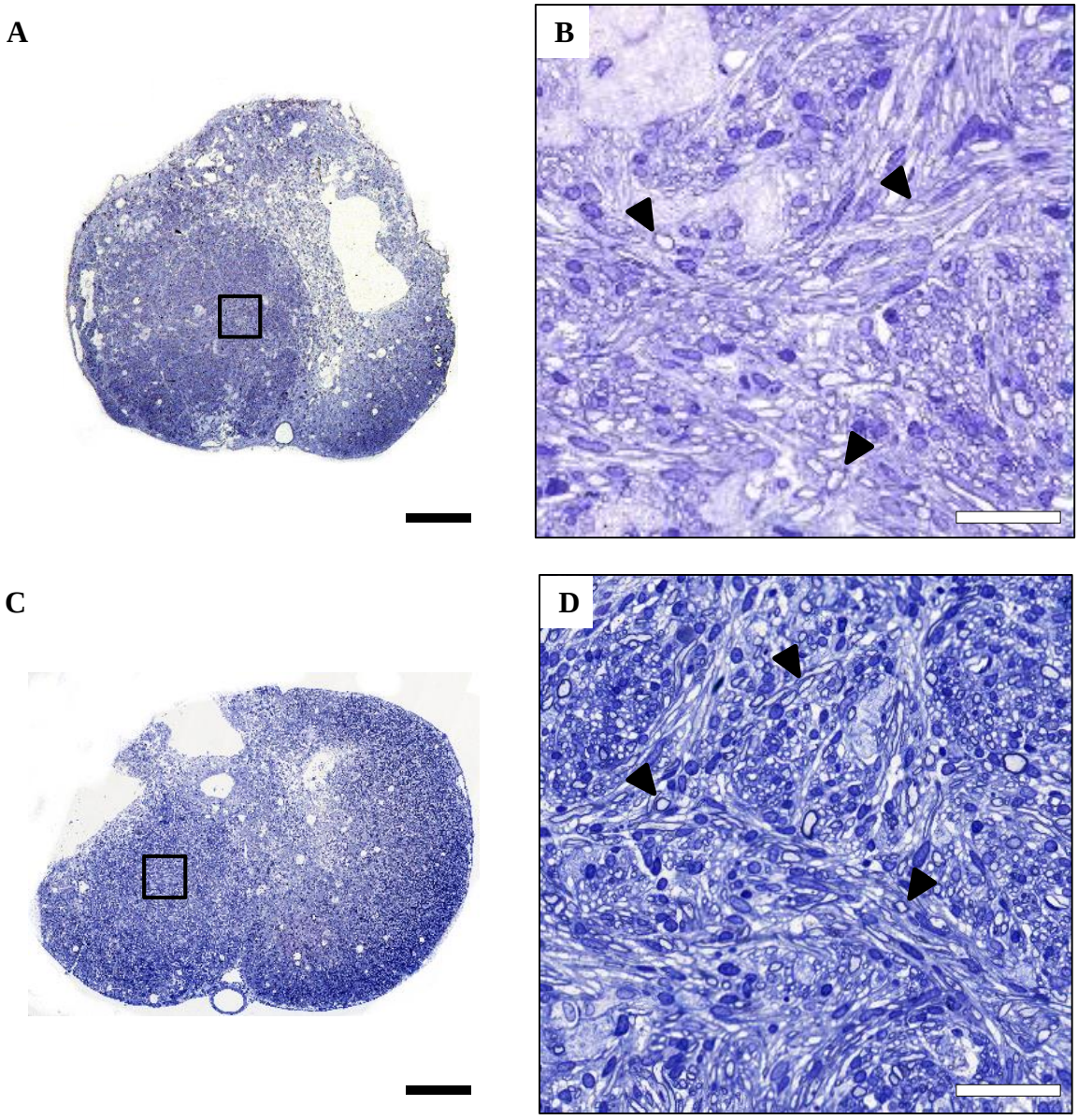

Figure 5.3: Toluidine blue staining reveals robust myelination by transplanted Schwann cells in both materials. Semi-thin plastic sections were stained with toluidine blue to label myelin deposits and imaged by light microscopy. Numerous myelinated axons were observed in animals treated with Matrigel (A and B) and injectable nerve (C and D). Black arrow heads indicate representative positive staining for myelin. Scale bars represent 500 µm for A and C and 50 µm for B and D.

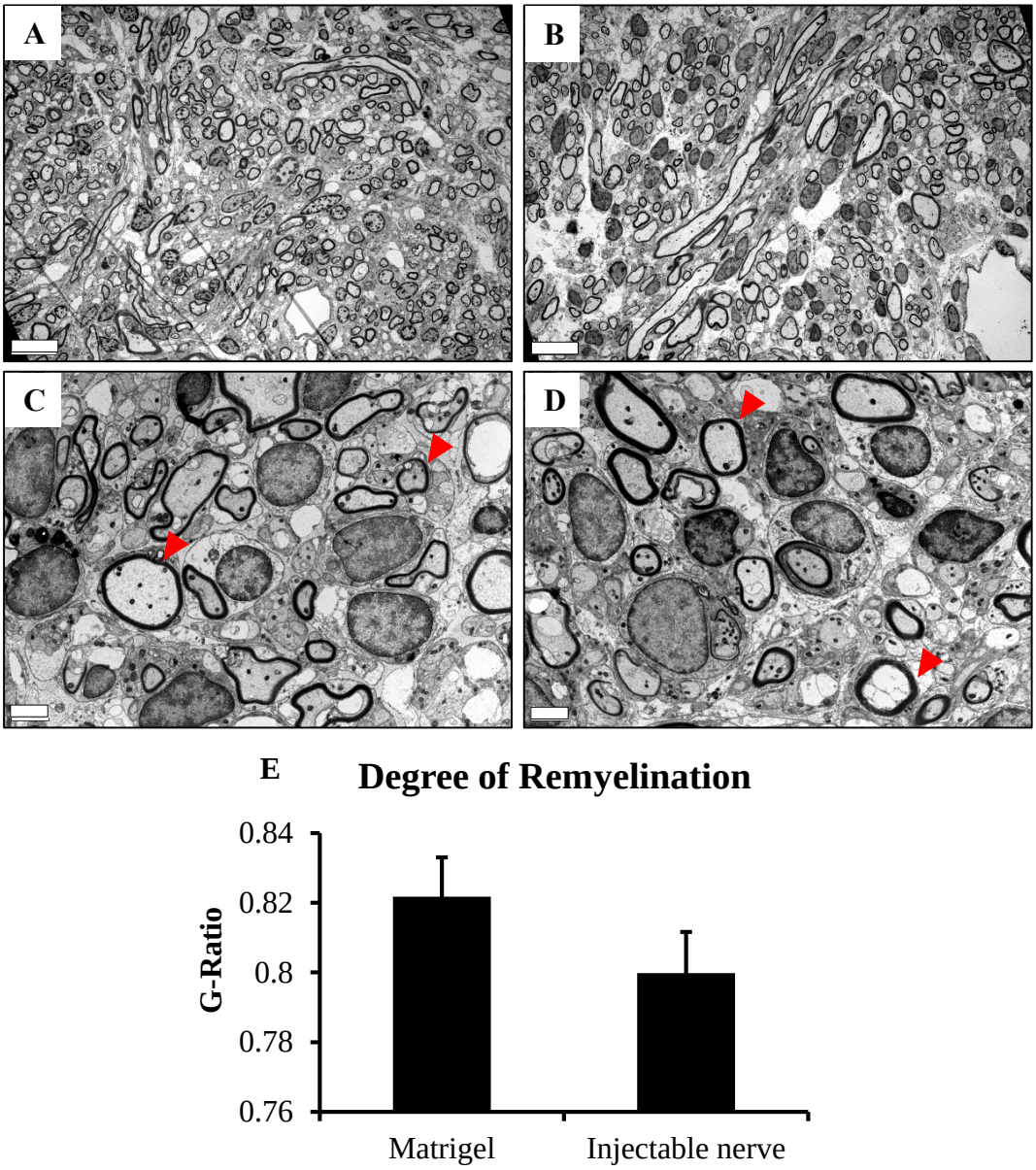

Figure 5.4: Myelination by transplanted Schwann cells is similar in Matrigel and injectable nerve matrices. Semi-thin plastic sections were stained with toluidine blue to label myelin deposits and imaged by transmission electron microscopy. Red arrow heads indicate representative myelinated axons. Scale bars indicate 10 µm in A and B and 2 µm in C and D. (E) Preliminary evidence suggests the g-ratio of myelinated axons was not statistically different for Matrigel and injectable nerve treated animals, though the latter exhibited a ratio closer to the optimal 0.77 (n=3 images per group).

5.2.3. Hindlimb Functional Recovery

To assess if the histological results correspond to functional recovery, three behavioral analyses were used to assess hindlimb function for 8 weeks following Schwann cell transplantation. The BBB test revealed no statistical differences between the three groups at any time point tested (**Figure 5.5A**). Noticeably faster recovery was observed using the nerve matrix in BBB subscores, although the differences were again not significant (**Figure 5.5B**). Grid walk analysis did reveal statistical differences, with animals in the injectable nerve group (without D15A) demonstrating fewer footslips at 4 weeks than the other two groups (**Figure 5.6D**). These differences were equalized by 8 weeks, however, and the differences in number of footfalls and total percentage of error did not achieve significance at either time. Surprisingly, the D15A Schwann cell group consistently scored below the other two groups, with BBB scores occasionally statistically below the others. These data demonstrate that neurotrophin supplementation is not required to support Schwann cell transplantation in nerve matrices and in fact may have a transitory, detrimental effect in combination with this material.

Increased sensitivity to pain was assessed using von Frey filaments to probe the animals' footpads prior to injury and 2, 4, and 8 weeks after transplantation. The minimum force required to elicit a motor response for each group is shown in **Figure 5.7**. The data were highly variable, with large standard deviations, and no differences were observed before and after injury or between treatment groups at these select time points.

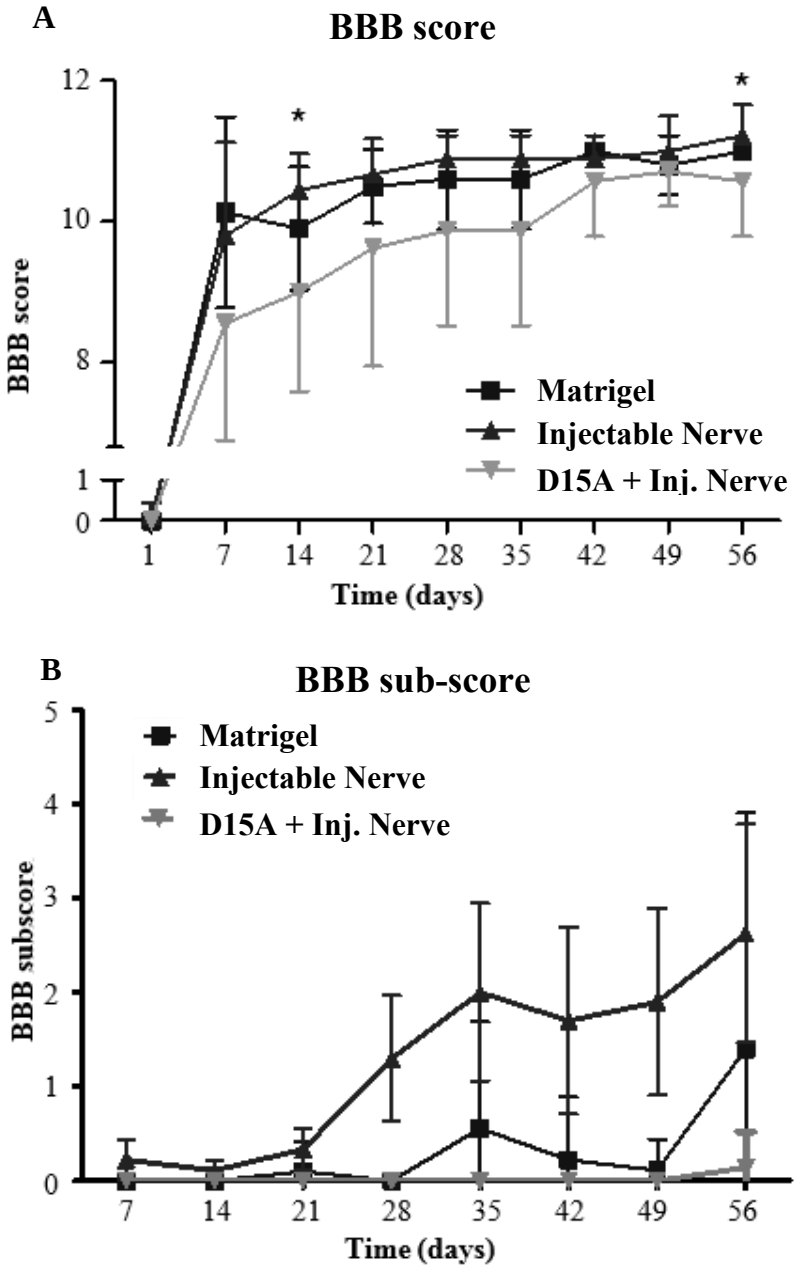

Figure 5.5: Locomotor function assessed by BBB tests. Animals were assessed for hindlimb functional recovery for 8 weeks post-Schwann cell transplantation using (A) BBB scores and (B) BBB subscores. Animals treated with injectable nerve and Matrigel matrices performed similarly and significantly better than animals treated using injectable nerve and transgenic Schwann cells expressing D15A at 2 and 9 weeks. (*$p<0.05$).

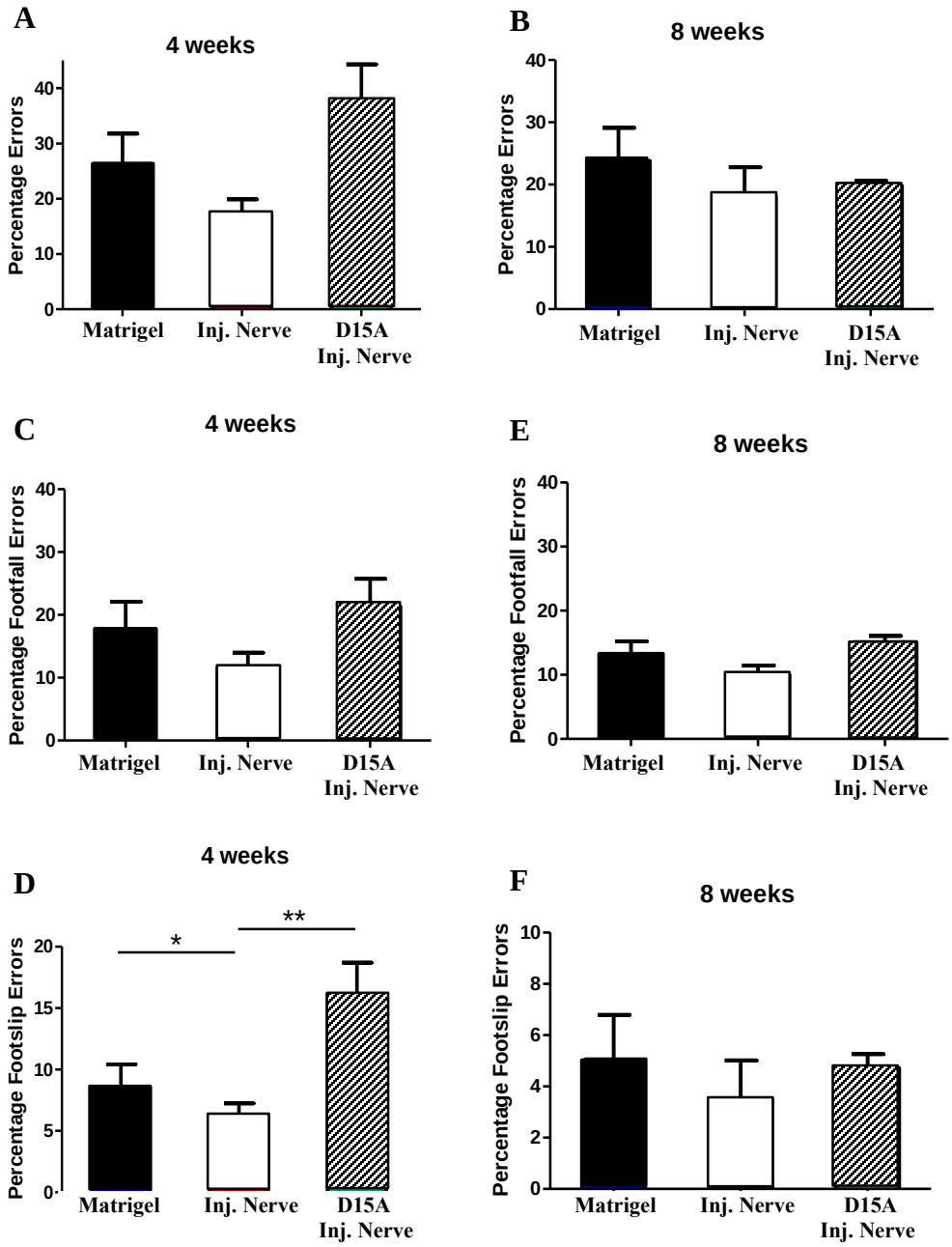

Figure 5.6: Motor coordination assessed by Grid Walk test revealed more rapid recovery with injectable nerve transplants but not D15A Schwann cells. Graphical representation of the footfall (left) and foot slip (right) errors counted, at 4 and 8 weeks post Schwann cell transplantation. *p<0.05; **p<0.01. Motor coordination assessed by Grid Walk test. Graphical representation of the total number of errors (footfalls + foot slips), 4 and 8 weeks after Schwann cell transplantation.

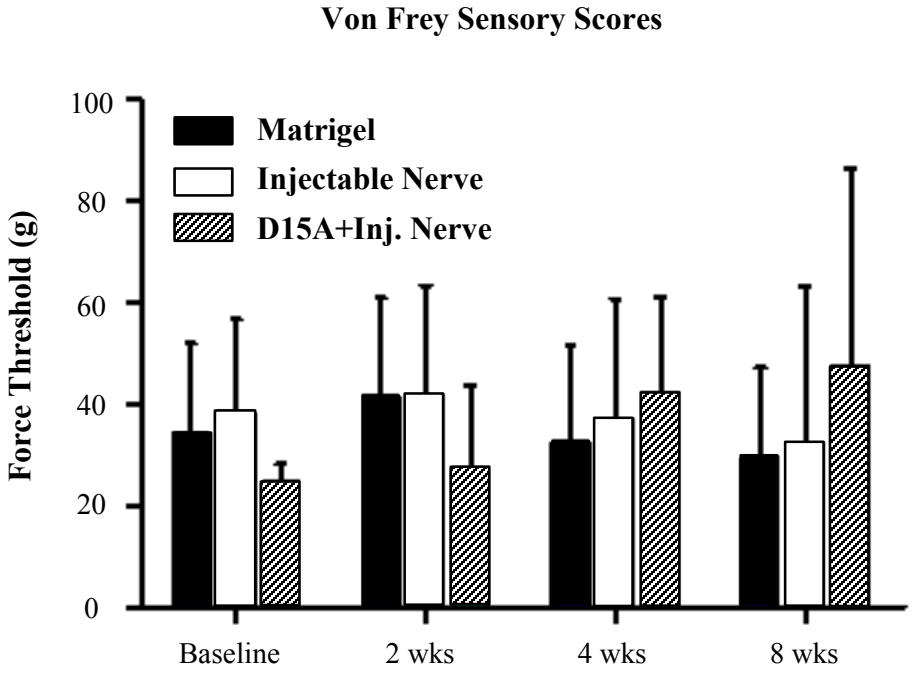

Figure 5.7: Application of Matrigel or injectable nerve after SCI did not increase sensitivity to mechanical stimuli. Von Frey filaments were used to probe the footpads of animals prior to injury and 2, 4, and 8 weeks after Schwann cell transplantation. No significant differences were observed for any treatment group at any time point as a result of large variation. Error bars represent standard deviation.

5.3. DISCUSSION

Given the promise of cell therapy for treating a number of pathologies, including SCI, there is a significant need for developing engineered materials to support and enhance cell transplantation. A key design criterion is that the materials are injectable such that they enable easier incorporation of exogenous cells. For SCI specifically, an injectable therapy can also limit the risk of causing additional damage during its application. It's also critical to consider the material's role in providing cell support. Detaching adherence-dependent cells from a substrate, effectively eliminating interactions with extracellular matrix ligands, increases the potential for cell death (Gilmore 2005). Resuspending these cells in solutions containing extracellular ligands such as in Matrigel can prevent this effect (He *et al.* 2015). In fact, Matrigel is widely used as a transplantation medium and is particularly useful for neural applications given the high laminin content. However, because tumor-derived Matrigel is unlikely to obtain FDA approval, biomaterial scientists are tasked with creating an alternative that is equivalent or better than Matrigel in supporting cell transplantation but with more translational potential.

One important solution in the field is injectable materials based on natural, decellularized tissue. These tissue matrices can provide cells with extracellular ligands at biologically-relevant concentrations, which may enhance the cellular response. Our approach was to implement an injectable matrix derived from acellular peripheral nerve to support Schwann cell transplantation after SCI. This new material is based on decellularized nerve tissue used clinically and therefore capitalizes on a translational precedent. Furthermore, because Schwann cells are native to peripheral nerve tissue, this

material may provide tissue-specific factors to bolster the efficacy of Schwann cell transplantation to treat SCI.

Both Matrigel and injectable nerve supported maintenance and survival of transplanted Schwann cells in the SCI lesion. Additionally, robust axonal myelination was observed by transplanted cells, achieving a g-ratio of 0.82 and 0.80 in Matrigel and injectable nerve, respectively, similar to an optimal value of 0.77 for CNS (Chomiak and Hu 2009). Myelination undoubtedly plays a role in reestablishing function, and injectable nerve transplants promoted equivalent recovery of hindlimb function compared to Matrigel transplants. Animals treated with the nerve scaffold also experienced faster recovery, demonstrating significantly fewer footslips at 4 weeks compared to Matrigel transplanted animals. Neither material contributed to an increase in sensitivity to mechanical stimuli.

5.4. CONCLUSIONS

An injectable acellular nerve matrix effectively supports Schwann cell transplantation after SCI. Both this material and Matrigel, a common positive control, enabled extensive myelination by grafted cells. Animals treated with injectable nerve demonstrated equivalent yet faster recovery of hindlimb function than Matrigel treated animals according to BBB and grid walk analysis. Despite the high growth factor content of Matrigel, the injectable nerve matrix did not require growth factor supplementation to achieve these effects. In fact, combining this material with Schwann cells expressing the neurotrophin D15A appeared to counterintuitively hinder recovery. Given that acellular nerve tissue is currently used in the clinic, an injectable acellular nerve may be a clinically-viable alternative to tumor-derived Matrigel for Schwann cell therapy after SCI.

Chapter 6: Dissertation Synopsis

6.1. Major Findings

This dissertation detailed development, characterization, and evaluation of an injectable acellular nerve graft for treating contusion SCI in rats. The described material recreates properties of native neural tissue and therefore offers a minimally-invasive method to provide chemical and mechanical cues similar to structured nerve grafts for promoting spinal cord regeneration. Once injected into a spinal cord lesion, injectable nerve grafts altered the immune response to injury after one week by decreasing the ratio of inflammatory to regenerative macrophages. Injecting this material alone after cervical contusion SCI increased the presence of axonal fibers in the lesion and also at the distal interface between lesion and intact spinal cord 8 weeks post-injection. Nonetheless, the functional baseline for injectable nerve was similar to PBS injection, indicating this scaffold can be used to support other therapies without causing detrimental effects. Combining injectable nerve scaffolds with Schwann cell transplantation, for example, promoted recovery of hindlimb functional after thoracic contusion in rats. This strategy resulted in functional and histological outcomes comparable to the commonly used but clinically-irrelevant Matrigel scaffold while also speeding recovery time.

6.1.1. Specific Aim 1

- An injectable, thermally gelling version of acellular nerve tissue was achieved by optimizing pepsin digestion
- Injectable acellular nerve tissue retained several compositional identifiers of native nerve tissue such as collagen, laminin, and glycosaminoglycans

- Acellular nerve hydrogels were tuned to match the mechanical properties of native rat neural tissue
- Schwann cells adhered to and survived on injectable nerve coated substrates *in vitro*
- Extracellular matrix components in injectable nerve altered the immune response to SCI, promoting more pro-regenerative macrophage phenotypes after one week *in vivo*

6.1.2. Specific Aim 2

- Histological outcomes showed no detriment to lesion volume and an increase in axonal fibers in the lesion and at the distal interface with the intact cord
- Delivery of injectable nerve after cervical SCI in rats did not negatively influence recovery of forelimb and respiratory recovery
- A therapeutic baseline similar to saline injection suggests injectable nerve may be used to support or enhance other interventions

6.1.3. Specific Aim 3

- Schwann cells transplanted in injectable nerve scaffolds exhibited robust myelination by 8 weeks after injection
- Combination of injectable nerve with Schwann cell therapy promoted equivalent yet faster recovery of hindlimb function compared to using Matrigel
- Neurotrophin supplementation using transgenic expression of D15A was not necessary for functional recovery using injectable nerve matrices

6.2. Overall Conclusions

Acellular nerve grafts can be reformulated into an injectable form that recreates native nerve chemical and mechanical cues following gelation at physiological conditions. This injectable nerve graft is biocompatible and promotes pro-regenerative immune cell phenotypes upon implantation into a contusion SCI cavity. While providing equivalent functional recovery to saline when implanted alone, injectable nerve scaffolds are a platform on which to build new intervention strategies for SCI. It was demonstrated that using injectable nerve grafts to support Schwann cell transplantation results in comparable yet significantly faster recovery of hindlimb function compared to using Matrigel in a rat model of thoracic contusion SCI. These results indicate injectable nerve scaffolds, based on clinically-approved acellular nerve technology, are an effective and clinically-viable alternative to non-translatable Matrigel for enhancing interventions for SCI.

6.3. Limitations and Future Work

A major limitation of this research was a lack of additional cell culture experiments for better characterizing the ability of injectable nerve scaffolds to support axon regeneration prior to *in vivo* assessment. Three dimensional cell culture in injectable nerve proved difficult. In assessing the cause, preliminary experiments suggested extensive washing of acellular nerves was necessary to eliminate CSPG fragments after chondroitinase treatment (data not presented). With minimal washing, as was initially performed, CSPG fragments remaining in the matrix were potentially promoting detachment and death of encapsulated Schwann cells. This factor proved a non-issue in preliminary *in vivo* experiments and hence that route was taken in place of additional

attempts at cell culture. Better in vitro characterization of the cellular response to injectable nerve should be performed given the issue is potentially resolved.

A second limitation is the use of singular cell markers to examine the immune response to material implantation. While CCR7 and CD206 are commonly used to identify M1 and M2 macrophages, respectively, they represent only one characteristic on the full spectrum of macrophage phenotype. Gene expression analysis should be conducted in future experiments to array a wider variety of phenotypic markers, such as CD80, CD86, and CD16/32 for M1 cells and Arginase 1 and CD163 for M2 cells (Kigerl *et al.* 2009). A more in-depth analysis should also be conducted to examine the influence of different subsets of M2 macrophages (M2a, M2b, and M2c) as well as the differential influence of invading macrophages and resident microglia (B. N. Brown *et al.* 2012; David and Kroner 2011). The latter may only be possible using transgenic animals or following better identification of cell markers to delineation these cell types after injury.

A final limitation of this work was the potential for low material residence time following application into an SCI cavity. Without adding exogenous cells, a pre-digested ECM scaffold may be subjected to faster clearance *in vivo*, limiting its potential to promote extended and robust axon regeneration. For material implantation alone, it may be necessary to delay ECM turnover using crosslinkers such as genipin (Tan *et al.* 2011) or small leucine rich proteoglycans such as decorin that coat and protect collagen from degradation and phagocytosis (Geng *et al.* 2006; Bhide *et al.* 2005). An alternative approach, as performed here, is to combine the material with exogenous cells that will replace the matrix over time. This method may prove most beneficial as cells can also secrete factors to promote axonal regeneration and further reform the injury environment.

Appendix

Image Threshold Information for Immune Cell Quantification

Initial Criteria	ED1 (488 nm)	CD206 (568 nm)	CCR7 (568 nm)
Threshold	1600-7842	1600-7842	1600-7842
Sharpen (Unsharp Mask)	0.5	0.5	0.5
Shed (Watershed)	count 3	count 3	count 3
Tolerance	3%	3%	3%
Neighbors	1	1	1
Minimum area	230	300	300
Refinement			
Max Area	815	900	900
Min Circularity	0.58	0.58	0.58
Max Circularity	1.00	1.00	1.00
Min Intensity, DAPI	N/A	1500	1500

References

Agrawal, V., S. Tottey, S. A. Johnson, J. M. Freund, B. F. Siu and S. F. Badylak (2011). "Recruitment of progenitor cells by an extracellular matrix cryptic peptide in a mouse model of digit amputation." Tissue Eng Part A **17**(19-20): 2435-2443.

Alilain, W. J., K. P. Horn, H. Hu, T. E. Dick and J. Silver (2011). "Functional regeneration of respiratory pathways after spinal cord injury." Nature **475**(7355): 196-200.

Allred, R. P., D. L. Adkins, M. T. Woodlee, L. C. Husbands, M. A. Maldonado, J. R. Kane, T. Schallert and T. A. Jones (2008). "The vermicelli handling test: a simple quantitative measure of dexterous forepaw function in rats." J Neurosci Methods **170**(2): 229-244.

Ansorena, E., P. De Berdt, B. Ucakar, T. Simon-Yarza, D. Jacobs, O. Schakman, A. Jankovski, R. Deumens, M. J. Blanco-Prieto, V. Preat and A. des Rieux (2013). "Injectable alginate hydrogel loaded with GDNF promotes functional recovery in a hemisection model of spinal cord injury." Int J Pharm **455**(1-2): 148-158.

Austin, J. W., C. E. Kang, M. D. Baumann, L. DiDiodato, K. Satkunendrarajah, J. R. Wilson, G. J. Stanisz, M. S. Shoichet and M. G. Fehlings (2012). "The effects of intrathecal injection of a hyaluronan-based hydrogel on inflammation, scarring and neurobehavioural outcomes in a rat model of severe spinal cord injury associated with arachnoiditis." Biomaterials **33**(18): 4555-4564.

Badylak, S. F., J. E. Valentin, A. K. Ravindra, G. P. McCabe and A. M. Stewart-Akers (2008). "Macrophage phenotype as a determinant of biologic scaffold remodeling." Tissue Eng Part A **14**(11): 1835-1842.

Baiguera, S., C. Del Gaudio, E. Lucatelli, E. Kuevda, M. Boieri, B. Mazzanti, A. Bianco and P. Macchiarini (2014). "Electrospun gelatin scaffolds incorporating rat decellularized brain extracellular matrix for neural tissue engineering." Biomaterials **35**(4): 1205-1214.

Barritt, A. W., M. Davies, F. Marchand, R. Hartley, J. Grist, P. Yip, S. B. McMahon and E. J. Bradbury (2006). "Chondroitinase ABC promotes sprouting of intact and injured spinal systems after spinal cord injury." J Neurosci **26**(42): 10856-10867.

Bartus, K., N. D. James, A. Didangelos, K. D. Bosch, J. Verhaagen, R. J. Yanez-Munoz, J. H. Rogers, B. L. Schneider, E. M. Muir and E. J. Bradbury (2014). "Large-scale chondroitin sulfate proteoglycan digestion with chondroitinase gene therapy leads to reduced pathology and modulates macrophage phenotype following spinal cord contusion injury." J Neurosci **34**(14): 4822-4836.

Basso, D. M., M. S. Beattie and J. C. Bresnahan (1995). "A sensitive and reliable locomotor rating scale for open field testing in rats." J Neurotrauma **12**(1): 1-21.

Basso, D. M., M. S. Beattie and J. C. Bresnahan (1996). "Graded histological and locomotor outcomes after spinal cord contusion using the NYU weight-drop device versus transection." Exp Neurol **139**(2): 244-256.

Baumann, M. D., C. E. Kang, C. H. Tator and M. S. Shoichet (2010). "Intrathecal delivery of a polymeric nanocomposite hydrogel after spinal cord injury." Biomaterials **31**(30): 7631-7639.

Bhide, V. M., C. A. Laschinger, P. D. Arora, W. Lee, L. Hakkinen, H. Larjava, J. Sodek and C. A. McCulloch (2005). "Collagen phagocytosis by fibroblasts is regulated by decorin." J Biol Chem **280**(24): 23103-23113.

Bible, E., F. Dell'Acqua, B. Solanky, A. Balducci, P. M. Crapo, S. F. Badylak, E. T. Ahrens and M. Modo (2012). "Non-invasive imaging of transplanted human neural stem cells and ECM scaffold remodeling in the stroke-damaged rat brain by (19)F- and diffusion-MRI." Biomaterials **33**(10): 2858-2871.

Blam, O. G., A. R. Vaccaro, J. S. Vanichkachorn, T. J. Albert, A. S. Hilibrand, J. M. Minnich and S. A. Murphey (2003). "Risk factors for surgical site infection in the patient with spinal injury." Spine (Phila Pa 1976) **28**(13): 1475-1480.

Bradbury, E. J., L. D. Moon, R. J. Popat, V. R. King, G. S. Bennett, P. N. Patel, J. W. Fawcett and S. B. McMahon (2002). "Chondroitinase ABC promotes functional recovery after spinal cord injury." Nature **416**(6881): 636-640.

Brown, A. and L. C. Weaver (2012). "The dark side of neuroplasticity." Exp Neurol **235**(1): 133-141.

Brown, B. N., B. D. Ratner, S. B. Goodman, S. Amar and S. F. Badylak (2012). "Macrophage polarization: an opportunity for improved outcomes in biomaterials and regenerative medicine." Biomaterials **33**(15): 3792-3802.

Brown, B. N., J. E. Valentin, A. M. Stewart-Akers, G. P. McCabe and S. F. Badylak (2009). "Macrophage phenotype and remodeling outcomes in response to biologic scaffolds with and without a cellular component." Biomaterials **30**(8): 1482-1491.

Busch, S. A., J. A. Hamilton, K. P. Horn, F. X. Cuascut, R. Cutrone, N. Lehman, R. J. Deans, A. E. Ting, R. W. Mays and J. Silver (2011). "Multipotent adult progenitor cells

prevent macrophage-mediated axonal dieback and promote regrowth after spinal cord injury." J Neurosci **31**(3): 944-953.

Cafferty, W. B., P. Duffy, E. Huebner and S. M. Strittmatter (2010). "MAG and OMgp synergize with Nogo-A to restrict axonal growth and neurological recovery after spinal cord trauma." J Neurosci **30**(20): 6825-6837.

Cantinieaux, D., R. Quertainmont, S. Blacher, L. Rossi, T. Wanet, A. Noel, G. Brook, J. Schoenen and R. Franzen (2013). "Conditioned medium from bone marrow-derived mesenchymal stem cells improves recovery after spinal cord injury in rats: an original strategy to avoid cell transplantation." PLoS One **8**(8): e69515.

Cao, Y., J. S. Shumsky, M. A. Sabol, R. A. Kushner, S. Strittmatter, F. P. Hamers, D. H. Lee, S. A. Rabacchi and M. Murray (2008). "Nogo-66 receptor antagonist peptide (NEP1-40) administration promotes functional recovery and axonal growth after lateral funiculus injury in the adult rat." Neurorehabil Neural Repair **22**(3): 262-278.

Cardenas, D. D. and T. M. Hooton (1995). "Urinary tract infection in persons with spinal cord injury." Arch Phys Med Rehabil **76**(3): 272-280.

Chaplan, S. R., F. W. Bach, J. W. Pogrel, J. M. Chung and T. L. Yaksh (1994). "Quantitative assessment of tactile allodynia in the rat paw." J Neurosci Methods **53**(1): 55-63.

Chen, J., Z. Zhang, J. Liu, R. Zhou, X. Zheng, T. Chen, L. Wang, M. Huang, C. Yang, Z. Li, C. Yang, X. Bai and D. Jin (2014). "Acellular spinal cord scaffold seeded with bone marrow stromal cells protects tissue and promotes functional recovery in spinal cord-injured rats." J Neurosci Res **92**(3): 307-317.

Chen, Z. L. and S. Strickland (2003). "Laminin gamma1 is critical for Schwann cell differentiation, axon myelination, and regeneration in the peripheral nerve." J Cell Biol **163**(4): 889-899.

Cheng, H., Y. C. Huang, P. T. Chang and Y. Y. Huang (2007). "Laminin-incorporated nerve conduits made by plasma treatment for repairing spinal cord injury." Biochem Biophys Res Commun **357**(4): 938-944.

Cheriyan, T., D. J. Ryan, J. H. Weinreb, J. Cheriyan, J. C. Paul, V. Lafage, T. Kirsch and T. J. Errico (2014). "Spinal cord injury models: a review." Spinal Cord **52**(8): 588-595.

Chernousov, M. A., R. C. Stahl and D. J. Carey (2001). "Schwann cell type V collagen inhibits axonal outgrowth and promotes Schwann cell migration via distinct adhesive activities of the collagen and noncollagen domains." J Neurosci **21**(16): 6125-6135.

Chomiak, T. and B. Hu (2009). "What is the optimal value of the g-ratio for myelinated fibers in the rat CNS? A theoretical approach." PLoS One **4**(11): e7754.

Christman, K. L., A. J. Vardanian, Q. Fang, R. E. Sievers, H. H. Fok and R. J. Lee (2004). "Injectable fibrin scaffold improves cell transplant survival, reduces infarct expansion, and induces neovasculature formation in ischemic myocardium." J Am Coll Cardiol **44**(3): 654-660.

Chua, J. S., C. P. Chng, A. A. Moe, J. Y. Tann, E. L. Goh, K. H. Chiam and E. K. Yim (2014). "Extending neurites sense the depth of the underlying topography during neuronal differentiation and contact guidance." Biomaterials **35**(27): 7750-7761.

Colin, S., J. C. Jeanny, F. Mascarelli, R. Vienet, S. Al-Mahmood, Y. Courtois and J. Labarre (1999). "In vivo involvement of heparan sulfate proteoglycan in the bioavailability, internalization, and catabolism of exogenous basic fibroblast growth factor." Mol Pharmacol **55**(1): 74-82.

Crapo, P. M., S. Tottey, P. F. Slivka and S. F. Badylak (2014). "Effects of biologic scaffolds on human stem cells and implications for CNS tissue engineering." Tissue Eng Part A **20**(1-2): 313-323.

Darlot, F., F. Cayetanot, P. Gauthier, V. Matarazzo and A. Kastner (2012). "Extensive respiratory plasticity after cervical spinal cord injury in rats: axonal sprouting and rerouting of ventrolateral bulbospinal pathways." Exp Neurol **236**(1): 88-102.

David, S. and A. J. Aguayo (1981). "Axonal elongation into peripheral nervous system "bridges" after central nervous system injury in adult rats." Science **214**(4523): 931-933.

David, S. and A. Kroner (2011). "Repertoire of microglial and macrophage responses after spinal cord injury." Nat Rev Neurosci **12**(7): 388-399.

De Waele, J., K. Reekmans, J. Daans, H. Goossens, Z. Berneman and P. Ponsaerts (2015). "3D culture of murine neural stem cells on decellularized mouse brain sections." Biomaterials **41**: 122-131.

Deister, C., S. Aljabari and C. E. Schmidt (2007). "Effects of collagen 1, fibronectin, laminin and hyaluronic acid concentration in multi-component gels on neurite extension." J Biomater Sci Polym Ed **18**(8): 983-997.

DeQuach, J. A., J. E. Lin, C. Cam, D. Hu, M. A. Salvatore, F. Sheikh and K. L. Christman (2012). "Injectable skeletal muscle matrix hydrogel promotes neovascularization and muscle cell infiltration in a hindlimb ischemia model." Eur Cell Mater **23**: 400-412; discussion 412.

DeQuach, J. A., S. H. Yuan, L. S. Goldstein and K. L. Christman (2011). "Decellularized porcine brain matrix for cell culture and tissue engineering scaffolds." Tissue Eng Part A **17**(21-22): 2583-2592.

Doperalski, N. J., M. S. Sandhu, R. W. Bavis, P. J. Reier and D. D. Fuller (2008). "Ventilation and phrenic output following high cervical spinal hemisection in male vs. female rats." Respir Physiol Neurobiol **162**(2): 160-167.

Duan, Y., Z. Liu, J. O'Neill, L. Q. Wan, D. O. Freytes and G. Vunjak-Novakovic (2011). "Hybrid gel composed of native heart matrix and collagen induces cardiac differentiation of human embryonic stem cells without supplemental growth factors." J Cardiovasc Transl Res **4**(5): 605-615.

Dupont, S., L. Morsut, M. Aragona, E. Enzo, S. Giulitti, M. Cordenonsi, F. Zanconato, J. Le Digabel, M. Forcato, S. Bicciato, N. Elvassore and S. Piccolo (2011). "Role of YAP/TAZ in mechanotransduction." Nature **474**(7350): 179-183.

Engler, A. J., S. Sen, H. L. Sweeney and D. E. Discher (2006). "Matrix elasticity directs stem cell lineage specification." Cell **126**(4): 677-689.

Faulk, D. M., C. A. Carruthers, H. J. Warner, C. R. Kramer, J. E. Reing, L. Zhang, A. D'Amore and S. F. Badylak (2014). "The effect of detergents on the basement membrane complex of a biologic scaffold material." Acta Biomater **10**(1): 183-193.

Fex Svennigsen, A. and L. B. Dahlin (2013). "Repair of the Peripheral Nerve-Remyelination that Works." Brain Sci **3**(3): 1182-1197.

Fitch, M. T. and J. Silver (2008). "CNS injury, glial scars, and inflammation: Inhibitory extracellular matrices and regeneration failure." Exp Neurol **209**(2): 294-301.

Flanagan, L. A., Y. E. Ju, B. Marg, M. Osterfield and P. A. Janmey (2002). "Neurite branching on deformable substrates." Neuroreport **13**(18): 2411-2415.

Forgione, N., S. K. Karadimas, W. D. Foltz, K. Satkunendrarajah, A. Lip and M. G. Fehlings (2014). "Bilateral contusion-compression model of incomplete traumatic cervical spinal cord injury." J Neurotrauma **31**(21): 1776-1788.

Fozdar, D. Y., J. Y. Lee, C. E. Schmidt and S. C. Chen (2011). "Selective axonal growth of embryonic hippocampal neurons according to topographic features of various sizes and shapes." International Journal of Nanomedicine **6**: 45-57.

Freytes, D. O., J. Martin, S. S. Velankar, A. S. Lee and S. F. Badylak (2008). "Preparation and rheological characterization of a gel form of the porcine urinary bladder matrix." Biomaterials **29**(11): 1630-1637.

Frith, J. E., R. J. Mills, J. E. Hudson and J. J. Cooper-White (2012). "Tailored integrin-extracellular matrix interactions to direct human mesenchymal stem cell differentiation." Stem Cells Dev **21**(13): 2442-2456.

Fruhstorfer, H., W. Gross and O. Selbmann (2001). "von Frey hairs: new materials for a new design." Eur J Pain **5**(3): 341-342.

Fuhrmann, T., L. M. Hillen, K. Montzka, M. Woltje and G. A. Brook (2010). "Cell-cell interactions of human neural progenitor-derived astrocytes within a microstructured 3D-scaffold." Biomaterials **31**(30): 7705-7715.

Fuhrmann, T., J. Obermeyer, C. H. Tator and M. S. Shoichet (2015). "Click-crosslinked injectable hyaluronic acid hydrogel is safe and biocompatible in the intrathecal space for ultimate use in regenerative strategies of the injured spinal cord." Methods.

Fuller, D. D., N. J. Doperalski, B. J. Dougherty, M. S. Sandhu, D. C. Bolser and P. J. Reier (2008). "Modest spontaneous recovery of ventilation following chronic high cervical hemisection in rats." Exp Neurol **211**(1): 97-106.

Fuller, D. D., F. J. Golder, E. B. Olson, Jr. and G. S. Mitchell (2006). "Recovery of phrenic activity and ventilation after cervical spinal hemisection in rats." J Appl Physiol (1985) **100**(3): 800-806.

Fuller, D. D., M. S. Sandhu, N. J. Doperalski, M. A. Lane, T. E. White, M. D. Bishop and P. J. Reier (2009). "Graded unilateral cervical spinal cord injury and respiratory motor recovery." Respir Physiol Neurobiol **165**(2-3): 245-253.

Geng, Y., D. McQuillan and P. J. Roughley (2006). "SLRP interaction can protect collagen fibrils from cleavage by collagenases." Matrix Biol **25**(8): 484-491.

Georgiou, M., S. C. Bunting, H. A. Davies, A. J. Loughlin, J. P. Golding and J. B. Phillips (2013). "Engineered neural tissue for peripheral nerve repair." Biomaterials **34**(30): 7335-7343.

Georgiou, M., J. P. Golding, A. J. Loughlin, P. J. Kingham and J. B. Phillips (2015). "Engineered neural tissue with aligned, differentiated adipose-derived stem cells promotes peripheral nerve regeneration across a critical sized defect in rat sciatic nerve." Biomaterials **37**: 242-251.

Gilbert, T. W. (2012). "Strategies for tissue and organ decellularization." J Cell Biochem **113**(7): 2217-2222.

Gilmore, A. P. (2005). "Anoikis." Cell Death Differ **12 Suppl 2**: 1473-1477.

Giusto, E., M. Donega, C. Cossetti and S. Pluchino (2014). "Neuro-immune interactions of neural stem cell transplants: from animal disease models to human trials." Exp Neurol **260**: 19-32.

Golden, K. L., D. D. Pearse, B. Blits, M. S. Garg, M. Oudega, P. M. Wood and M. B. Bunge (2007). "Transduced Schwann cells promote axon growth and myelination after spinal cord injury." Exp Neurol **207**(2): 203-217.

Gomez-Pinilla, F., J. R. Huie, Z. Ying, A. R. Ferguson, E. D. Crown, K. M. Baumbauer, V. R. Edgerton and J. W. Grau (2007). "BDNF and learning: Evidence that instrumental training promotes learning within the spinal cord by up-regulating BDNF expression." Neuroscience **148**(4): 893-906.

Gu, Y., Y. Ji, Y. Zhao, Y. Liu, F. Ding, X. Gu and Y. Yang (2012). "The influence of substrate stiffness on the behavior and functions of Schwann cells in culture." Biomaterials **33**(28): 6672-6681.

Guo, S. Z., X. J. Ren, B. Wu and T. Jiang (2010). "Preparation of the acellular scaffold of the spinal cord and the study of biocompatibility." Spinal Cord **48**(7): 576-581.

Gupta, D., C. H. Tator and M. S. Shoichet (2006). "Fast-gelling injectable blend of hyaluronan and methylcellulose for intrathecal, localized delivery to the injured spinal cord." Biomaterials **27**(11): 2370-2379.

Hardy, J. G., R. C. Cornelison, R. C. Sukhavasi, R. J. Saballos, P. Vu, D. L. Kaplan and C. E. Schmidt (2015). "Electroactive Tissue Scaffolds with Aligned Pores as Instructive Platforms for Biomimetic Tissue Engineering." Bioengineering **2**(1): 15-34.

Hargreaves, K., R. Dubner, F. Brown, C. Flores and J. Joris (1988). "A new and sensitive method for measuring thermal nociception in cutaneous hyperalgesia." Pain **32**(1): 77-88.

He, N., Y. Xu, W. Du, X. Qi, L. Liang, Y. Wang, G. Feng, Y. Fan, Z. Han, D. Kong, Z. Cheng, J. C. Wu, Z. He and Z. Li (2015). "Extracellular Matrix can Recover the Downregulation of Adhesion Molecules after Cell Detachment and Enhance Endothelial Cell Engraftment." Sci Rep **5**: 10902.

Hill, C. E., D. M. Brodak and M. Bartlett Bunge (2012). "Dissociated predegenerated peripheral nerve transplants for spinal cord injury repair: a comprehensive assessment of their effects on regeneration and functional recovery compared to Schwann cell transplants." J Neurotrauma **29**(12): 2226-2243.

Hill, J. J., K. Jin, X. O. Mao, L. Xie and D. A. Greenberg (2012). "Intracerebral chondroitinase ABC and heparan sulfate proteoglycan glypican improve outcome from chronic stroke in rats." Proc Natl Acad Sci U S A **109**(23): 9155-9160.

Hofstetter, C. P., E. J. Schwarz, D. Hess, J. Widenfalk, A. El Manira, D. J. Prockop and L. Olson (2002). "Marrow stromal cells form guiding strands in the injured spinal cord and promote recovery." Proc Natl Acad Sci U S A **99**(4): 2199-2204.

Horn, K. P., S. A. Busch, A. L. Hawthorne, N. van Rooijen and J. Silver (2008). "Another barrier to regeneration in the CNS: activated macrophages induce extensive retraction of dystrophic axons through direct physical interactions." J Neurosci **28**(38): 9330-9341.

Hudson, T. W., S. Y. Liu and C. E. Schmidt (2004). "Engineering an improved acellular nerve graft via optimized chemical processing." Tissue Eng **10**(9-10): 1346-1358.

Hurtado, A., J. M. Cregg, H. B. Wang, D. F. Wendell, M. Oudega, R. J. Gilbert and J. W. McDonald (2011). "Robust CNS regeneration after complete spinal cord transection using aligned poly-L-lactic acid microfibers." Biomaterials **32**(26): 6068-6079.

Imaizumi, T., K. L. Lankford and J. D. Kocsis (2000). "Transplantation of olfactory ensheathing cells or Schwann cells restores rapid and secure conduction across the transected spinal cord." Brain Res **854**(1-2): 70-78.

Inskip, J. A., L. M. Ramer, M. S. Ramer and A. V. Krassioukov (2009). "Autonomic assessment of animals with spinal cord injury: tools, techniques and translation." Spinal Cord **47**(1): 2-35.

Irvine, K. A., A. R. Ferguson, K. D. Mitchell, S. B. Beattie, A. Lin, E. D. Stuck, J. R. Huie, J. L. Nielson, J. F. Talbott, T. Inoue, M. S. Beattie and J. C. Bresnahan (2014). "The Irvine, Beatties, and Bresnahan (IBB) Forelimb Recovery Scale: An Assessment of Reliability and Validity." Front Neurol **5**: 116.

Jain, A., Y. T. Kim, R. J. McKeon and R. V. Bellamkonda (2006). "In situ gelling hydrogels for conformal repair of spinal cord defects, and local delivery of BDNF after spinal cord injury." Biomaterials **27**(3): 497-504.

Jakeman, L. B. (2012). Assessment of Lesion and Tissue Sparing Volumes Following Spinal Cord Injury. Animal Models of Acute Neurological Injuries II. J. X. Chen, X. ; Xu, Z. C. ; Zhang, J. H. , Humana Press. **2:** 417-442.

Jiao, X., P. C. Billings, M. P. O'Connell, F. S. Kaplan, E. M. Shore and D. L. Glaser (2007). "Heparan sulfate proteoglycans (HSPGs) modulate BMP2 osteogenic bioactivity in C2C12 cells." J Biol Chem **282**(2): 1080-1086.

Johnson, T. D., S. Y. Lin and K. L. Christman (2011). "Tailoring material properties of a nanofibrous extracellular matrix derived hydrogel." Nanotechnology **22**(49).

Ju, Y. E., P. A. Janmey, M. E. McCormick, E. S. Sawyer and L. A. Flanagan (2007). "Enhanced neurite growth from mammalian neurons in three-dimensional salmon fibrin gels." Biomaterials **28**(12): 2097-2108.

Kang, C. E., P. C. Poon, C. H. Tator and M. S. Shoichet (2008). "A New Paradigm for Local and Sustained Release of Therapeutic Molecules to the Injured Spinal Cord for Neuroprotection and Tissue Repair." Tissue Eng Part A **15**(3): 595-604.

Kanno, H., Y. Pressman, A. Moody, R. Berg, E. M. Muir, J. H. Rogers, H. Ozawa, E. Itoi, D. D. Pearse and M. B. Bunge (2014). "Combination of engineered Schwann cell grafts to secrete neurotrophin and chondroitinase promotes axonal regeneration and locomotion after spinal cord injury." J Neurosci **34**(5): 1838-1855.

Karimi-Abdolrezaee, S., E. Eftekharpour, J. Wang, C. M. Morshead and M. G. Fehlings (2006). "Delayed transplantation of adult neural precursor cells promotes remyelination and functional neurological recovery after spinal cord injury." J Neurosci **26**(13): 3377-3389.

Karimi-Abdolrezaee, S., E. Eftekharpour, J. Wang, D. Schut and M. G. Fehlings (2010). "Synergistic effects of transplanted adult neural stem/progenitor cells, chondroitinase, and growth factors promote functional repair and plasticity of the chronically injured spinal cord." J Neurosci **30**(5): 1657-1676.

Keyvan-Fouladi, N., G. Raisman and Y. Li (2003). "Functional repair of the corticospinal tract by delayed transplantation of olfactory ensheathing cells in adult rats." J Neurosci **23**(28): 9428-9434.

Khaing, Z. Z., S. A. Geissler, S. Jiang, B. D. Milman, S. V. Aguilar, C. E. Schmidt and T. Schallert (2012). "Assessing forelimb function after unilateral cervical spinal cord injury: novel forelimb tasks predict lesion severity and recovery." J Neurotrauma **29**(3): 488-498.

Khaing, Z. Z., B. D. Milman, J. E. Vanscoy, S. K. Seidlits, R. J. Grill and C. E. Schmidt (2011). "High molecular weight hyaluronic acid limits astrocyte activation and scar formation after spinal cord injury." J Neural Eng **8**(4): 046033.

Kigerl, K. A., J. C. Gensel, D. P. Ankeny, J. K. Alexander, D. J. Donnelly and P. G. Popovich (2009). "Identification of two distinct macrophage subsets with divergent effects causing either neurotoxicity or regeneration in the injured mouse spinal cord." J Neurosci **29**(43): 13435-13444.

Kim, Y. T., V. K. Haftel, S. Kumar and R. V. Bellamkonda (2008). "The role of aligned polymer fiber-based constructs in the bridging of long peripheral nerve gaps." Biomaterials **29**(21): 3117-3127.

Kwon, J. S., S. M. Yoon, S. W. Shim, J. H. Park, K. J. Min, H. J. Oh, J. H. Kim, Y. J. Kim, J. J. Yoon, B. H. Choi and M. S. Kim (2013). "Injectable extracellular matrix hydrogel developed using porcine articular cartilage." Int J Pharm **454**(1): 183-191.

Lammertse, D. P., L. A. Jones, S. B. Charlifue, S. C. Kirshblum, D. F. Apple, K. T. Ragnarsson, S. P. Falci, R. F. Heary, T. F. Choudhri, A. L. Jenkins, R. R. Betz, D. Poonian, J. P. Cuthbert, A. Jha, D. A. Snyder and N. Knoller (2012). "Autologous incubated macrophage therapy in acute, complete spinal cord injury: results of the phase 2 randomized controlled multicenter trial." Spinal Cord **50**(9): 661-671.

Lane, M. A., K. Z. Lee, K. Salazar, B. E. O'Steen, D. C. Bloom, D. D. Fuller and P. J. Reier (2012). "Respiratory function following bilateral mid-cervical contusion injury in the adult rat." Exp Neurol **235**(1): 197-210.

Lang, B. T., J. M. Cregg, M. A. DePaul, A. P. Tran, K. Xu, S. M. Dyck, K. M. Madalena, B. P. Brown, Y. L. Weng, S. Li, S. Karimi-Abdolrezaee, S. A. Busch, Y. Shen and J. Silver (2015). "Modulation of the proteoglycan receptor PTPsigma promotes recovery after spinal cord injury." Nature **518**(7539): 404-408.

Lau, L. W., R. Cua, M. B. Keough, S. Haylock-Jacobs and V. W. Yong (2013). "Pathophysiology of the brain extracellular matrix: a new target for remyelination." Nat Rev Neurosci **14**(10): 722-729.

Leach, J. B., X. Q. Brown, J. G. Jacot, P. A. Dimilla and J. Y. Wong (2007). "Neurite outgrowth and branching of PC12 cells on very soft substrates sharply decreases below a threshold of substrate rigidity." J Neural Eng **4**(2): 26-34.

Lee, J., A. A. Abdeen, D. Zhang and K. A. Kilian (2013). "Directing stem cell fate on hydrogel substrates by controlling cell geometry, matrix mechanics and adhesion ligand composition." Biomaterials **34**(33): 8140-8148.

Lee, Y. S., C. Y. Lin, H. H. Jiang, M. Depaul, V. W. Lin and J. Silver (2013). "Nerve regeneration restores supraspinal control of bladder function after complete spinal cord injury." J Neurosci **33**(26): 10591-10606.

Leipzig, N. D. and M. S. Shoichet (2009). "The effect of substrate stiffness on adult neural stem cell behavior." Biomaterials **30**(36): 6867-6878.

Levental, I., P. C. Georges and P. A. Janmey (2007). "Soft biological materials and their impact on cell function." Soft Matter **3**(3): 299-306.

Levi, A. D., H. Dancausse, X. Li, S. Duncan, L. Horkey and M. Oliviera (2002). "Peripheral nerve grafts promoting central nervous system regeneration after spinal cord injury in the primate." J Neurosurg **96**(2 Suppl): 197-205.

Li, C., X. Zhang, R. Cao, B. Yu, H. Liang, M. Zhou, D. Li, Y. Wang and E. Liu (2012). "Allografts of the acellular sciatic nerve and brain-derived neurotrophic factor repair spinal cord injury in adult rats." PLoS One **7**(8): e42813.

Li, Y., P. Decherchi and G. Raisman (2003). "Transplantation of olfactory ensheathing cells into spinal cord lesions restores breathing and climbing." J Neurosci **23**(3): 727-731.

Liesi, P. and T. Kauppila (2002). "Induction of type IV collagen and other basement-membrane-associated proteins after spinal cord injury of the adult rat may participate in formation of the glial scar." Exp Neurol **173**(1): 31-45.

Liu, J., J. Chen, B. Liu, C. Yang, D. Xie, X. Zheng, S. Xu, T. Chen, L. Wang, Z. Zhang, X. Bai and D. Jin (2013). "Acellular spinal cord scaffold seeded with mesenchymal stem cells promotes long-distance axon regeneration and functional recovery in spinal cord injured rats." J Neurol Sci **325**(1-2): 127-136.

Liu, T., J. Xu, B. P. Chan and S. Y. Chew (2012). "Sustained release of neurotrophin-3 and chondroitinase ABC from electrospun collagen nanofiber scaffold for spinal cord injury repair." J Biomed Mater Res A **100**(1): 236-242.

Liu, Y., H. Ye, K. Satkunendrarajah, G. S. Yao, Y. Bayon and M. G. Fehlings (2013). "A self-assembling peptide reduces glial scarring, attenuates post-traumatic inflammation and promotes neurological recovery following spinal cord injury." Acta Biomater **9**(9): 8075-8088.

Man, A. J., H. E. Davis, A. Itoh, J. K. Leach and P. Bannerman (2011). "Neurite outgrowth in fibrin gels is regulated by substrate stiffness." Tissue Eng Part A **17**(23-24): 2931-2942.

Marchand, R. and S. Woerly (1990). "Transected spinal cords grafted with in situ self-assembled collagen matrices." Neuroscience **36**(1): 45-60.

Marchand, R., S. Woerly, L. Bertrand and N. Valdes (1993). "Evaluation of two cross-linked collagen gels implanted in the transected spinal cord." Brain Res Bull **30**(3-4): 415-422.

McKinley, W. O., A. B. Jackson, D. D. Cardenas and M. J. DeVivo (1999). "Long-term medical complications after traumatic spinal cord injury: a regional model systems analysis." Arch Phys Med Rehabil **80**(11): 1402-1410.

Medberry, C. J., P. M. Crapo, B. F. Siu, C. A. Carruthers, M. T. Wolf, S. P. Nagarkar, V. Agrawal, K. E. Jones, J. Kelly, S. A. Johnson, S. S. Velankar, S. C. Watkins, M. Modo and S. F. Badylak (2013). "Hydrogels derived from central nervous system extracellular matrix." Biomaterials **34**(4): 1033-1040.

Metz, G. A., A. Curt, H. van de Meent, I. Klusman, M. E. Schwab and V. Dietz (2000). "Validation of the weight-drop contusion model in rats: a comparative study of human spinal cord injury." J Neurotrauma **17**(1): 1-17.

Metz, G. A., D. Merkler, V. Dietz, M. E. Schwab and K. Fouad (2000). "Efficient testing of motor function in spinal cord injured rats." Brain Res **883**(2): 165-177.

Miki, T., T. Lehmann, H. Cai, D. B. Stolz and S. C. Strom (2005). "Stem cell characteristics of amniotic epithelial cells." Stem Cells **23**(10): 1549-1559.

Miron, V. E., A. Boyd, J. W. Zhao, T. J. Yuen, J. M. Ruckh, J. L. Shadrach, P. van Wijngaarden, A. J. Wagers, A. Williams, R. J. Franklin and C. ffrench-Constant (2013). "M2 microglia and macrophages drive oligodendrocyte differentiation during CNS remyelination." Nat Neurosci **16**(9): 1211-1218.

Mokarram, N., A. Merchant, V. Mukhatyar, G. Patel and R. V. Bellamkonda (2012). "Effect of modulating macrophage phenotype on peripheral nerve repair." Biomaterials **33**(34): 8793-8801.

Moshayedi, P., F. Costa Lda, A. Christ, S. P. Lacour, J. Fawcett, J. Guck and K. Franze (2010). "Mechanosensitivity of astrocytes on optimized polyacrylamide gels analyzed by quantitative morphometry." J Phys Condens Matter **22**(19): 194114.

Mothe, A. J., R. Y. Tam, T. Zahir, C. H. Tator and M. S. Shoichet (2013). "Repair of the injured spinal cord by transplantation of neural stem cells in a hyaluronan-based hydrogel." Biomaterials **34**(15): 3775-3783.

Mothe, A. J. and C. H. Tator (2013). "Review of transplantation of neural stem/progenitor cells for spinal cord injury." International Journal of Developmental Neuroscience **31**(7): 701-713.

Nagao, R. J., S. Lundy, Z. Z. Khaing and C. E. Schmidt (2011). "Functional characterization of optimized acellular peripheral nerve graft in a rat sciatic nerve injury model." Neurol Res **33**(6): 600-608.

Nagao, R. J., Y. Ouyang, R. Keller, C. Lee, L. J. Suggs and C. E. Schmidt (2013). "Preservation of Capillary-beds in Rat Lung Tissue Using Optimized Chemical Decellularization." J Mater Chem B Mater Biol Med **1**(37): 4801-4808.

Nakayama, K. H., C. A. Batchelder, C. I. Lee and A. F. Tarantal (2010). "Decellularized rhesus monkey kidney as a three-dimensional scaffold for renal tissue engineering." Tissue Eng Part A **16**(7): 2207-2216.

Neubauer, D., J. B. Graham and D. Muir (2007). "Chondroitinase treatment increases the effective length of acellular nerve grafts." Exp Neurol **207**(1): 163-170.

Nicaise, C., T. J. Hala, D. M. Frank, J. L. Parker, M. Authelet, K. Leroy, J. P. Brion, M. C. Wright and A. C. Lepore (2012). "Phrenic motor neuron degeneration compromises phrenic axonal circuitry and diaphragm activity in a unilateral cervical contusion model of spinal cord injury." Exp Neurol **235**(2): 539-552.

Nomura, H., Y. Katayama, M. S. Shoichet and C. H. Tator (2006). "Complete spinal cord transection treated by implantation of a reinforced synthetic hydrogel channel results in syringomyelia and caudal migration of the rostral stump." Neurosurgery **59**(1): 183-192; discussion 183-192.

Norenberg, M. D., J. Smith and A. Marcillo (2004). "The pathology of human spinal cord injury: defining the problems." J Neurotrauma **21**(4): 429-440.

Novak, M. L. and T. J. Koh (2013). "Macrophage phenotypes during tissue repair." J Leukoc Biol **93**(6): 875-881.

Novikova, L. N., S. Lobov, M. Wiberg and L. N. Novikov (2011). "Efficacy of olfactory ensheathing cells to support regeneration after spinal cord injury is influenced by method of culture preparation." Exp Neurol **229**(1): 132-142.

NSCISC (2014). Spinal Cord Injury Facts and Figures at a Glance, National Spinal Cord Injury Statistics Center.

O'Neill, J. D., D. O. Freytes, A. J. Anandappa, J. A. Oliver and G. V. Vunjak-Novakovic (2013). "The regulation of growth and metabolism of kidney stem cells with regional specificity using extracellular matrix derived from kidney." Biomaterials **34**(38): 9830-9841.

Ott, H. C., B. Clippinger, C. Conrad, C. Schuetz, I. Pomerantseva, L. Ikonomou, D. Kotton and J. P. Vacanti (2010). "Regeneration and orthotopic transplantation of a bioartificial lung." Nat Med **16**(8): 927-933.

Ott, H. C., T. S. Matthiesen, S. K. Goh, L. D. Black, S. M. Kren, T. I. Netoff and D. A. Taylor (2008). "Perfusion-decellularized matrix: using nature's platform to engineer a bioartificial heart." Nat Med **14**(2): 213-221.

Ottoboni, L., D. De Feo, A. Merlini and G. Martino (2015). "Commonalities in immune modulation between mesenchymal stem cells (MSCs) and neural stem/precursor cells (NPCs)." Immunol Lett.

Oudega, M. and X. M. Xu (2006). "Schwann cell transplantation for repair of the adult spinal cord." J Neurotrauma **23**(3-4): 453-467.

Parr, A. M., C. H. Tator and A. Keating (2007). "Bone marrow-derived mesenchymal stromal cells for the repair of central nervous system injury." Bone Marrow Transplant **40**(7): 609-619.

Patel, V., G. Joseph, A. Patel, S. Patel, D. Bustin, D. Mawson, L. M. Tuesta, R. Puentes, M. Ghosh and D. D. Pearse (2010). "Suspension matrices for improved Schwann-cell survival after implantation into the injured rat spinal cord." J Neurotrauma **27**(5): 789-801.

Pearse, D. D., F. C. Pereira, A. E. Marcillo, M. L. Bates, Y. A. Berrocal, M. T. Filbin and M. B. Bunge (2004). "cAMP and Schwann cells promote axonal growth and functional recovery after spinal cord injury." Nat Med **10**(6): 610-616.

Pearse, D. D., A. R. Sanchez, F. C. Pereira, C. M. Andrade, R. Puzis, Y. Pressman, K. Golden, B. M. Kitay, B. Blits, P. M. Wood and M. B. Bunge (2007). "Transplantation of

Schwann cells and/or olfactory ensheathing glia into the contused spinal cord: Survival, migration, axon association, and functional recovery." Glia **55**(9): 976-1000.

Petersen, O. W., L. Ronnov-Jessen, A. R. Howlett and M. J. Bissell (1992). "Interaction with basement membrane serves to rapidly distinguish growth and differentiation pattern of normal and malignant human breast epithelial cells." Proc Natl Acad Sci U S A **89**(19): 9064-9068.

Podratz, J. L., E. Rodriguez and A. J. Windebank (2001). "Role of the extracellular matrix in myelination of peripheral nerve." Glia **35**(1): 35-40.

Poon, P. C., D. Gupta, M. S. Shoichet and C. H. Tator (2007). "Clip compression model is useful for thoracic spinal cord injuries: histologic and functional correlates." Spine (Phila Pa 1976) **32**(25): 2853-2859.

Portmann-Lanz, C. B., A. Schoeberlein, R. Portmann, S. Mohr, P. Rollini, R. Sager and D. V. Surbek (2010). "Turning placenta into brain: placental mesenchymal stem cells differentiate into neurons and oligodendrocytes." Am J Obstet Gynecol **202**(3): 294 e291-294 e211.

Powers, J. C., A. D. Harley and D. V. Myers (1977). "Subsite specificity of porcine pepsin." Adv Exp Med Biol **95**: 141-157.

Ramon-Cueto, A., M. I. Cordero, F. F. Santos-Benito and J. Avila (2000). "Functional recovery of paraplegic rats and motor axon regeneration in their spinal cords by olfactory ensheathing glia." Neuron **25**(2): 425-435.

Rao, Y. J., W. X. Zhu, Z. Q. Du, C. X. Jia, T. X. Du, Q. A. Zhao, X. Y. Cao and Y. J. Wang (2014). "Effectiveness of olfactory ensheathing cell transplantation for treatment of spinal cord injury." Genet Mol Res **13**(2): 4124-4129.

Rapalino, O., O. Lazarov-Spiegler, E. Agranov, G. J. Velan, E. Yoles, M. Fraidakis, A. Solomon, R. Gepstein, A. Katz, M. Belkin, M. Hadani and M. Schwartz (1998). "Implantation of stimulated homologous macrophages results in partial recovery of paraplegic rats." Nat Med **4**(7): 814-821.

Reilly, G. C. and A. J. Engler (2010). "Intrinsic extracellular matrix properties regulate stem cell differentiation." J Biomech **43**(1): 55-62.

Reynolds, B. A. and S. Weiss (1992). "Generation of neurons and astrocytes from isolated cells of the adult mammalian central nervous system." Science **255**(5052): 1707-1710.

Risling, M., K. Fried, H. Linda, T. Carlstedt and S. Cullheim (1993). "Regrowth of motor axons following spinal cord lesions: distribution of laminin and collagen in the CNS scar tissue." Brain Res Bull **30**(3-4): 405-414.

Santos-Silva, A., R. Fairless, M. C. Frame, P. Montague, G. M. Smith, A. Toft, J. S. Riddell and S. C. Barnett (2007). "FGF/heparin differentially regulates Schwann cell and olfactory ensheathing cell interactions with astrocytes: a role in astrocytosis." J Neurosci **27**(27): 7154-7167.

Sawkins, M. J., W. Bowen, P. Dhadda, H. Markides, L. E. Sidney, A. J. Taylor, F. R. Rose, S. F. Badylak, K. M. Shakesheff and L. J. White (2013). "Hydrogels derived from demineralized and decellularized bone extracellular matrix." Acta Biomater **9**(8): 7865-7873.

Schallert, T., S. M. Fleming, J. L. Leasure, J. L. Tillerson and S. T. Bland (2000). "CNS plasticity and assessment of forelimb sensorimotor outcome in unilateral rat models of stroke, cortical ablation, parkinsonism and spinal cord injury." Neuropharmacology **39**(5): 777-787.

Seidlits, S. K., Z. Z. Khaing, R. R. Petersen, J. D. Nickels, J. E. Vanscoy, J. B. Shear and C. E. Schmidt (2010). "The effects of hyaluronic acid hydrogels with tunable mechanical properties on neural progenitor cell differentiation." Biomaterials **31**(14): 3930-3940.

Seif-Naraghi, S. B., D. Horn, P. J. Schup-Magoffin and K. L. Christman (2012). "Injectable extracellular matrix derived hydrogel provides a platform for enhanced retention and delivery of a heparin-binding growth factor." Acta Biomater **8**(10): 3695-3703.

Seif-Naraghi, S. B., M. A. Salvatore, P. J. Schup-Magoffin, D. P. Hu and K. L. Christman (2010). "Design and characterization of an injectable pericardial matrix gel: a potentially autologous scaffold for cardiac tissue engineering." Tissue Eng Part A **16**(6): 2017-2027.

Shin, H., B. D. Olsen and A. Khademhosseini (2012). "The mechanical properties and cytotoxicity of cell-laden double-network hydrogels based on photocrosslinkable gelatin and gellan gum biomacromolecules." Biomaterials **33**(11): 3143-3152.

Shupe, T., M. Williams, A. Brown, B. Willenberg and B. E. Petersen (2010). "Method for the decellularization of intact rat liver." Organogenesis **6**(2): 134-136.

Sicari, B. M., J. L. Dziki, B. F. Siu, C. J. Medberry, C. L. Dearth and S. F. Badylak (2014). "The promotion of a constructive macrophage phenotype by solubilized extracellular matrix." Biomaterials **35**(30): 8605-8612.

Singelyn, J. M., P. Sundaramurthy, T. D. Johnson, P. J. Schup-Magoffin, D. P. Hu, D. M. Faulk, J. Wang, K. M. Mayle, K. Bartels, M. Salvatore, A. M. Kinsey, A. N. Demaria, N. Dib and K. L. Christman (2012). "Catheter-deliverable hydrogel derived from decellularized ventricular extracellular matrix increases endogenous cardiomyocytes and preserves cardiac function post-myocardial infarction." J Am Coll Cardiol **59**(8): 751-763.

Somerson, S. K. and B. T. Stokes (1987). "Functional analysis of an electromechanical spinal cord injury device." Exp Neurol **96**(1): 82-96.

Sorokin, L. (2010). "The impact of the extracellular matrix on inflammation." Nat Rev Immunol **10**(10): 712-723.

Stachowiak, M. R., M. A. Smith, E. Blankman, L. M. Chapin, H. E. Balcioglu, S. Wang, M. C. Beckerle and B. O'Shaughnessy (2014). "A mechanical-biochemical feedback loop regulates remodeling in the actin cytoskeleton." Proceedings of the National Academy of Sciences of the United States of America **111**(49): 17528-17533.

Stokols, S., J. Sakamoto, C. Breckon, T. Holt, J. Weiss and M. H. Tuszynski (2006). "Templated agarose scaffolds support linear axonal regeneration." Tissue Eng **12**(10): 2777-2787.

Stokols, S. and M. H. Tuszynski (2006). "Freeze-dried agarose scaffolds with uniaxial channels stimulate and guide linear axonal growth following spinal cord injury." Biomaterials **27**(3): 443-451.

Stonehill, W. H., R. R. Dmochowski, A. L. Patterson and C. E. Cox (1996). "Risk factors for bladder tumors in spinal cord injury patients." J Urol **155**(4): 1248-1250.

Suri, S. and C. E. Schmidt (2010). "Cell-laden hydrogel constructs of hyaluronic acid, collagen, and laminin for neural tissue engineering." Tissue Eng Part A **16**(5): 1703-1716.

Takami, T., M. Oudega, M. L. Bates, P. M. Wood, N. Kleitman and M. B. Bunge (2002). "Schwann cell but not olfactory ensheathing glia transplants improve hindlimb locomotor performance in the moderately contused adult rat thoracic spinal cord." J Neurosci **22**(15): 6670-6681.

Teng, Y. D., E. B. Lavik, X. Qu, K. I. Park, J. Ourednik, D. Zurakowski, R. Langer and E. Y. Snyder (2002). "Functional recovery following traumatic spinal cord injury mediated by a unique polymer scaffold seeded with neural stem cells." Proc Natl Acad Sci U S A **99**(5): 3024-3029.

Tom, V. J., H. R. Sandrow-Feinberg, K. Miller, L. Santi, T. Connors, M. A. Lemay and J. D. Houle (2009). "Combining peripheral nerve grafts and chondroitinase promotes functional axonal regeneration in the chronically injured spinal cord." J Neurosci **29**(47): 14881-14890.

Tysseling-Mattiace, V. M., V. Sahni, K. L. Niece, D. Birch, C. Czeisler, M. G. Fehlings, S. I. Stupp and J. A. Kessler (2008). "Self-assembling nanofibers inhibit glial scar formation and promote axon elongation after spinal cord injury." J Neurosci **28**(14): 3814-3823.

Tysseling, V. M., V. Sahni, E. T. Pashuck, D. Birch, A. Hebert, C. Czeisler, S. I. Stupp and J. A. Kessler (2010). "Self-assembling peptide amphiphile promotes plasticity of serotonergic fibers following spinal cord injury." J Neurosci Res **88**(14): 3161-3170.

Uygun, B. E., A. Soto-Gutierrez, H. Yagi, M. L. Izamis, M. A. Guzzardi, C. Shulman, J. Milwid, N. Kobayashi, A. Tilles, F. Berthiaume, M. Hertl, Y. Nahmias, M. L. Yarmush and K. Uygun (2010). "Organ reengineering through development of a transplantable recellularized liver graft using decellularized liver matrix." Nat Med **16**(7): 814-820.

Wang, J. Y., A. K. Liou, Z. H. Ren, L. Zhang, B. N. Brown, X. T. Cui, S. F. Badylak, Y. N. Cai, Y. Q. Guan, R. K. Leak, J. Chen, X. Ji and L. Chen (2013). "Neurorestorative effect of urinary bladder matrix-mediated neural stem cell transplantation following traumatic brain injury in rats." CNS Neurol Disord Drug Targets **12**(3): 413-425.

Webb, A. A. and G. D. Muir (2005). "Sensorimotor behaviour following incomplete cervical spinal cord injury in the rat." Behav Brain Res **165**(2): 147-159.

Wen, X., Y. Wang, Z. Guo, H. Meng, J. Huang, L. Zhang, B. Zhao, Q. Zhao, Y. Zheng and J. Peng (2015). "Cauda equina-derived extracellular matrix for fabrication of nanostructured hybrid scaffolds applied to neural tissue engineering." Tissue Eng Part A **21**(5-6): 1095-1105.

West, M. J. (2012). "Estimating volume in biological structures." Cold Spring Harb Protoc **2012**(11): 1129-1139.

Wewetzer, K., N. Kern, C. Ebel, C. Radtke and G. Brandes (2005). "Phagocytosis of O4+ axonal fragments in vitro by p75- neonatal rat olfactory ensheathing cells." Glia **49**(4): 577-587.

Whishaw, I. Q., S. M. Pellis, B. Gorny, B. Kolb and W. Tetzlaff (1993). "Proximal and distal impairments in rat forelimb use in reaching follow unilateral pyramidal tract lesions." Behav Brain Res **56**(1): 59-76.

Williams, R. R., M. Henao, D. D. Pearse and M. B. Bunge (2015). "Permissive Schwann cell graft/spinal cord interfaces for axon regeneration." Cell Transplant **24**(1): 115-131.

Xie, J., S. M. Willerth, X. Li, M. R. Macewan, A. Rader, S. E. Sakiyama-Elbert and Y. Xia (2009). "The differentiation of embryonic stem cells seeded on electrospun nanofibers into neural lineages." Biomaterials **30**(3): 354-362.

Xiong, Z., Y. N. Yan, S. G. Wang, R. J. Zhang and C. Zhang (2002). "Fabrication of porous scaffolds for bone tissue engineering via low-temperature deposition." Scripta Materialia **46**(11): 771-776.

Xu, H., K. Miki, S. Ishibashi, J. Inoue, L. Sun, S. Endo, I. Sekiya, T. Muneta, J. Inazawa, M. Dezawa and H. Mizusawa (2010). "Transplantation of neuronal cells induced from human mesenchymal stem cells improves neurological functions after stroke without cell fusion." J Neurosci Res **88**(16): 3598-3609.

Xu, X. M., S. X. Zhang, H. Li, P. Aebischer and M. B. Bunge (1999). "Regrowth of axons into the distal spinal cord through a Schwann-cell-seeded mini-channel implanted into hemisected adult rat spinal cord." Eur J Neurosci **11**(5): 1723-1740.

Xue, H., X. Y. Zhang, J. M. Liu, Y. Song, Y. F. Li and D. Chen (2013). "Development of a chemically extracted acellular muscle scaffold seeded with amniotic epithelial cells to promote spinal cord repair." J Biomed Mater Res A **101**(1): 145-156.

Ydens, E., A. Cauwels, B. Asselbergh, S. Goethals, L. Peeraer, G. Lornet, L. Almeida-Souza, J. A. Van Ginderachter, V. Timmerman and S. Janssens (2012). "Acute injury in the peripheral nervous system triggers an alternative macrophage response." J Neuroinflammation **9**: 176.

Zeev-Brann, A. B., O. Lazarov-Spiegler, T. Brenner and M. Schwartz (1998). "Differential effects of central and peripheral nerves on macrophages and microglia." Glia **23**(3): 181-190.

Zhang, X. Y., H. Xue, J. M. Liu and D. Chen (2012). "Chemically extracted acellular muscle: A new potential scaffold for spinal cord injury repair." Journal of Biomedical Materials Research Part A **100A**(3): 578-587.

Zhu, T., Q. Tang, Y. Shen, H. Tang, L. Chen and J. Zhu (2015). "An acellular cerebellar biological scaffold: Preparation, characterization, biocompatibility and effects on neural stem cells." Brain Res Bull **113**: 48-57.

Zimmer, M. B., K. Nantwi and H. G. Goshgarian (2007). "Effect of spinal cord injury on the respiratory system: basic research and current clinical treatment options." J Spinal Cord Med **30**(4): 319-330.

Zimmermann, D. R. and M. T. Dours-Zimmermann (2008). "Extracellular matrix of the central nervous system: from neglect to challenge." Histochemistry and Cell Biology **130**(4): 635-653.

Zuidema, J. M., C. J. Rivet, R. J. Gilbert and F. A. Morrison (2014). "A protocol for rheological characterization of hydrogels for tissue engineering strategies." J Biomed Mater Res B Appl Biomater **102**(5): 1063-1073.